21–22 April 2021

Online

PROCEEDINGS OF IX INTERNATIONAL COMPETITION OF COOMET "THE BEST YOUNG METROLOGIST 2021"

COOMET

PROCEEDINGS OF
IX INTERNATIONAL
COMPETITION OF
COOMET "THE BEST
YOUNG METROLOGIST
2021"

CONTENTS

SCIENTIFIC COMMITTEE
OF IX INTERNATIONAL
COMPETITION OF COOMET
"THE BEST YOUNG
METROLOGIST 2021"

Approach to validation of calibration procedures based on a process for estimating of measurement uncertainty

Anastasiya Tumilovich, Anna Chunovkina
D.I. Mendeleyev Institute for Metrology (VNIIM)
190005, Russia, St.Petersbur, Moskovsky pr.,19
Tel: +7 (812) 251-79-29, fax: +7 812 713-0114
E-mail: a.a.koroleva@vniim.ru

Abstract

Many of calibration laboratories, regardless of their organizational and legal form, are accredited to carry out calibration work. During accreditation, calibration laboratories are checked for compliance with the requirements, specified in the document ISO/IEC 17025—2019 «General requirements for the competence of testing and calibration laboratories», where in clause 7.2.2 it is said about necessity to validate measurement methods. This requirement also applies to calibration laboratories of national metrology institutes that support CMC's (Calibration and Measurement Capabilities) through participation in comparison of national measurement standards and implementation of quality systems. At present, there is no document regulating the process of validation of calibration procedures. With considering received experience, authors proposed an approach to the validation of calibration procedures, related with estimating measurement uncertainty algorithms. Analysis of calibration procedures VNIIM made it possible to single out typical algorithms for validation of measurement procedure, which are supposed to be taken as a basis for developing corresponding Recommendations.

Key words: *validation of calibration procedures, calibration laboratories, measurement uncertainty, algorithms of estimation, quality assurance, situation approach.*

The relevance of the research and problem statement

COOMET National Metrology Institutes (NMIs) participate in the implementation of the mutual recognition agreement CIPM MRA [1], where a necessary condition for confirming calibration capabilities is participation in comparisons of national measurement standards and audit of measurement quality systems at NMIs. When performing measurements in the framework of comparisons, the laboratory follows a calibration procedure, which is verified by experts of external quality assessment. ISO/IEC 17025-2019 [2] specifies requirements for calibration laboratories, including the validation of methods developed by laboratories. At the moment there is no normative document governing the process of validation of calibration procedures.

There are several national and international normative documents describing the method validation process. In particular, the EURACHEM guide [3], which applies to analytical measurement methods. This recommendation clarifies the understanding of the validation process in general, but validation process of calibration procedures has its specific features. Therefore, there is a need to create a structured approach that would regulate the process of validation of MI calibration procedures based on their intended application.

Approach to problem solving

Each calibration procedure is unique, as it is developed to establish the individual metrological characteristics of the MI. Calibration procedures include the formulation of a measurement model, choice of measurement standards and MI (used for influence quantity control), justification of the method for transferring a unit of quantity, processing of measurement results, estimation of uncertainty, etc. Calibration procedures implement the calibration capabilities of the laboratory and meet the needs of the calibration customer.

When developing a calibration procedure, establish:

- determined metrological properties (MP) of calibrated instrument (performance characteristics);
- target measurement uncertainty (if necessary);
- measurement standards and measuring instruments (MI) used in calibration;
- stages of measurement process;
- algorithms for processing experimental data, estimating measurement uncertainty,
- form of data reported and checking of compliance with the established requirements (if necessary).

The documents [3,4] provide definitions of the concept of "validation". Based on them, it can be concluded that the validation of a calibration procedures is a confirmation of the suitability of the application of this procedure for the intended purposes through analysis and confirmation of the compliance of the studied calibration procedure with the established requirements.

At the validation process the following requirements are checked:

(1) the correspondence of the determined MP to the customer's requirements;

(2) the correctness of the measurement method chosen, of requirements for the accuracy of the measurement standards and auxiliary measuring instruments used, control of influence quantities (at the stage of checking the choice of measurement standards and auxiliary measuring instruments);

(3) the choice of the number of calibration points over the range, the number of repeated measurements, as well as control of the measurement conditions (at the stage of analyzing the measurement experiment at calibration);

(4) the correctness of the algorithm for data processing and the application of statistical criteria (at the stage of data processing/analysis);

(5) the correctness of the formulation of the measurement model, the estimation of the uncertainty of the input quantities, the compilation of the uncertainty budget, the calculation of the expanded uncertainty (at the stage of checking the correctness of the uncertainty estimation);

(6) the correctness of the decision-making algorithm at the stage of checking compliance with the established requirements;

(7) the correctness of reporting of the calibration results in accordance with the customer's requirements.

Based on the experience of validating calibration procedures at VNIIM, it can be stated that there is a close relation between validation process and the process of measurement uncertainty evaluation.

This relationship is presented in Table 1. The left column indicates the steps in the calibration procedure being validated, the right column indicates the uncertainty estimation steps associated with the corresponding steps from the left column.

Table 1 - Relationship of uncertainty with stages of validation

Measured quantities / determinable MP. Unit transfer method	Formulation of a measurement equation, determination of input and output quantities.
Sources of uncertainty and related quantitative uncertainty information.	Determination of input quantities. Standard uncertainty evaluation based on information available. Choice of absolute or relative form of recording uncertainty.
Design of a measurement experiment (planning to achieve target uncertainty).	Choice of the number of repeated measurements for type A evaluation (analysis of the ratio of contributions by type A and B). Uncertainty budget analysis.

	The choice of the coverage factor, *k*, depending on the distribution law and the ratio of uncertainty contributions.
The reporting of the calibration results and analysis of the algorithm used for checking of compliance.	The procedure of checking the compliance of the calibration result with the established requirements, taking into account the uncertainty.

Through the analysis of the process of uncertainty estimation of the measurement result, a comprehensive approach for analyzing the completeness and correctness of the calibration procedure can be realized. This becomes possible due to the fact that when analyzing the correctness of the estimation of the measurement uncertainty [5-7] the following items should be checked: the correctness of the choice of the measurement standards and auxiliary measuring instruments, the conditions for the calibration, the measurement model, the method of transferring the unit quantity and other factors affecting the accuracy of the measurement results.

Thus, the process of analyzing the estimation uncertainty is core point in validating a calibration procedure. Figure 1 illustrates a diagram that clearly shows the relationship of the measurement uncertainty evaluation process with all the elements of the calibration procedure and the requirements that determine the validation process.

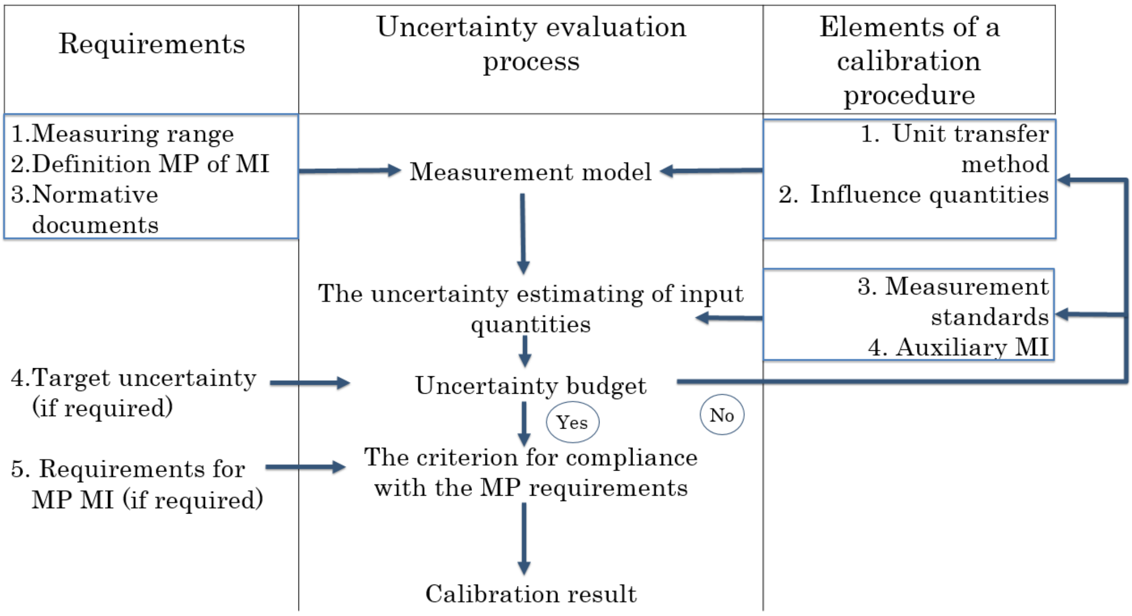

Figure 1 - Relationship between uncertainty evaluation process and validation process of calibration procedures

Research results

Experience shows that the process of validating calibration procedures can be reduced to typical situations. These situations can be identified (classified) through various combinations of the following elements, shown in Figure 2.

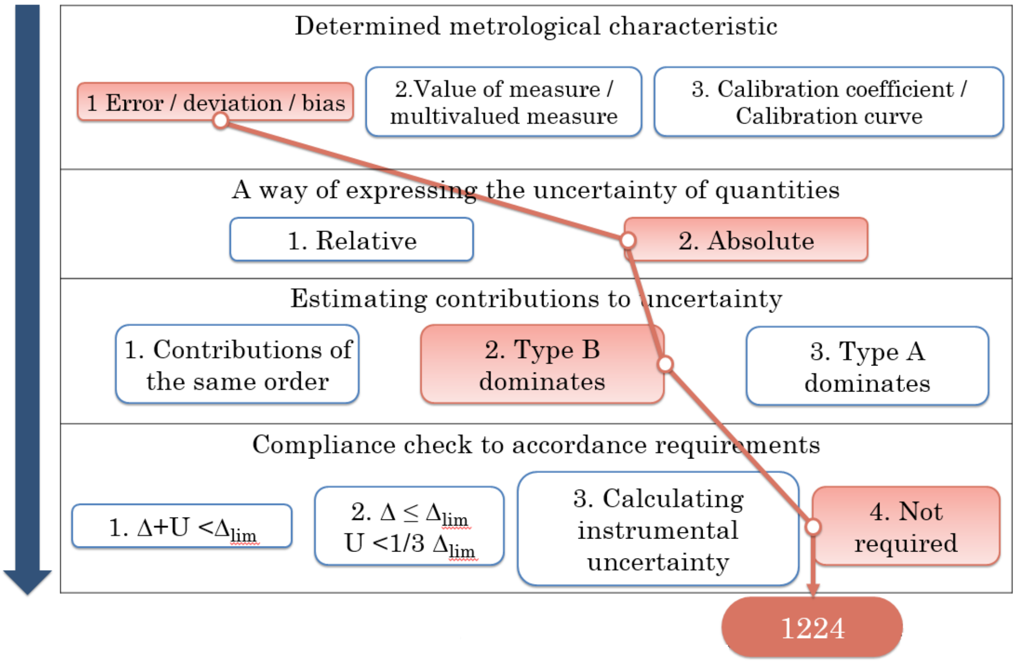

Figure 2 – Classification of algorithms for calibration procedure validation

Thus, we have many options when choosing a validation algorithm for a calibration procedure. Each algorithm can be specified through a sequence of numbers. For example, {1224}, which means the determination of the error {1} when calibrating a measuring instrument with the expression of the uncertainty of the measurement result in absolute units {2}, where the dominant contributions to the total uncertainty are those that were estimated by type B {2}, and checking of compliance with the established requirements was not required {4}.

On the basis of the described approach, the developed and validated at VNIIM in the period from 2015 to 2020 calibration procedures were analyzed. The experience shows that there are some more frequently used algorithms for validation. The results of such analysis are presenting in Figure 3, where the most common algorithms for validating calibration procedures (more than 7% of the total number of calibration procedures) are highlighted in red.

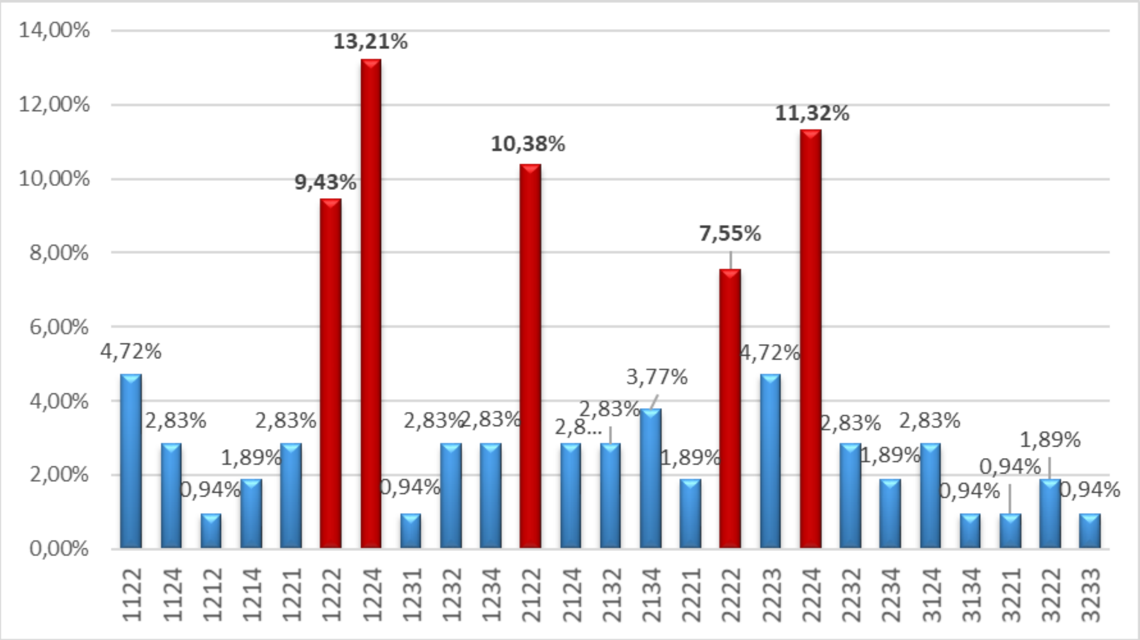

Figure 3 - Analysis of the used validation algorithms for calibration procedures

Conclusions

The paper proposes an approach to the validation of calibration procedures based on the processes of evaluating the measurement uncertainty during calibration and ensuring compliance with customer requirements. Descriptions of typical situations, which are illustrated based on the experience of validating calibrations at VNIIM, are given.

The results of the work are supposed to be used when updating the form of calibration procedure validation protocol used at the VNIIM.

In the opinion of the authors, it seems possible to initiate a COOMET project on the development of Recommendations for the validation of calibration procedures in case of interest of COOMET NMIs.

References:

1. CIPM MRA Mutual recognition of national measurement standards and of calibration and measurement certificates issued by national metrology institutes (CIPM MRA), 1999– 48p.
2. ISO/IEC 17025-2019. General requirements for the competence of testing and calibration laboratories, 2019– 36p;
3. Guide Eurachem. The Fitness for Purpose of Analytical Methods: A Laboratory Guide to Method Validation and Related Topics: Second edition, 2016–96 p;
4. International vocabulary of metrology – Basic and general concepts and associated terms (VIM), 3rd edition, 2008– 108p;
5. Guide to the Expression of Uncertainty in Measurement (GUM), 1999– 126p;
6. ISO/IEC Guide 98-1:2009. Uncertainty of measurement — Part 1: Introduction to the expression of uncertainty in measurement, 2009– 40p;
7. EA-4/02 M: 2013. Evaluation of the uncertainty of measurement in calibration, 2013– 75p;

Obtaining Uncertainty Estimates Compatible with Estimates of Monte Carlo Method using the example of weight calibration

Oleksandra Patsenko
National Scientific Centre "Institute of Metrology",
Kharkov, Ukraine
+38 093 579 35 50,
E-mail: sashapatsenko@ukr.net

Abstract

The paper describes obtaining uncertainty estimates of measurements taking into account the nonlinearity models using the example from item 9.3.1.1 of JCGM-S1 "Mass calibration", which describes the comparison in air of reference and calibrated weights having the same nominal mass. Uncertainty evaluation procedures based on the GUM uncertainty framework and the Monte Carlo method are compared in JCGM. The article uses the procedure developed by the authors and consists in decomposing the measurement model into a Taylor series of the second order taking into account the kurtosis of the distributions of input quantities. To find expanded uncertainty, the kurtosis method is used. Good agreement between the results obtained by the proposed method and the result obtained by the Monte Carlo method is shown.

Relevance of the work: consists in expanding the base of analytical methods for assessing measurement uncertainty, taking into account the nonlinearity of the model and the laws of distribution of input quantities, with obtaining a full budget of uncertainty.

Aim of work: Expansion and popularization of the theoretical foundations for assessing measurement uncertainty by the method of excesses.

The developed method allows to obtain unbiased estimates of the measured quantity and its uncertainty, to obtain a hollow uncertainty budget, taking into account the excesses of the distributions of the input quantities.

Objectives of the work: It is necessary to obtain estimates of the measurement uncertainty comparable with the estimates obtained by the Monte Carlo method using the example of the calibration of a weight.

Weight calibration is carried out by comparing its mass with a reference weight having the same mass using balance working in the air. Measurement uncertainty evaluating for this example is discussed in regulatory document JCGM-S1, 9.3.1.1. [1]. In [1], the measurement uncertainty evaluation using the methods of GUM [2] and Monte Carlo [3] is performed. At this, a significant bias in the measurement uncertainty evaluation obtained using GUM is discovered.

The final model for deviation δm of conventional mass of calibrated weight from its nominal value takes the form [1]:

$$\delta m = (m_{R,c} + \delta m_{R,c})\frac{(1-\rho_a/\rho_R)(1-\rho_{a0}/\rho_W)}{(1-\rho_{a0}/\rho_R)(1-\rho_a/\rho_W)} - m_{nom} \tag{1}$$

where $m_{R,c}$ - actual mass of the reference weight, 100 g;

δm_R - actual mass of small weight, added to equalize balance, 1,234 mg;

ρ_a, ρ_{a0} – air mass density, 1,2 kg/m^3;

ρ_W - mass density of calibrated weight, 8000 kg/m^3;

ρ_R - mass density of reference weight, 8000 kg/m^3;
m_{nom}- nominal value, 100 g.

Calculated value for deviation δm of conventional mass of calibrated weight from its nominal value is 1,234 mg.

Formula (1) gives an unbiased estimate of the numerical value of the measurand only in the absence of uncertainties of input quantities.

For equation (1) the calculation of the bias for δm is performed by the formula:

$$\Delta_c = -\frac{1}{2}[c(m_{R,c})_2 u^2(m_{R,c}) + c(\delta m_{R,c})_2 u^2(\delta m_{R,c}) + c(\rho_a)_2 u^2(\rho_a) + c(\rho_R)_2 u^2(\rho_R) + c(\rho_W)_2 u^2(\rho_W)]$$

where $c(x_i)_2$ – partial derivative of the second order of the measured quantity with respect to the corresponding input quantity.

To make it easier to calculate the bias $\acute{\Delta}_c$ is convenient to use the method of partial increments [4].

The expressions for $c(x_i)_2$ are given in Table 1. [7]. All of their values are zero.

Since the second-order partial derivatives of the measurand with respect to all input quantities turned out to be equal to zero, the bias of the measurand numerical value will also be zero.

In the first approximation, the calculation of the standard uncertainty of the measurand is carried out based on the equation:

$$u(\delta m) = \sqrt{c^2(m_{R,c})u^2(m_{R,c}) + c^2(\delta m_{R,c})u^2(\delta m_{R,c}) + c^2(\rho_a)u^2(\rho_a) + c^2(\rho_R)u^2(\rho_R) + c^2(\rho_W)u^2(\rho_W)} \qquad (2)$$

where $u(x_i)$ and $c(x_i)$ – the standard uncertainty of the input quantity x_i and the partial derivative of the measurand with respect to this input quantity (sensitivity coefficient), respectively.

Expressions for $c(x_i)$ and their values are given in Table 2. [7].

For the above evaluations of input quantities, as well as for the standard uncertainty of the input quantities specified in [1]: $u(m_{R,c})$ = 0,05 mg; $u(\delta m_{R,c})$ = 0,02 mg; $u(\rho_a)$ = 0,05774 kg/m^3; $u(\rho_W)$ = 577,35 kg/m^3; $u(\rho_R)$ =28,87 kg/m^3, $u(\delta m)$ = 0,05385 mg.

Formula (2) provides an unbiased estimate of the standard uncertainty of the measurand only in the absence of uncertainties of the input quantities.

The calculation of the bias for $u(\delta m)$ is made by the formula [5]:

$$\Delta[u^2(\delta m)] = \frac{1}{4}\{[c(\rho_a)_2 u^2(\rho_a)]^2[\eta(\rho_a)+2] + [c(\rho_R)_2 u^2(\rho_R)]^2[\eta(\rho_R)+2] + [c(\rho_W)_2 u^2(\rho_W)]^2[\eta(\rho_W)+2]\} +$$
$$+\{[c(\delta m_{R,c},\rho_R)u(m_{R,c})u(\rho_R)]^2 + [c(m_{R,c},\rho_a)u(m_{R,c})u(\rho_a)]^2 + [c(m_{R,c},\rho_W)u(m_{R,c})u(\rho_W)]^2 +$$
$$+\{[c(\delta m_{R,c},\rho_R)u(\delta m_{R,c})u(\rho_R)]^2 + [c(\delta m_{R,c},\rho_a)u(\delta m_{R,c})u(\rho_a)]^2 + [c(\delta m_{R,c},\rho_W)u(\delta m_{R,c})u(\rho_W)]^2 +$$
$$+\{[c(\rho_a,\rho_R)u(\rho_a)u(\rho_R)]^2 + [c(\rho_a,\rho_W)u(\rho_a)u(\rho_W)]^2 + [c(\rho_R,\rho_W)u(\rho_R)u(\rho_W)]^2, \qquad (3)$$

where $c(x_i,x_j)$ – second-order mixed partial derivatives of the measurand with respect to the corresponding input quantities; $\eta(x_i)$ – kurtosis of input quantities.

Expressions for $c(x_i,x_j)$ and their values are given in Table 4 [7].

To facilitate the calculation of mixed partial derivatives, it is convenient to use the method of partial increments.

For the above input quantities estimates and their standard uncertainties, as well as for kurtosis corresponding to the distribution laws of input quantities $\eta(m_{R,c}) = \eta(\delta m_{R,c})$=0; $\eta(\rho_a) = \eta(\rho_R) = \eta(\rho_W)$=-1,2, we obtain $\Delta(u^2)$=0,00272 mg^2.

The unbiased estimate of the combined standard uncertainty calculated by the formula:

$$u_0(\delta m) = \sqrt{u^2(\delta m) + \Delta(u^2)}\,. \tag{4}$$

For the above values $u(\delta m)$ and $\Delta(u^2)$, we obtain $u_0(\delta m)$=0,075 mg, which is very close to the value calculated in [1] by the Monte Carlo method (0.0754 mg).

Since there is no bias of the measurand, this indicates that the nonlinearity of the model does not introduce additional asymmetry into the distribution law of the measurand, therefore, to calculate the expanded uncertainty, we can use the kurtosis method proposed by the authors [6].

In this case, the kurtosis of the measurand is calculated by the formula:

$$\eta(\delta m) = \frac{1}{u^4(\delta m)}[\eta(m_{R,c})c^4(m_{R,c})u^4(m_{R,c}) + \eta(\delta m_{R,c})c^4(\delta m_{R,c})u^4(\delta m_{R,c}) +$$

$$+\eta(\rho_a)c^4(\rho_a)u^4(\rho_a) + \eta(\rho_W)c^4(\rho_W)u^4(\rho_W) + \eta(\rho_R)c^4(\rho_R)u^4(\rho_R)\,. \tag{5}$$

For the above estimates of input quantities, standard uncertainties, and their kurtosis we have $\eta(\delta m)$=0.

The value of the coverage factor for the probability of 0.95 is calculated by the formula [6]:

$$k_{0,95} = \begin{cases} 0{,}1085\eta^3 + 0{,}1\eta + 1{,}96, \text{ при } \eta < 0; \\ 1{,}96, \text{ при } \eta \geq 0. \end{cases} \tag{6}$$

Since $\eta(\delta m) = 0$, we take $k_{0,95} = 1{,}96$. In this case $U(\delta m)$=0,147 mg, which is very close to the value obtained in [1] by the Monte Carlo method (0,148 mg).

The results are summarized in the uncertainty budget (Table 1).

Table 1 – Measurement uncertainty budget for weight calibration

X_i	x_i	$u(x_i)$	$\eta(x_i)$	c_i	$u_i(y)$, mg	$\Delta_i(y)$, mg	$\Delta[u_i(y)]$, mg
$m_{R,c}$	100 000 mg	0,05 mg	0	1	0,05	0	0
$\delta m_{R,c}$	1,234 mg	0,02 mg	0	1	0,02	0	0
ρ_a	1,2 kg/m^3	0,05774 kg/m^3	-1,2	0	0	0	0
ρ_R	8000 kg/m^3	577,4 kg/m^3	-1,2	0	0	0	-0,0521
ρ_W	8000 kg/m^3	28,87 kg/m^3	-1,2	0	0	0	0,0026
Y	y_0	$u_0(y)$	$\eta(y)$	$k_{0.95}$	$U(y)$	Δ_y, mg	$\Delta[u(y)]$
δm	1,234 mg	0,077 mg	0	1,96	0,15, mg	0	0,0522, mg

In contrast to the usual uncertainty budget for the kurtosis method [6], two columns are added to Table 1 that take into account the nonlinearity of the measurement model.

In the penultimate column of the budget $\Delta_i(y)$ – bias of the measurand caused by each i-th input quantity; $\Delta_y = \sum_{i=1}^{N} \Delta_i(y)$ – combined bias of the measurand. In the last column of the budget

$\Delta[u_i(y)]$ – bias of the standard uncertainty of the measurand caused by the i-th input quantity and the combined bias $\Delta[u(y)] = \sqrt{\Delta[u^2(y)]}$, which is calculated by the formula:

$$\Delta[u(y)] = \sqrt{\sum_{i=1}^{N} \{\Delta[u_i(y)]\}^2} \cdot \qquad (7)$$

The presence of additional columns makes it possible to obtain an unbiased estimate of the measurand and its uncertainty in the nonlinear model equation.

Table 2 shows the analysis of the compared methods.

Table 2 – Comparison of results obtained by GUM, Monte-Carlo Method [1] and Excess Method [7[

	GUM	Monte-Carlo method	Excess Method
Standard uncertainty	0.053	0,0754 mg	0,0750 mg
Expanded uncertainty	0,106	0,148	0,147

Conclusion

1. In the example of estimating the measurement uncertainty when calibrating a weight, taking into account the second-order partial derivatives of the measured quantity with respect to the corresponding input it is possible to estimate the displacement of the numerical value of the measured quantity due to the nonlinearity of the model.

2. It is shown that the nonlinearity of the measurement model in the example under consideration leads to a bias in the estimate of the standard uncertainty of the measured quantity, which can be eliminated by calculating the second-order mixed partial derivatives of the measured quantity from the corresponding input quantities, taking into account the excesses of their distributions.

3. Application of the method of excesses made it possible to evaluate the expanded uncertainty of the deviation of the conventional mass of the calibrated weight from its nominal value, taking into account the distribution laws of the input quantities.

4. The validation of the developed methodology using the Monte Carlo procedure has shown its suitability for the intended use. In contrast to the Monte Carlo method, the considered technique allows to draw up a measurement uncertainty budget, which is a necessary element of the measurement uncertainty estimation procedure.

References:

1. JCGM 101:2008 Evaluation of measurement data − Supplement 1 to the “Guide to the expression of uncertainty in measurement” − Propagation of distributions using a Monte Carlo method.

2. JCGM 100:2008 Evaluation of measurement data − Guide to the expression of uncertainty in measurement.

3. Zakharov I.P., Vodotyka S.V. Application of Monte Carlo simulation for the evaluation of measurements uncertainty // Metrology and Measurement Systems, 2008, Vol. XV, № 1. – pp. 118-123.

4. Zakharov, I., Neyezhmakov, P., Botsiura, O. (2018) Reduction of the measurand estimate bias for nonlinear model equation. Journal of Physics: Conf. Series 1065, 212002.

5. Zakharov I., Neyezhmakov P., Botsiura O. Reduction of the bias of measurement uncertainty estimates with significant non-linearity of a model equation // Conf. Series 1379 (2019).

6. Zakharov, I.P., Botsyura, O.A. Calculation of Expanded Uncertainty in Measurements Using the Kurtosis Method when Implementing a Bayesian Approach // Measurement Techniques, 2019, Volume: 62, Issue: 4, pp. 327-331.

7. Zakharov I., Botsiura O., Patsenko O.. Accounting for the kurtosis of input quantities in the procedure of evaluating measurement uncertainty using the example of weight calibration. Ukrainian Metrological Journal, 2020, № 3, pp. 36 – 41. DOI: 10.24027/2306-7039.3.2020.216839.

Coupling ionics with electronics for a new resistance standard based on memristive devices

Gianluca Milano
Advanced Materials Metrology and Life Science Division, Italian National Institute of Metrological Research (INRiM), Strada delle Cacce 91, Torino 10135, Italy
E-mail: g.milano@inrim.it,
Telephone: +39 +011 3919344

Abstract

With the revision of the International System of Units (SI) in 2019, where units were defined in terms of fundamental physical constants, memristive devices coupling ionics with electronics represent promising platforms for the realization of a quantum-based standard of resistance working at room temperature, in air and without applying a magnetic field, differently from conventional resistance standards based on the Quantum-Hall effect. By coupling ionics with electronics, the conductance levels of these devices can be electrically controlled and programmed to be quantized in multiples in the fundamental quantum of conductance $G_0 = 2e^2/h$. Since both the elementary charge and the Planck constant are fixed in the revised SI, the quantized conductance levels of memristive devices can be exploited for the practical realization of a quantum-based standard of resistance. These devices, that can be miniaturized down to the nanometer scale and are CMOS compatible, represent promising candidates for the realization of a resistance standard for next-generation self-calibrating electrical systems with zero-chain traceability, in the spirit of the revised SI.

The ratification of the revised International System of Units (SI) in 2019 represents an historic revolution for metrology [1], since the seven base SI units (second, meter, kilogram, ampere, kelvin, mole, and candela) were defined in terms of seven fundamental constants of Nature (the hyperfine transition frequency of the cesium 133 atom, the speed of light in vacuum, the Planck constant, the elementary charge, the Boltzmann constant, the Avogadro constant, and the luminous efficacy of a defined visible radiation). Since these seven constants were assigned to fixed values without uncertainty, these constants have not to be measured anymore. It follows that each experiment that is able to correlate a measurable quantity to a fundamental constant of nature or a combination of fundamental constants is a direct realization of the corresponding SI units. This means that the revised SI lays the foundations for the development of new experiments where the uncertainties associated to units are related on the specific scientific/technical purpose.

Quantum effects such as the quantum Hall effect (QHE), the single electron transistor effect and the Josephson effect are conventionally exploited for the practical realization of electrical units. However, the working principles of these effects require cryogenic temperatures, vacuum conditions, and/or high magnetic fields. This would require a laboratory environment, hindering on-chip implementation of these devices as required in self-calibrating systems that can independently refer to the fundamental constants of nature with zero-chain traceability. As a promising alternative, it has been demonstrated that memristive devices can exhibit reproducible quantized conductance states multiples of the fundamental quantum of conductance at room temperature, in air and without applying a magnetic field [2]. Importantly, parasitic electrical parameters and operating/quiescent currents have the potential to be optimized by a proper device design and through a rational choice of involved materials.

Memristors (i.e. resistors with memory) are two-terminal devices where the internal state of resistance depends on the history of applied voltage and current [3]. The working principle is related to the so-called resistive switching mechanism that imply a reconfiguration of atomic configuration and nanoionic processes occurring in a metal-insulator-metal structure at the nanoscale [4]. An applied voltage to an electrochemically active electrode (such as Ag or Cu) lead to redox reactions with dissolution of metal atoms to form metal ions that subsequently migrates in the insulating layer driven by the action of the applied electric field. The electrocrystallization of these ions is responsible for the formation of a metallic conductive pathway termed “filament” that bridges the two electrodes. The formation of this conductive filament turns the internal state of the device from an initial high resistance state to a lower resistance state. This process is reversible, meaning that an applied voltage in the opposite direction is responsible for retraction of metal atoms causing the formation of a gap in the filament and turning the device state again to an high resistance state. A schematization of this process is depicted in Figure 1a, where the hysteretic loop in the *I-V* plane represents the typical fingerprint of a memristive device. Due the aforementioned characteristics together with the high scalability, fast switching speed and possibility to program the internal state of resistance in an analogue fashion, these devices have been proposed for the realization of memory devices and for next-generation in-memory and neuromorphic computing architectures for overcoming the Von-Neumann computing bottleneck [5]–[7].

If the size of the conductive filaments is shrinked down to the atomic scale, ballistic electron transport through a constriction occurs in the so-called atomic-point contact (Figure 1b). In this conduction regime, the device exhibits quantized conductance levels. Indeed, when the filament size is in the order of the phase coherence length of electrons, the conductive pathway behaves as an electron waveguides where ballistic transport occurs through discrete conduction channels. Each of these channels contributes to the total device conductivity with a maximum of one fundamental quantum of conductance $G_0 = 2e^2/h$.

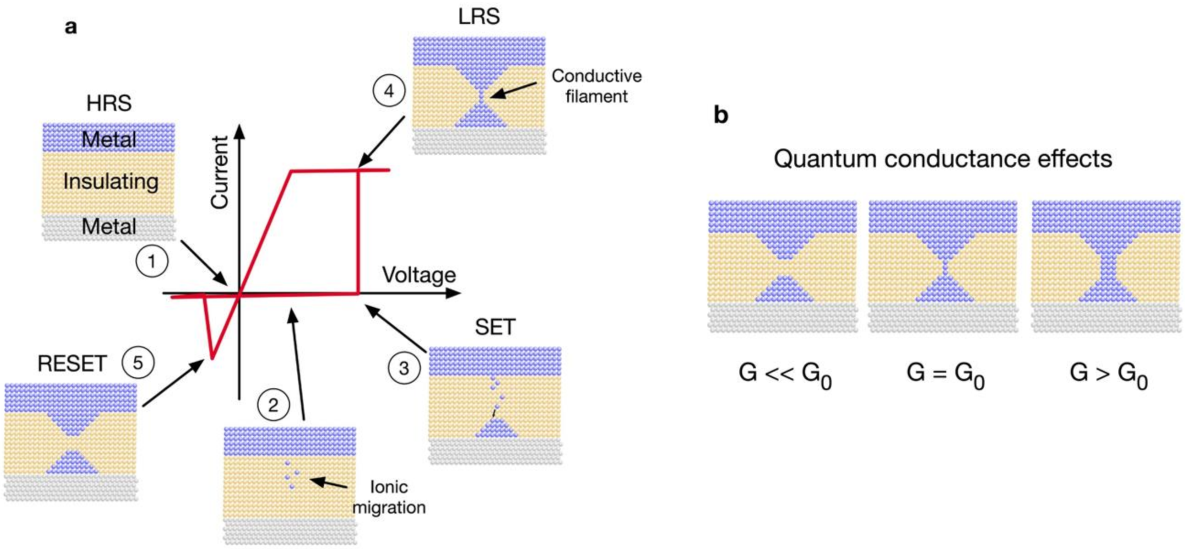

Figure 1. Resistive switching phenomena in memristive devices and quantum conductance effects. a) Working principle of a memristive device that rely on the formation/rupture of a conductive pathway upon external electrical stimulation. b) Quantized conductance phenomena can be observed when the filament size is scaled down to the atomic scale forming a quantum point contact.

After the seminal works of Terabe et al. that observed quantized conductance values in memristive devices based on silver-sulfide [8], evidences of quantized conductance phenomena were reported in a wide range of memristive cells [9]. In this framework, the key aspect is that the observation of quantized phenomena relies on the accurate control of the filament size and morphology at the atomic level by means of an appropriate external electrical device stimulation. Quantized effects can be observed by applying a voltage sweep that induces dissolution and electromigration of ions with consequent rearrangement of the atomic configuration of the atomic-sized conductive filament as reported in ref. [9]. Also, quantized conductance levels can be observed by properly controlling the kinetic of filament formation or dissolution by applying a positive voltage bias [10]. Moreover, quantized conductance levels of the cells can be programmed by means of voltage pulses as reported in ref. [10], where the device can be programmed into discrete multiples of G_0 depending on the voltage pulse amplitude and polarity. Note also that memristive device programming with pulses down to the ns scale have been demonstrated [11], thus paving the way for the realization of an high-speed programmable standard of resistance.

It is important to remark that, due to the presence of parasitic resistances, the state-of-art of memristive devices cannot compete with the precise quantization effects reported in resistance standards based on quantum Hall effect where a relative uncertainty of few parts in 10^8 can be achieved [12]. However, the main advantage of memristive devices is that the quantization effects can be observed in much more relaxed experimental conditions since these devices can work not only in air but also in harsh environment, in a wide range of temperatures (4–600 K) and without applying an external magnetic field [2]. In addition, it should be remarked that by coupling a memristive resistance standard with a voltage standard (for example based on the Josephson effect) represent a viable strategy for the practical realization of a current standard as indicated by the Bureau International des Poids et Mesures [13]

To summarize, here we discuss the use of memristive devices as a viable solution for the practical realization of a standard of resistance based on quantized conductance effects phenomena. These devices, where the internal resistance state can be programmed depending on the external electrical stimulation, can exhibit quantized conductance levels multiples of G_0 without applying a magnetic field, in different ambient conditions and in a wide range of temperatures. For this reason, together with high scalability down to the nanometer scale and CMOS compatibility, these devices are particularly promising for the realization of a resistance standard implementable on-chip for nano electronics as well as for space applications, high-end electronics and for the realization of embedded self-calibrating electrical systems with traceability to the fundamental physical quantities, in the spirit of the revised SI.

References:

[1] E. Göbel and U. Siegner, *The New International System of Units (SI)*. Wiley, 2019.

[2] G. Milano, F. Ferrarese Lupi, M. Fretto, C. Ricciardi, N. De Leo, and L. Boarino, “Memristive Devices for Quantum Metrology,” *Adv. Quantum Technol.*, vol. 3, no. 5, p. 2000009, May 2020.

[3] D. B. Strukov, G. S. Snider, D. R. Stewart, and R. S. Williams, “The missing memristor found,” *Nature*, vol. 453, no. 7191, pp. 80–83, May 2008.

[4] Z. Wang *et al.*, “Resistive switching materials for information processing,” *Nat. Rev. Mater.*, vol. 5, no. 3, pp. 173–195, Mar. 2020.

[5] J. Tang *et al.*, “Bridging Biological and Artificial Neural Networks with Emerging Neuromorphic Devices: Fundamentals, Progress, and Challenges,” *Adv. Mater.*, vol. 31, no. 49, p. 1902761, Dec. 2019.

[6] N. K. Upadhyay, H. Jiang, Z. Wang, S. Asapu, Q. Xia, and J. Joshua Yang, “Emerging Memory Devices for Neuromorphic Computing,” *Adv. Mater. Technol.*, vol. 4, no. 4, p. 1800589, Apr. 2019.

[7] G. Milano *et al.*, “Self-limited single nanowire systems combining all-in-one memristive and neuromorphic functionalities,” *Nat. Commun.*, vol. 9, no. 1, p. 5151, Dec. 2018.

[8] K. Terabe, T. Hasegawa, T. Nakayama, and M. Aono, “Quantized conductance atomic switch,” *Nature*, vol. 433, no. 7021, pp. 47–50, Jan. 2005.

[9] Y. Li *et al.*, “Conductance Quantization in Resistive Random Access Memory,” *Nanoscale Res. Lett.*, vol. 10, no. 1, p. 420, Dec. 2015.

[10] T. Tsuruoka, T. Hasegawa, K. Terabe, and M. Aono, “Conductance quantization and synaptic behavior in a Ta 2 O 5 -based atomic switch,” *Nanotechnology*, vol. 23, no. 43, p. 435705, Nov. 2012.

[11] L. Jiang *et al.*, “Conductance quantization in an AgInSbTe-based memristor at nanosecond scale,” *Appl. Phys. Lett.*, vol. 109, no. 15, p. 153506, Oct. 2016.

[12] N.-H. Kaneko, “Review of quantum electrical standards and benefits and effects of the implementation of the ‘revised SI,’” *IEEJ Trans. Electr. Electron. Eng.*, vol. 12, no. 5, pp. 627–637, Sep. 2017.

[13] BIPM Bureau International des Poids et Mesures, “The international System of Units (SI Brochure) [9th edition],” 2019.

Ensuring the traceability of measurements of nanoparticle diameters by atomic force microscopy based on the nanomeasuring machine (NMM)

Bagdun A.A.
Republican Unitary Enterprise "Belarusian State Institute of Metrology"
93 Starovilensky trakt, 220053, Minsk, phone +375 17 379 35 82,
e-mail: bagdun@belgim.by

Abstract

It is accepted worldwide to use electron microscopes as a measuring instrument of the highest accuracy for measuring nanoparticle diameters and ensuring traceability. In particular, NIST uses the electron microscope to ensure traceability, to which most of the produced standard samples of nanoparticle diameters are traceable. However, the operation of an electron microscope requires large financial expenses, and the preparation of a sample takes much effort and time.

The paper proposes and describes the possibility of using a nanomeasuring machine (NMM) with an atomic force microscope as a measuring instrument of the highest accuracy, for measuring nanoparticle diameters and ensuring traceability to international standards of the unit of length, while maintaining the previously achieved metrological characteristics. The proposed method makes it possible to carry out measurements in the lateral plane, to provide a quantitative assessment of the results on the samples of particles of a sufficiently large size and to reduce the time for sample preparation.

The paper presents a method for generating and collecting nanoparticles on a substrate for subsequent measurements. A measurement method is also proposed and described to ensure the traceability of nanoparticle measurements. The budget of the uncertainty of measurements of nanoparticles was calculated using an atomic force microscope based on the nanomeasuring machine (NMM) in the vertical and lateral planes.

Main provisions for ensuring the traceability of nanoparticle measurements by microscopy

The size of nanoparticles is a basic parameter that affects the physicochemical properties of the final nanotechnology product. In this regard, it is important to quickly and accurately control the dimensional parameters of nanoparticles, which is impossible without ensuring the metrological traceability of measurements of nanoparticle sizes. Due to the fact that nanoparticles have various shapes, from a sphere to a polygonal element (Figure 1), a model in the form of a sphere was adopted to analyze them and to determine the size characteristics, and for its dimensional analysis the concept of an equivalent diameter of a spherical object - an object with the same physical properties as the measured particle [1] -was introduced.

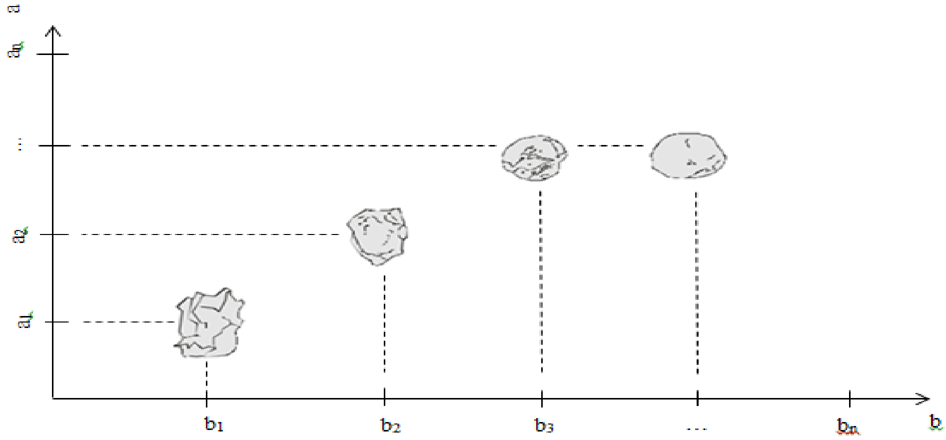

$a_1, a_2, \ldots, a_n$ – sphericity
$b_1, b_2, \ldots, b_n$ – roundness

Figure 1 - Examples of nanoparticle shapes

Also, given that the sizes of nanoparticles are random quantities, it is customary to display information about them in the form of a distribution. By the distribution of particles we shall mean the distribution of the number of particles depending on their sizes [2].

Thus, to ensure the metrological traceability of nanoparticle size measurements to the SI units, it is necessary to use spherical standard samples with normal particle size distribution (for example, PSL polyurethane latex nanoparticles).

Before particles can be measured with a microscope, they should be dispersed and collected on a substrate. Aerosol generators are used to disperse particles. The principle of their operation is that compressed air is supplied to a solution of particles in a liquid, which results in the generation of aerosols. However, it is impractical to use conventional aerosol generators for nanoparticles due to the fact that besides particles aerosols contain multiple drops from the solution and a surfactant, so the aerosol is nonhomogeneous.

The Electrospray aerosol generator is suitable for resolving this task. Electrospray is a method used in mass spectrometry to obtain ions in the gas phase from a solution.

Then the disperse aerosol of nanoparticles should be turned into a monodisperse one. For this purpose we propose to use an electrostatic classifier together with a nanoparticle differential mobility analyzer. It allows generating a stream of monodisperse aerosol with particles of known size from the incoming polydisperse aerosol.

The next step is to collect the dispersed nanoparticles for their subsequent measurement with a microscope. A nanometric aerosol sampler, typically used for sampling of the aerosol, which was well conditioned and positively charged, is suitable for this purpose. When particles are collected, their measurement with a microscope can start.

All the above information can be presented in the form of a block diagram given in Figure 2.

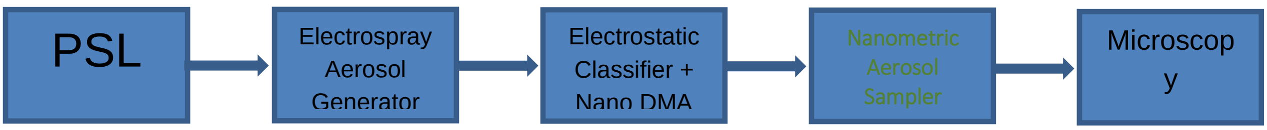

Figure 2 - Block diagram of dispersion and collection of nanoparticles for measurements using microscopy

Measurement of nanoparticles by atomic force microscopy based on the nano-measuring machine (NMM)

We are planning to carry out measurements of nanoparticles using a nanomeasuring machine (NMM) with an atomic force microscope (hereinafter referred to as AFM) as a sensor. This configuration of the equipment will allow exploring several options for nanoparticle measurements.

The first task to be resolved is to choose the density of particles deposited on the substrate, which is suitable for accurate measurements, i.e. optimal concentration of particles per unit area. Since the information about the particles is displayed as a distribution, it is necessary to collect a sufficient array of data on the size of nanoparticles.

We assume that due to the interaction of particles, processes can occur affecting the accuracy of particle measurements. The most obvious problem is the agglomeration and deposition of particles in several layers. Consequently, it is better to deposit particles with a low deposition density. The use of a deposition electrode in a 9.5 mm nanometer sampler allows obtaining a sufficient array of data on the particle size at a low deposition density and excluding agglomerates from measurements. The use of NMM makes it possible to increase the AFM measurement range in the lateral plane up to 25 mm, which enables the analysis of the entire area of deposition of nanoparticles.

The use of NMM with AFM makes it possible to implement two methods of nanoparticles size measurement: measurement in the vertical and lateral planes.

When measuring particles in the vertical plane, the distance between the tip of a single particle and the substrate is measured. There is an additional source of methodological error that affects the measurement accuracy in this method of measurement: the roughness of the substrate. Accordingly, the result of the nanoparticles size measurement can be represented as follows:

$$\mathrm{Y} = \mathrm{X}_{\text{и}} + \delta_{\mathrm{p}} + \delta_{\text{м}} + \delta_{\text{ш}} + \delta_{\mathrm{R}} \qquad (1)$$

where Y is the results of measurements of nanoparticles, nm;
$X_{\text{и}}$is the arithmetic mean of AFM readings, nm;
δ_{p} is the correction for the NMM resolution, nm;
$\delta_{\text{м}}$ is the correction for the standard gauge, nm;
$\delta_{\text{ш}}$ is the correction for the AFM noise level, nm;
δ_{R} if the correction for the substrate roughness, nm.

The characteristics of the input quantities are given in Table 1. The calculation of the measurement uncertainty budget is given in Table 2.

Table 1

Input quantity	Characteristic of the input quantity
δ_{p}- correction for the NMM resolution, nm	Type of uncertainty evaluation - B Type of distribution - rectangular Evaluation value 0 The interval ±a_p, within which the value of the input quantity lies, is determined by the NMM resolution. D =0,1 nm, a_p =0,5D = 0,05 nm Standard uncertainty u(δ_{p})= a_p / 3 = 0,03 nm
$\delta_{\text{м}}$- correction for the standard gauge, nm	Type of uncertainty - B Type of distribution - normal Evaluation value: 0 nm Standard uncertainty $u(\delta_{\text{м}}) = \frac{U_{\text{м}}}{k}$, where $U_{\text{м}}$ is the expanded uncertainty (k = 2, p = 95%) The expanded measurement uncertainty $U_{\text{м}}$, nm, is given in the gauge calibration certificate

	$U_м$ = 0,013 nm $u(\delta_м)= \frac{0,013}{2}$ = 0,0065 nm
$\delta_ш$- correction for the AFM noise level, nm	Type of uncertainty evaluation - B Type of distribution - rectangular Evaluation value 0 The interval, within which the value of the input quantity lies, is $\pm a_ш$ = 0,08nm Standard uncertainty $u(\delta_ш) = a_ш / \sqrt{3}$ = 0,05 nm
δ_R- correction for the substrate roughness, nm	Type of uncertainty evaluation - B Type of distribution - rectangular Evaluation value 0 The interval, within which the value of the input quantity lies, is $\pm a_R$ = 0,4 nm [3] Standard uncertainty $u(\delta_R) = a_R / \sqrt{3}$ = 0,23 nm

Table 2

Input quantity	Value x_i, nm	± r, nm	Type of uncertainty	Probability distribution	$u(x_i)$, nm	Sensitivity factor C_i	Uncertainty contribution $u_i(y)$	Interest contribution, %
δ_p	-	0,5	B	Rectangular	0,03	1	0,03	1,60
$\delta_ш$	-	0,08	B	Rectangular	0,05	1	0,05	0,09
$\delta_м$	-	0,013	B	Normal	0,007	1	0,007	4,44
δ_R	-	0,4	B	Rectangular	0,23	1	0,23	93,88
Y	**-**				**0,24**			

Expanded uncertainty $U = k \cdot u_c(y) = 2 \cdot 0{,}24 = 0{,}48$ nm

When measuring nanoparticles in the lateral plane, the distance between two parallel straight lines, which are tangent lines to two opposite edges of the particle, is measured. If measurements are carried out only using AFM, then this method eliminates the impact of the substrate roughness and the noise level of the probe on the measurement result, but the nonlinearity error of the AFM scanner appears. However, due to the fact that measurements are carried out using the AFM installed on the NMM, this error does not affect the measurements, since the movement of the AFM probe in the lateral plane is performed by the NMM. So the result of measurement of nanoparticles can be represented as follows:

$$Y = X_и + \delta_p \,, \tag{2}$$

где Y is the results of measurements of nanoparticles, nm;
$X_и$ is the arithmetic mean of AFM readings, nm;
δ_p- is the correction for the NMM resolution, nm.

The characteristics of the input quantities are given in Table 3. The calculation of the measurement uncertainty budget is given in Table 4.

Table 3

Input quantity	Characteristic of the input quantity
δ_p- correction for the NMM resolution, nm	Type of uncertainty evaluation - B Type of distribution - rectangular Evaluation value 0 The interval $\pm a_p$, within which the value of the input quantity

	lies, is determined by the NMM resolution. D =0,1 nm, a_p =0,5D = 0,05 nm Standard uncertainty u(δ_p)= a_p / 3 = 0,03 nm
δ_M- correction for the standard gauge, nm	Type of uncertainty - B Type of distribution - normal Evaluation value: 0 nm Standard uncertainty $u(\delta_M) = \frac{U_M}{k}$, where U_M is the expanded uncertainty (k = 2, p = 95%) The expanded measurement uncertainty U_M, nm, is given in the gauge calibration certificate U_M = 0,013 nm $u(\delta_M)= \frac{0,013}{2}$ = 0,0065 nm

Table 4

Input quantity	Value x_i, nm	± r, nm	Type of uncertainty	Probability distribution	u(x_i), nm	Sensitivity factor C_i	Uncertainty contribution $u_i(y)$	Interest contribution, %
δ_p	-	0,5	B	Rectangular	0,03	1	0,03	94,84
δ_M	-	0,013	B	Normal	0,007	1	0,007	5,16
Y	**-**				**0,03**			

Expanded uncertainty U=k·u_c(y) = 2·0,03 = 0,06 nm

These calculations are not final and they do not take into account the effect of repeatability of NMM measurements, however, they lead to the conclusion that the nanoparticle size measurement in the lateral plane will have a lower uncertainty value than the measurement in the vertical plane, and the use of an AFM, installed on a NMM, eliminates the impact of the nonlinearity error of the AFM scanner on the measurement results. Hence, due to the fact that the resolution of the NMM is comparable with electron microscopes, it can be concluded that the use of a nanomeasuring machine (NMM) with an AFM as a measuring instrument of the highest accuracy for measuring the diameters of nanoparticles and ensuring the traceability of measurements to international standards of the length unit, realizing the determination of the unit of length-meter by means of three stabilized HE-NE lasers installed on the X coordinate axes; Y; Z, allows achievement of the accuracy no worse than when using electron microscopes, while performing measurements in the lateral plane, providing a sufficiently large sample of particles and not spending a lot of time on the preparation of the sample.

The result of this work is the creation of a basis for the production of standard samples of the micro- and nanoparticles size and their certification in the territory of the Republic of Belarus, the accuracy of which corresponds to the requirements of any standards used in the field of particle size measurements.

References:

1 Particle characterization of particle systems. Vocabulary: ISO 26824: 2013; introduced 07/15/2013 - ISO / TC 24 / SC 4 Particle characterization other than sieving, 2013 - Clause 1.6

2 CLEANROOMS AND ASSOCIATED CONTROLLED ENVIRONMENTS. Part 1. Classification of air cleanliness: GOST ISO 14644-1-2002; introduced 04/01/2004 - Moscow: Gosstandart of Russia, 2004. - Clause 2.2

3 Ivenin, S.V. Monocrystalline silicon carbide wafers processing / S.V. Ivenin //Mordovia University Bulletin. - 2015. - Vol. 25, No. 4. - P. 37–50.

Calibration uncertainty and thermal influences of the Coordinate Measuring Machines

Mussatayev Meirbek[1),2),3)], Huang Meifa[3),*], Marat Nurtas[4)], Azamat Arynov[5)]

1) EPSRC Centre for Doctoral Training in Future Innovation in NDE (FIND-CDT) Faculty of Engineering, University of Bristol, UK, meirbek.mussatayev@bristol.ac.uk +447747074821.
2) Guilin University of Electronic Technology, School of Mechanical & Electrical Engineering, 1 Jinji Rd, Guilin, Guangxi, 541004, China.
3) RA Metrology Verification Lead of the Future Growth Project (FGP) of "Tengizchevroil", Kazakhstan.
4) International Information Technology University, Department of Mathematical and Computer Modelling, Kazakhstan.
5) School of Engineering at Warwick University, UK.

Abstract

Tight tolerances and accurate dimensions have become the reality of precision engineering, especially when parts are assembled into mechanical system dimensions for which the reliability of functions has to be proven by measurements. This paper presents the uncertainty analysis in commercial coordinate measuring machine (CMM)-based Coordinate Metrology. Due to the operation of a CMM and the fluctuations in an operating environment, temperature changes can occur for the workpiece and measurement system, introducing significant errors into the measurement and lowering the accuracy and precision. Uncertainty, as an integral part of every calibration and verification process, should be taken into consideration. The conventional GUM-method cannot be applied to CMM measurements primarily because of the lack of an analytical relationship between the input quantities and the measurement. However, only a few assessment techniques are available to integrate this knowledge. This paper presents the improved calibration uncertainty assessment technique for CMM based Coordinate Metrology. Our findings have highlighted some practical issues related to the importance of maintaining thermal equilibrium before the measurement. The authors concluded that the thermal influence as an uncertainty contributor of CMM calibration process has a significant influence for this example.

Key words*: Coordinate Measuring Machine, Coordinate Metrology, uncertainty, Quality Control, thermal influence.*

1. Introduction

High quality inspection performance is one of the major factors of evaluating the quality of products in manufacturing. Single inspection tasks of a product are performed by commonly used (1D) inspection measurement instruments, such as Vernier calipers, screw micrometers, and rulers. For more complex inspection tasks, e.g., positional tolerances or repetitive measurements, conventional CMMs are used. The ISO 10360-2:2001 [1] standard requires that all decisions regarding conformance to specifications follow the rules listed in [2].

The main point of inspection is primarily related to ensuring compliance with the tolerance requirements of dimensional properties.

Therefore the CMM should be calibrated in the same way it functions, which is the main requirement of identity. Therefore, if a material standard is used at other temperatures, the calibration and the verification are not necessarily valid, and additional uncertainty is present due to the unknown thermal expansion coefficient. Consequently, this increases the total uncertainty budget [3]. Finally, because CMMs are installed in a typical shop floor, the environmental temperatures may vary. In the experimental part of this research, only some major points were examined in order to pay special attention to thermal influences. It should be noted that the definition of error in this research was based on the measurement difference between a known value from the PTB and a measured value from a CMM. The PTB, which is the German National Metrology Institute, is a higher federal authority research institute with scientific and technical service tasks that is based in Braunschweig and Berlin.

A similarly uncertainty assessment approach for time-varying temperature environment is that of reference [4]. However, it is inherently not suitable for ease up calculation method and still has not been implemented of the calibration uncertainty for variety of workpieces. Another research [5] presented uncertainty evaluation model (distance between a point and a plane defined by 3 points) enables uncertainty evaluation for different measuring tasks. The limitation of this research is that the uncertainty assessment technique would only be applicable to estimating the discussed cases of position and out-of-plane parallelism of axes. In the research [6] authors make an analysis of the various elements to be considered in the implementation uncertainty of circular features. Another research was conducted [7] to compare two uncertainty combined methods based on Guide to the Expression of Uncertainty in Measurement (GUM) with Monte Carlo method. The feasibility of the evaluation method has been verified by measurement example of flatness. Conducted experiments show that precision significance of uncertainty determined by GUM is unreliable, the expanded uncertainty increased by 11.1% compared with actual situation. Task specific uncertainty assessment techniques are still up-to-date and investigated by researchers [8-10]. However only a few uncertainty assessment techniques are available for the specific points of the calibration of CMMs, including those mentioned above.

The objective of this research was to carry out a calibration procedure of a CMM and to present a more sophisticated assessment technique to improve former research. We emphasized the importance of temperature induced uncertainty and many of the situations where consideration of it would be most useful, such as: 1) non-20°C temperature CMM error as an uncertainty contributor; 2) Machine repeatability and reproducibility; 3) Temporal gradients; 4) Sampling strategies, i.e., the number and location of points in the workpiece coordinate system.

2. Presentation of the problem and the chosen solution approach

In practice, the error induced due to thermal influences causes CMM components to expand and bend. This error has a complex non-linear nature, which is why it is quite difficult to handle. Some of the contributing components to the development of thermal errors are a) The distribution of the temperature of a CMM influenced by external sources, b) the gradient of the temperature, c) uniform temperature changes, and d) the material of a machine component and its thermal properties.

Initially, we discussed in a review paper [11] the importance of the uncertainty of measurement using CMMs in the manufacturing industry. In a previous study [12], the state-of-the-art technique for the assessment of uncertainty was described in detail. A case study of the hole distance measurement from 50 mm to 750 mm was used. The measurement results showed that the uncertainty under the improved industrial conditions (IIC) was doubled compared to the low industrial conditions (LIC) (terminology borrowed from ISO 230-9) [13]. Consequently, the thermal influence as an uncertainty component was the most significant contributor to the last study. Since this paper describes the examination of the effect of thermal fluctuations on the calibration uncertainty of CMM measurements, which are commonly used instruments, it will be of interest to readers in the field of manufacturing.

3. Case study

3.1 Calibration object

The accuracy of the CMMs was tested by a hole-plate. This method is time- and cost-effective compared to the use of lasers. Because of weight, elasticity and thermal problems ball plates cannot be simply upscaled for the error mapping for CMMs. Therefore, in our case study the verification object was a hole-plate with 52 holes. The serial number of the object was PTB 5.32-95/5. The measurand was made of grey cast iron ($\alpha \approx 10.5 \times 10^{-6}$°$C^{-1}$). The relative locations of the round holes contained in a common plane were highly adapted for the verification of the CMMs. It should be noted that an artifact should be measured with different orientations and locations in the CMM measurement range. This allows the estimation of the CMM accuracy of length measurement. The verification process was performed without compensation in order to compare our case study results with the calibration certificate of the PTB for the same hole-plate.

The experiments were performed with the use of a high accuracy machine, DEA GLOBAL Silver CMM (with touch-trigger TESASTAR probes and High-Speed-Scanning Leitz sensors) manufactured by Hexagon MI. The sensor type was chosen based on the application. The main machine properties were a) Work volume: 1000 × 700 × 660 mm^3, and b) Specified volumetric accuracy: u = 1.4 μm + $3 \cdot 10^{-6}$ L at (20±1) °C, with L in units of mm. The conducted measurement process is illustrated in Figure 1.

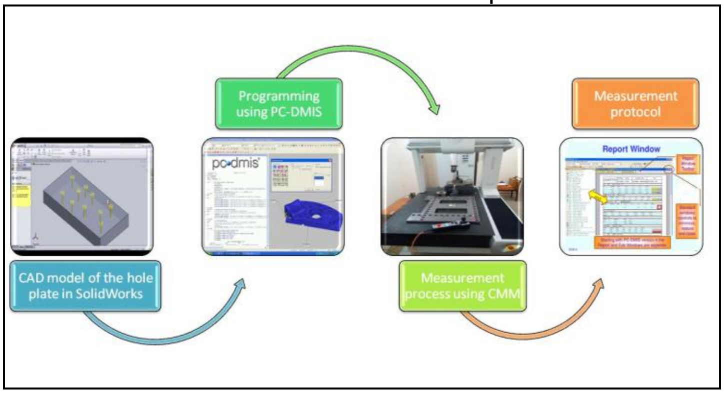

Figure 1: Coordinate measurement process to obtain geometric measurements.

3.2 Measurement conditions

An appropriate environmental condition is one of the key factors for experimentation because the effects of environmental changes on machine accuracy are highly important. Air temperature, pressure, humidity, and vibration all influence the length scales of a machine. Hence, it is recommended that a CMM environment should be in line with high settings, representing “improved working conditions” [14]. In addition, in order to maintain the room temperature at a nearly constant level, as many heat sources as possible were controlled.

For instance, 1) the room had indirect lighting to prevent shadows; 2) the measurement was completely automated so that no human heat source needed to be present near the machine after the run began; 3) thermocouples were placed at each axis on the machine. They were used to measure the thermal profile of the machine as the experimental measurements are made to check on the actual thermal stability of the machine frame; 4) generally, the machine was run through a warm-up cycle to assure that the thermal equilibrium was reached before the measurement run began.

The environmental condition in the room was quite good over long periods of time, within 0.2°C, but since the room was not separately thermostated, occasional temperature excursions might occur. A human heat source might create a negative effect on the air temperature within 0.5°C, which was not suitable to this kind of experiment. Therefore, we tried to eliminate operator interaction with the experiment by creating a program in PC DMIS 2013 MR1 software. PC-DMIS is metrology CMM software that is used to measure parts with all shapes, sizes, and tolerances, and it links Computer-Aided Design (CAD) models with CMMs, as shown in Figure 1. Consequently, we conducted completely automated measurements.

3.3 Verification method

In our case study, the adopted version of the procedure described in ISO 10360-2 [1] was used. Experimental measurement was carried out at 52 reference points. Each of the measurements started at the center of each hole (the CMM measured all three axes of each point) and the intersection length between the hole centers. The errors measured during the uncertainty assessment with the calibrated workpiece were used to determine the measurement uncertainties for the actual measurements. A calibrated workpiece is a workpiece whose dimensions are known with high accuracy. The described method utilized calibrated workpieces. Therefore, it took into account systematic measurement errors, which simplified the process of proving traceability. Metrological traceability was essential to ensure that the measurement results were repeatable, reproducible, and reliable regardless of the place where the methods and instruments were implemented. The method mentioned above is reliable for the determination of the measurement uncertainty. However, it is generally costly and time consuming [15].

In the experimental part, we conducted long-term measurements. They were normally started after more than a six-hour working time of the CMM. However, short-term measurements were performed with a two-hour thermal relaxation time after each measurement. In addition, low and improved industrial environments (borrowing terminology from ISO 230-9) were created and set. Measurements were taken to evaluate the effect of the temperature deviation as a factor in calculating the CMM uncertainty. It should be remarked upon that we tried to replicate medium industrial environment for the LIC. Moreover, medium environmental conditions (MIC) were created, which was another common environment that could be applied between the LIC and the IIC. This aided understanding of the thermal effects in a typical industry environment. The material temperature sensors were located close to the X-axis, Y-axis, and Z-axis scales and on the surface of the measurand. Moreover, there was no significant discrepancy in temperature for more than five days of testing. The experimental settings for five repeated measurements are displayed in Table 1. To better understand the thermal effect on the degree of uncertainty of the measurement result of CMM, we carried out experiments with various parameters:

Table 1. Parameters of experiments

Parameters	**Low industrial conditions (ISO 230-9)**	**Long-term measurements in improved industrial conditions**	**Short-term measurements in medium industrial conditions**
Temperature range	23 ± 1.5°C	19 ± 0.2°C	20.5 ± 0.5°C
Measurement strategy	Before rotating the workpiece 180° degree	Before rotating the workpiece 180° degree	After rotating the workpiece 180° degree
Average sensor measurements of temperature gradient: CMM structure Workpiece Probe	 23.3 ± 0.5°C 23.2 ± 0.4°C 23.2 ±0.2	 19.2 ± 0.1°C 19.2 ± 0.15°C 19.2 ±0.1	 20.5 ± 0.45°C 20 ± 0.4°C 20 ±0.4

4. Measurement results

The following diagrams (Figures 2–4) display the results of the measurements of the LIC, MIC, and IIC. Figure 3 illustrates the measurement results under the LIC. The abscissa shows the number of sampling points and the ordinate shows the error of the CMM in µm. Figure 2 illustrates the proof that the environmental influence on the measurement was not negligible. The other pairs of diagrams illustrate the MIC and IIC measurements, which were performed short term and long term, respectively.

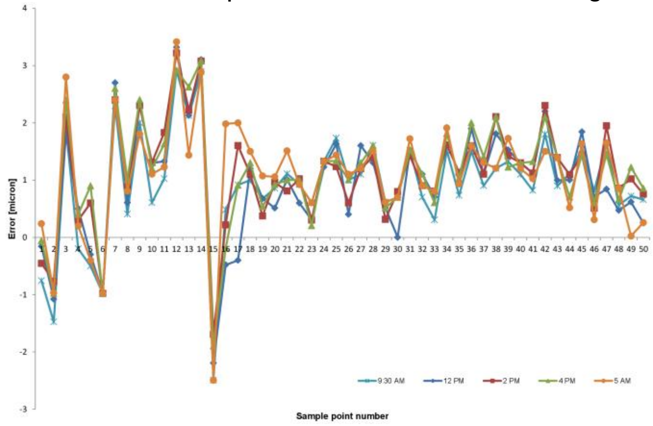

Figure 2. Whole measurement results under the low industrial conditions

From Figure 2, it is clear that the measurement results under the LIC lacked accuracy because almost all of the calibration points moved to $2 \cdot 10^{-6}$ m.

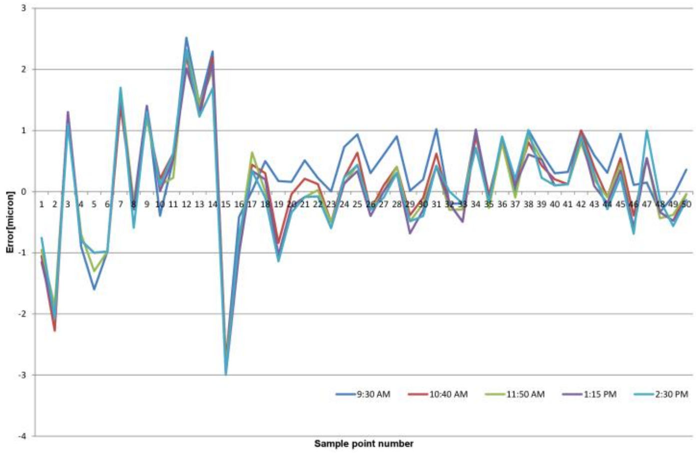

Figure 3. Whole measurement results under the MIC (short term)

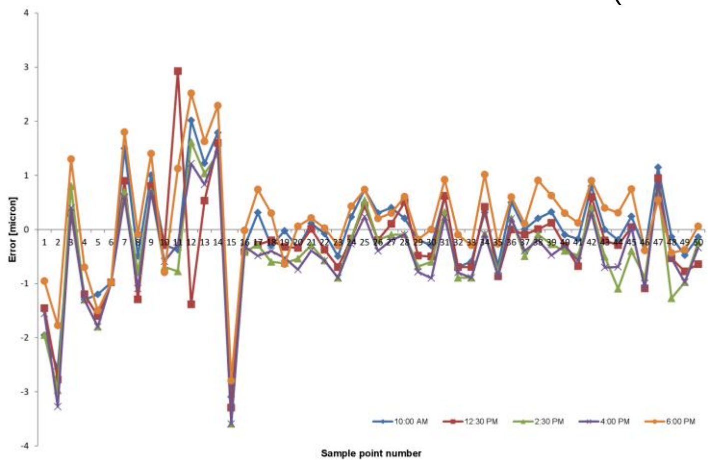

Figure 4. Whole measurement results under the IIC (long term)

It is clear from Figures 2–4 that the measurements, which were conducted under the MIC and IIC, had both precise accuracy and repeatability. However, it should be noted that first 20 minutes of the measurements still had sharp resonances. The difference curves that were obtained for each environmental condition under the IIC were identical on the micrometer level for the temperature range under consideration. They could be considered to have measurement durations that were independent for this research.

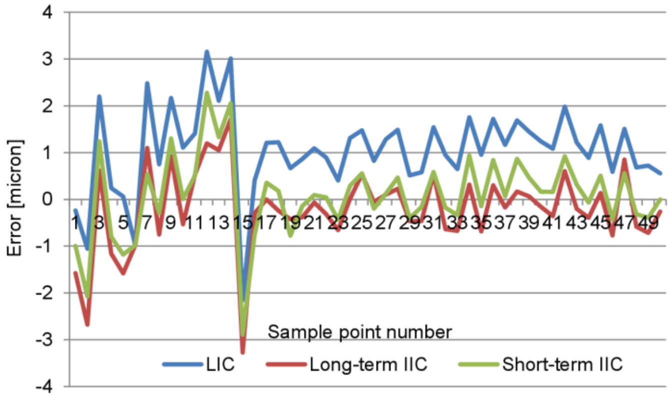

Figure 5. Average measurement results for each industrial condition: LIC, IIC (long term), and MIC (short term).

After comparing the data, the following observations were made. The difference between the errors of the LIC and IIC in coordinates was within a range of $1.2 \cdot 10^{-6}$ m. The difference between the errors of the long-term IIC and short-term MIC in coordinates was within a range of $2 \cdot 10^{-5}$ m. The last difference was not significant due to a close temperature range with comparison between the LIC and IIC data for which all of the measurement results moved by more than 1 micron. Figure 5 shows the residual errors for each industrial condition.

The differences for each industrial condition are illustrated in Figure 5, which shows the average measurement results between the LIC and IIC (long term) and the MIC (short term). In both cases (IIC and MIC), the distance measurement errors (EL values) could not exceed the maximum permissible error of the CMM. Despite the fact that the MIC (short term) measurements were conducted in higher temperature ranges than the IIC (long term) measurements, the results of the MIC were almost the same as those of the IIC. The reason for this might have been the heat emission from the CMM components, which increased the error in the IIC (long term) measurement results. However, as shown by the graph, the LIC had the highest rate of error compared to the other industrial conditions.

5. Improved CMM calibration uncertainty assessment technique

An improved version of the current level in assessing this calibration and verification uncertainty was discussed, in some detail, in references [12, 16]. Task-specific experiments based on the identification of residual errors using a hole plate standard were performed, and the authors concluded that thermal fluctuations were a major source of uncertainty in the measurements. According to reference [16], the main causes of uncertainty are a) machine uncertainty, b) thermally-induced uncertainty, and c) sampling uncertainty (See Appendix).

Table 2. Uncertainty contributors for the hole plate measurement under various environmental conditions

Source	**Equation number**	**Result ($1{\cdot}10^{-6}$ m) under the LIC at 23.7ºC**	**Result ($1{\cdot}10^{-6}$ m) under the MIC at 20.3ºC**	**Result ($1{\cdot}10^{-6}$ m) under the IIC at 19.2ºC**
Machine				
u_M	3	0.9	0.9	0.9
S	4	0.92	0.98	0.91
u_r	5	0.13	0.14	0.13
u_R	6	0.93	0.98	0.89
uu_c	7	1.6	1.65	1.56
Sampling u_S	8	0.36	0.04	0.03
Thermal				
UNE_S	10	0.02	0.002	0.005
UNE_W	10	0.11	0.013	0.016
$LUTM_S$	11	0.05	0.014	0.01
$LUTM_W$	11	0.26	0.1	0.07
u_T	9	0.29	0.1	0.07
Combined uncertainty u_c	1	1.69	1.65	1.56
Expanded uncertainty U (k=2)	2	3.4	3.3	3.1

Based on the results obtained (Table 2), there were several inferences: 1) the result of the proposed method was within the acceptable uncertainty tolerance of the CMM measurement. 2) the total uncertainty of the measurement result under the LIC was higher than the uncertainties obtained under other industrial conditions; 3) the main part of the uncertainty component was associated with the CMM accuracy and the repeatability; 4) each component of the total thermal uncertainty was doubled in comparison to other environmental conditions.

Following the obtained results from both research studies [11,12] for the case study, it was evident that the main sources of measurement uncertainty included the CMM error, sampling uncertainty, and thermal influence. Disregarding the uncertainty component associated with the Maximum Permissible Indication Error (EL, MPE), which was mainly related to CMM errors, one could conclude that the environmental impact was the main contributing factor to the uncertainty, and it completely dominated the overall uncertainty budget for the given study. Additionally, the dispersion of the gradient of the temperature by the X, Y, and Z axes of the CMM and the workpiece could be a significant issue. However, other thermal influences related aspects also needed to be considered. In this regard, the best solution was to compensate for the thermal error with the control of the heat fluxes into the system. Thus, it would be possible to compensate for the error by means of the controlled relative motion in the frame [14]. Even with precise temperature-controlled rooms and compensation systems, when it came to long length calibrations, the main contributor of the uncertainty budget was still related to the thermal influences of the internal heat sources of the machine [3].

6. Conclusion

The proposed improved uncertainty assessment technique was suitable for the estimation of calibration and verification uncertainty of the CMM for the given study. The main issues for the calibration uncertainty of Coordinate Metrology were discussed, and some specific points were identified for further improvement. The solution, as the calibration and verification uncertainty technique, was given to fulfill a number of issues related to the time-varying temperature environment and machine repeatability that would normally be considered in a calibration and verification uncertainty analysis. The proposed technique was experimentally proved in the technical base of the National Scientific Centre “Institute of Metrology,” Ukraine.

Thermal contributions to the overall performance of a CMM can be the single most influential part of the error budget. Additionally, the performance of the precision of a CMM is often dictated by thermal stability. The main reason for this is the number of different materials and interfaces found in a mechanical design. The mechanical properties of independent materials such as thermal expansion coefficients and mechanical joints can cause stress distributions to arise as a system reacts to thermal changes. That is why the mechanism to distort, grow, or contract with the temperature changes with time [15].

An analysis of the calibration of the CMM dependent upon the ambient thermal environment in which it operated was attempted. Therefore it is critical that the approach to estimating uncertainty is well defined and unilaterally applied. This is especially true in the context of measurements in workshops where temperature is difficult to control.

Eliminating thermal errors can be one of the most difficult aspects of any precision design. It should be noted that there are three general mechanisms [14] for heat transfer that are all relevant to precision machine design. A thermal error can be considered a systematic error that can be corrected, while temperatures are recorded and used by the software. However, this is an (unknown) bias error for the case of the correction system being incompatible for use with thermometer data.

Acknowledgments

This research was funded by the National Natural Science Foundation of China (grant number 51765012). Special thanks to Kostrikov A. – Acting Head of Dimensional Laboratory of National Scientific Centre "Institute of Metrology", Ukraine for kindly help in performing experimental part of this research and the many helpful suggestions

References:

[1] International Organization for Standardization. (2009). ISO 10360-2: 2009—Geometrical Product Specifications (GPS)—Acceptance and Reverification Tests for Coordinate Measuring Machines (CMM)—Part 2: CMMs Used for Measuring Linear Dimensions, International Organization for Standardization.
[2] International Organization for Standardization. (1998). ISO 14253-1:1998 – Geometrical Product Specifications (GPS)–Inspection by measurement of workpieces and measuring equipment—Part 1: Decision rules for proving conformance or non-conformance with specifications, International Organization for Standardization.
[3] European cooperation for Accreditation of Laboratories. (2019) WELAC Guidance Document WGD 8 EAL-G17 – Coordinate Measuring Machine Calibration EAL European cooperation for Accreditation of Laboratories Publication Reference.
[4] Fang, C.-Y., Sung, C. K., Lui, K.-W. (2005). Measurement Uncertainty Analysis of CMM with ISO GUM, ASPE Proceedings.

[5] Płowucha, W., (2020). Point plane distances model for uncertainty evaluation of coordinate measurement. Metrology and Measurement Systems, 27(4), pp. 625–639. https://doi.org/10.24425/mms.2020.134843
[6] Ruffa, S., Panciani, G.D., Ricci, F., Vicario, G. Assessing measurement uncertainty in CMM measurements: comparison of different approaches, Int. J. Metrol. Qual. Eng. 2014, 4, 163–168, EDP Sciences. DOI: 10.1051/ijmqe/2013057
[7] Cheng Y. B.; Chen X. H.; Li Y. R. Uncertainty Analysis and Evaluation of Form Measurement Task for CMM Jiliang Xuebao/Acta Metrologica Sinica, 2020, 41(2), 134-138.
[8] Rost, K., Wendt, K., Härtig, F. (2016). Evaluating a task-specific measurement uncertainty for gear measuring instruments via Monte Carlo simulation. Precision Engineering 04 Vol. 44 , https://doi.org/10.1016/j.precisioneng.2016.01.001
[9] Valdez, M. O., Morse, E. P. (2017). The role of extrinsic factors in industrial task-specific uncertainty. Precision Engineering 01, Vol. 49, pp. 78-84 https://doi.org/10.1016/j.precisioneng.2017.01.013
[10] Yang, J., Li, G., Wu, B., Gong, J., Wang, J., Zhang, M. (2015). Efficient Methods for Evaluating Task-Specific Uncertainty in Laser-Tracking Measurement. MAPAN 30, pp. 105–117 Springer-Verlag. https://doi.org/10.1007/s12647-014-0126-9
[11] Mussatayev, M., Huang, M., Rysbayeva, G. (2019). Role of uncertainty calculation in dimensional metrology using Coordinate Measuring Machine, ARCTIC Journal, 6.
[12] Mussatayev, M., Huang, M., Beshleyev, S. (2020). Thermal influences as an uncertainty contributor of the coordinate measuring machine (CMM). Int J Adv Manuf Tech, 111, pp. 537–547. https://doi.org/10.1007/s00170-020- 06012-3.
[13] International Organization for Standardization. (2005). ISO/TR 230-9:2005 – Test code for machine tools – Part 9: Estimation of measurement uncertainty for machine tool tests according to series ISO 230, basic equations. International Organization for Standardization
[14] Saunders, P.; Verma, M.; Orchard, N; Maropoulos, P. (2013). The application of uncertainty evaluating software for the utilisation of machine tool systems for final inspection 10th International Conference and Exhibition on Laser Metrology, Coordinate Measuring Machine and Machine Tool Performance, LAMDAMAP, EUSPEN publication, 219-228.
[15] Leach, R., Smith, S. T. (2018). Basics of Precision Engineering. Taylor & Francis Group, LLC.

Cheng, Y., Wang, Z., Chen, X., Li, Y., Li, H., Li H., Wang, H. (2019). Evaluation and optimization of task-oriented measurement uncertainty for coordinate measuring machines based on geometrical product specifications. Appl Sci 9(1):6, doi: https://10.3390/app9010006

Design, construction, and calibration of a step gauge of nests for performance evaluation of Laser Trackers

Iván Espinosa Nulutagua[1]
Company: Centro Nacional de Metrología (CENAM)[1],
km 4.5 carretera a Los Cués, El Marqués, 76246-
Querétaro. Phone: +52 4422110500. Fax: +52
4422110577.
email: iespinos@cenam.mx,
Co-author: Octavio Icasio Hernández[1]

Abstract

According to documentary standards for the performance evaluation of Laser Trackers (LT), long length reference artifacts are required. We will discuss the design, construction, and calibration of a long length artifact called step gauge of nests (SGN). The SGN has several nests in line to place the LT probe; the two extreme nests of the SGN are at 3 m approximately. However, for long gauges, factors like gravitational force, fixturing forces, change in the environmental conditions, among others, deforms the gauge, and its length changes when its orientation changes. To evaluate these factors, in the design stage, we employ finite element simulation of the SGN to predict such deformations (mainly length variations between the two extreme nests). The simulation considers the used material, its stiffness, straightness, distribution of the nest's weight, and geometry's change of the SGN to reduce the variations in its length. The results of the finite element simulation show a length variation of around 20 ppm between the horizontal and vertical SGN positions. That variation was validated with the calibration results using two different methods. The line of sight (LOS) method, which involves the same LT under evaluation and the Overlap method which uses an accurate CMM.

1. Introduction

The present work describes the design, construction, and calibration of the reference length that CENAM (the National Metrology Institute (NMI) of Mexico) uses for the performance evaluation of Laser Trackers (LTs). The use of LTs has been growing in Mexico and around the world, thus there is increasing demand for metrological support from our NMI perform the corresponding Proficiency Tests. The work described in this paper addresses this critical need.

The performance is evaluated according to written standards such as ASME B89.4.19 [1], ISO 10360-10 [2], and VDI/VDE 2617-Part 10 [3], which test the instruments to meet their Maximum Permissible Error (MPE) specified by the manufacturer.

According to [1], the performance evaluation of LTs requires a calibrated length of at least 2.3 m. For this reason, the gauge presented here has several nests where the LT probe (SMR) may be fixed so that two positions are at an approximate distance of 3 m. There are other nests between the two extreme nests to help with the calibration process and allow to establish shorter reference lengths. We will refer to this calibration artifact a Step Gauge of Nests (SGN).

According to Sawyer et al. [4], the design, construction, and calibration of such a long scale bar create challenges for manufacturers, as well as for customers of these scale bars. The main challenge is that the length of a long-scale bar will suffer a significant change in dimension at different orientations and over time. These changes come among others from its material, how it was designed, the structural bending under gravity loading, fixturing forces, and atmospheric changes. To solve these challenges, in the design stage of our SGN, we use a CAD model and finite element simulation to predict such length variations between the two extreme nests. The simulation considers the material, its stiffness, and straightness so as to reduce the length variations by determining support locations for the SGN and changing the weights distribution of the spherically mounted retroreflector (SMR) nests.

In the construction stage, we describe how the SGN was manufactured and how using high module carbon fiber with a low thermal expansion coefficient (CTE), we reduce the variation in the length coming from environmental factors like temperature. The finite element simulation shows a variation in the length of around 20 ppm in the two extreme nests between the horizontal and vertical SGN positions. Such variation was validated with the calibration results using two calibration methods. The first method is the overlap with CMM introduced by Icasio-Hernández et. al. [5] which uses the intermediate nests and the second method is the Line of Sight (LOS) method, which uses an LT, see Wang et al. [6].

2. Design, construction, and calibration of SGN

2.1. Design stage

The main parts of the SGN are:

Nests – the nests serve to hold the LT probe, the SMR, using a magnet to ensure repeatability during the measurement. The nests are made of steel. Steps – this piece works as a connection between the carbon fiber bars and the nests. The step is also made of steel. Carbon fiber bars – are the SGN body. The distance between every step is determined by holes positioned in the bars. The SGN body material is a high module carbon fiber with unidirectional fibers with CTE of around 0.3 ppm per 1 °C. Because the SGN must be calibrated on a CMM, it was designed to be placed in such a way that there are always two nests that define a length of 1 m. There are additional nests between these nests to allow overlapping. The labels at the top of Fig. 1 shows the main parts of the SGN.

The parts to support the SGN are shown with labels at the bottom of Fig. 1; the components are: Points of support –are the parts that are in contact with a stand. Based on simulation studies, we choose the Bessel points of the length of the carbon fiber pipe to minimize the transmission of deformation to the SGN. Carbon fiber pipe – is the main part of the support. It works as a filter, absorbing the external loads, to attenuate them as they reach the step gauge. It is made of carbon fiber with crossed fibers. Holders – these are the contacts between the support parts and the SGN body through O-rings. Considering that X-axis is along the length of the SGN, these block the Y and Z movement and allow expansion along the X-axis.

The finite element simulation allows us to visualize the deformation behavior of the SGN in the different orientations proposed by the documentary standard [1]. With the simulation, we define the location and number of holders that are needed to reduce variation in the length between the extreme nests.

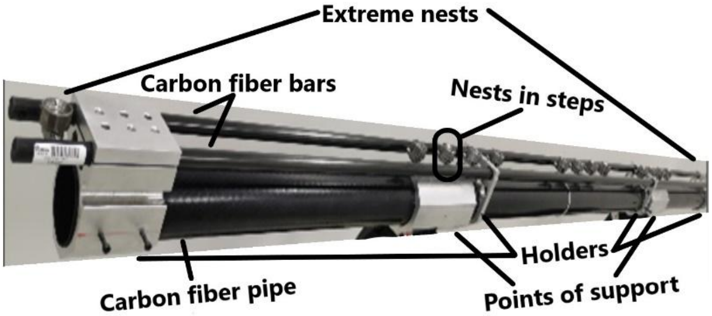

Fig. 1. Components of the step gauge of nest.

2.2 Construction

The main challenge in the construction of the SGN was how to make that the holes in the two carbon fiber bars as coincident as possible. The carbon fiber bars, and the carbon fiber pipe were acquired from an external provider. The rest of the components were designed and built at CENAM.

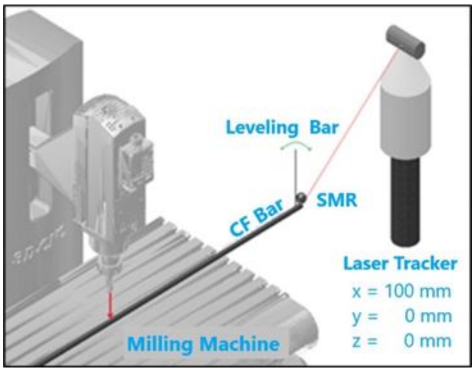

Fig. 2.- Milling machine making the holes on the carbon fiber bars.

The short axis travel of the milling machine did not allow us to drill the carbon fibers bars along its entire length and both fibers at the same time. Therefore, to drill the holes, we had to use an LT to establish the position of the corresponding holes on both bars of the SGN. The holes were made, as shown in Fig. 2. We drill a hole in one extreme of the bar to set a temporary nest. We place the LT SMR on that nest to help identify the position of the hole in the bar. The leveling bar helps to control the rotation between each hole and keep them aligned. We fix the pins of the steps into the holes in the bars using Araldite 20/20 glue.

2.3 Calibration

For the overlap method, we use a calibrated Mitutoyo Legex CMM model 9106. It has a range of motion of 1000 mm, 900 mm and 600 mm in its X, Y and Z axis respectively, with an MPE of ± (0.28 + 1 L/m) μm. For the LT line of sight method (LOS) method, we employed a calibrated Leica AT901-B LT with MPEs of ± (0.4 + 0.3 L/m) μm for range, and ± (15 + 6 L/m) μm for angles. The SGN design allows using four nests for overlap inside the CMM interval. According to [5], four elements are enough to establish the link between two segments to stitch together longer lengths. We measure the SGN in four sections setting a solid steel sphere of 1.5 in diameter on the nests every time we want to measure a nest. The spheres fulfill the function of the LT SMR.

Fig. 3 left shows the calibration of the SGN with CMM, a steel rail bar serves as support for the SGN and its structural base. To measure every section of the SGN, we translated the array of components on the table.

Fig. 3.- CMM calibrating the SGN using the overlap method and LT using the LOS method.

The LOS method using LT interferometer is the second method used to calibrate the SGN, see Fig. 3 right. The figure show that we set the LT in line with the center of the SMR on the nests of the SGN. For misalignment error reduction, we must minimize the angular errors, see Muralikrishnan et al. [7], and Loser et al. [8]. The reference length is the distance between nests 1 and 14. If the line describing these two points is collinear with the LT laser beam, all the mechanical errors of the LT no longer influence the measurement, then only interferometer (IFM) errors are present. According to Wang et al. [6], we must ensure that the differences among the measured horizontal/vertical angles between nests 1 and 14 are less than 0.05°, through manual adjustment. We must clarify that this method is more versatile than the overlap method because unlike the overlap method where only the horizontal position of the SGN can be measured, the LOS method allows us to measure the SGN in any position and orientation by placing a mirror between the LT and the SGN in such a way that the IFM of the LT is aligned along the line joining the nests.

3. Results and uncertainty evaluation

3.1 Uncertainty evaluation

We use two methods for the calibration of the SGN. We show the uncertainty in the length for both methods.

Uncertainty component	Method	Value (mm)	Uncertainty component	Method	Value (mm)
Overlap Method			LOS method		
Workpiece calibration, u(cal)	B	0.0004	Optical Alignment, Interferometer Uncertainty, and angular encoders, u(L)	B	0.001
Measurement procedure, u(p)	A	0.0002	Repeatability of Nests	A	0.002
Systematic error, u(b)		0.0007	Gravity Loading, u(G)	B	0.002
Material and manufacturing variations, u(w)	A o B	0.0049	Retroreflector, u(R)	B	0.001
Combined uncertainty, uc		0.0049	Artifact Temperature, u(T)	B	0.002
Expanded uncertainty, U (k=2)		0.010	Length Stability During Testing Time, u(S)	B	0.001
			Combined Uncertainty, uc		0.004
			Expanded Uncertainty, U (k=2)		0.008

Table 1.- Uncertainty budgets for both methods

The uncertainty budget considered for the calibration using the overlap is based on the standard ISO 15530:3 2011 [9]. A description of uncertainty's components for LOS method can be found in [10]. According with table 1, the LOS method has lower uncertainty than the overlap method, but both are close to the required uncertainty considering the LT MPE and the rule established in [1] that the uncertainty must be no more than a quarter of the MPE.

3.2 Calibration results

According to section 2.2, the holes were drilled with a drilling machine and an LT, the straightness value found during calibration was 0.51 mm, which is not large considering the employed technique. Table 2 shows the length result between the two extreme nests of the SGN using CMM with the overlap method [5], LT measurements using the LOS method [6], and finite element simulation. The CMM result works as validation of the measurements with LT interferometry using the LOS method. The LT results and the simulation results are similar, showing compression of the SGN between horizontal and vertical positions. These two represent the deformation (variation in the length) expected by simulation and the real deformation between horizontal and vertical position. The results show a difference between the CMM and LT in the horizontal position. Considering the uncertainties of both methods and taking the LT method as a reference, we found a normalized error of 0.8. If NE is less than 1, then there is a correlation between the results. Then the measurement of the LT is validated with the CMM and vice versa.

Method	**CMM**	**U k=2**	**LT**	**U k=2**	**Finite element**
Horizontal (mm)	**2940.143**	0.010	**2940.153**	0.008	**2940.023**
45° (mm)	**No info.**		**2940.144**	0.008	**No info.**
Vertical (mm)	**No info.**		**2940.132**	0.008	**2940.003**

Table 2.- Calibration Results

4. Discussions and conclusions

In this paper, we have described the design, construction, and calibration stages of a long length artifact for the performance evaluation of LT under different documentary standards [1-3]. The construction of a long length artifact is not an easy task. The 21 μm compression of the SGN that we found between horizontal and vertical positions was expected but not desired. We verified this difference from a lot of measurements, and these differences remain. It is important to avoid variation in the length when a gauge is designed, but if there is a method for the calibration of the length at different orientations, the problem is reduced. We believe that our current design has a problem in that the nests of the SGN are not on the neutral axis between the two carbon fiber bars, and the slice of the SGN isn't enough to absorb the deformation in the Z-axis. The next design will take this problem into consideration to see if we can reduce that compression. The LOS method for calibration of long length artifacts described here shows that it is a valid method for evaluation of the length. LOS method was validated using the overlap method with a CMM. Unfortunately, it was not validated in straightness; in the future, we are planning to do the validations of straightness (Y, Z, coordinates) using a large CMM. Also, the evaluated uncertainty of the calibrated distance is inside the one-quarter of the MPE, if we consider a distance measurement of 3 m from the LT. In the case of new LTs with only ADM, the range accuracy of such devices could represent a problem. This problem was solved by designing an SGN with extra targets and using the overlap method, and a CMM. Finally, we conclude that the construction of a long dimensional gauge is possible. In the future, we are planning the redesign of our SGN looking for construction schemes that could reduce deformations and explore other methods for calibration.

References:

[1] ASME B89.4.19-2006 Performance Evaluation of Laser-Based Spherical Coordinate Measurement Systems, Copyright ASME International.

[2] ISO 10360-10:2016 Geometrical product specifications (GPS) - Acceptance and reverification tests for coordinate measuring systems (CMS) - Part 10: Laser trackers for measuring point-to-point distances.

[3] VDI/VDE 2617-10:2011 Accuracy of Coordinate Measuring Machines - Characteristics and Their Checking - Acceptance and Reverification Tests of Laser Trackers

[4] Sawyer D, Parry B, Phillips S, Blackburn C, Muralikrishnan B. 2012 A model for geometry-dependent errors in length artifacts. J Res Natl Inst Stand Techno; 117:216.

[5] Icasio-Hernandez O, Trapet E, and Arizmendi-Reyes E, Valenzuela-Galvan M and Brau A. 2020 Overlap method for performance evaluation of coordinate measurement systems and the calibration of one-dimensional artifacts. Meas Sci Technol.

[6] Wang L, Muralikrishnan B, Lee V, Rachakonda P, Sawyer D, Gleason J 2019 Methods to calibrate a three-sphere scale bar for laser scanner performance evaluation per the ASTM E3125-17https://doi.org/10.1016/j.measurement. 107274

[7] Muralikrishnan B, Sawyer D, Blackburn C, Phillips S, Borchardt B, Estler WT. ASME B89.4.19 2009 Performance Evaluation Tests and Geometric Misalignments in Laser Trackers. J Res Natl Inst Stand Technol. 2009; 114(1):2135. 2009 Feb 1. doi:10.6028/jres.114.003

[8] Loser R, Kyle S 1999 Alignment and field check procedures for the Leica Laser Tracker LTD 500.In: Boeing Large Scale Optical Metrology Seminar.

[9] ISO 15530-3 2011 Geometrical Product Specifications (GPS) coordinate measuring machines (CMM): Technique for determining the uncertainty of measurements Part3: Use of calibrated workpieces or measurement standards.

[10] Hudlemeyer A, Meuret M, Sawyer DS, Blackburn CJ, Lee VD, Shakarji CM 2015 Considerations for design and in-situ calibration of high-accuracy length artifacts for field testing of laser trackers. Journal of the Coordinate Metrology Society Conference 10(1):26-32.

Improvement of the metrological support system for measuring the mass and volume of liquid in the flow, mass and volume fluid flow rates in the range from 10^{-6} to 10^{-2} t/h (m³/h)

R.R. Tukhvatullin
VNIIR – Affiliated Branch of D.I. Mendeleyev Institute for Metrology – VNIIM-VNIIR
Contact details: 420088, Russia, Republic of Tatarstan, Kazan, 2nd Azinskaya, 7 «a»
e-mail: rustam_vniir@bk.ru

Abstract

A critical analysis of literature related the current state of the world system of metrological support for measurements in the low-flow range is presented. A hydraulic diagram of the standard and a program of research of metrological characteristics were developed. The equipment of the main modules of the standard was installed. The main sources of uncertainty of the standard were determined. The main sources of uncertainty characteristic of the low flow range were estimated. Physical modeling of the process of liquid evaporation from the weighing container was performed, and methods of minimizing this source of uncertainty for the metrological characteristics of the standard in the conditions of a multifactorial experiment were determined.

1. Introduction

The need to study the metrological characteristics of measuring instruments in the flow range from 10^{-6} to 10^{-2} t/h (m³/h) (low flow range) is accounted for by the urgent needs of various sectors of the economy: pharmaceuticals, medicine, chemical, food and oil industries, mechanical engineering.

A significant contribution to the issue of improving the metrological infrastructure, in the period from 2010 to 2020, was provided out by foreign national research centers in Germany, Portugal, France, the Czech Republic, Denmark, Switzerland, Great Britain, and the Netherlands. Currently, the European Union is implementing a joint research project - "Metrology for Drug Delivery II". This project is aimed at improving the accuracy of measuring instruments for units of quantity and flow rate, operating in the range of low flow rates, in existing drug delivery devices.

The creation of a full-scale metrological infrastructure in the Russian Federation covering the transfer of units of volume and mass of liquid in a stream, volumetric and mass flow rates in the range from 10^{-6} to 10^{-2} t/h (m^3/h), is due to the appearance of a large number of measuring instruments on the market, which are applied in the specified flow range.

2. Review of the experience of operating national primary standards

A review of literary sources [1-6, etc.] and the experience of foreign national research centers in the creation and operation of standards for units of mass and volume of liquid in a stream, mass and volumetric liquid flow rate in the range of low flow rates [7-15, etc.] determined the basic technical solutions of the modules, allowing to create a state primary special standard with the necessary metrological and technical characteristics. The forced pressure flow of a liquid stream in the standards is created in various ways: by displacing the previously prepared liquid from the expansion tank with a membrane by air with excess pressure; using pumps; by squeezing out of syringes (provers); using a hydrostatic liquid column. The standard includes a balance of accuracy class I, connected to a computer via digital interfaces, which makes it possible to record each mass value obtained in real time with a dynamic model of measuring units. To neutralize the effect of water evaporation from the weighing container during the measurement process, it is recommended to use evaporation traps in the weighing zone [7], create a layer of highly viscous liquid, such as oil, above the liquid layer in the weighing container [16]. Liquid from the capillary tube flows into the weighing container onto a porous glass filter [7], or the outlet section of the capillary tube is arranged below the water level in the weighing container [16], and if the outlet section of the capillary tube is located above the water level in the weighing container, a sprinkler is used to minimize the effect of the jet on balance readings [17].

Ensuring the reliability of the estimation of flow rate values and the amount of water in a stream in the range of low flow rates is a difficult task due to the need to control and manage a large number of influencing factors, including the human factor. The implementation of optimal technical solutions in the design of a standard determines the level of its metrological characteristics.

The purpose of this work: improvement of the system of metrological support of means and systems for measuring the flow rate and amount of liquid in the low flow range.

Tasks: 1) perform a critical review of the experience of operating foreign standards in the low flow range; 2) develop a hydraulic diagram of the primary standard and a program of research of metrological characteristics; 3) install the equipment for the main modules of the standard; 4) identify the sources of uncertainty; 5) develop new technical solutions to minimize the main sources of uncertainty.

3. Instrumentation

The best design solutions and algorithms of operation described in [7-14] formed the basis for the development of a hydraulic schematic diagram of the standard (Figure 1), which made it possible to ensure the smallest values of uncertainty. The standard consists of three hydraulic lines, made according to the same design scheme, which makes it possible to implement a direct method of dynamic weighing of the mass of distilled water (hereinafter – water).

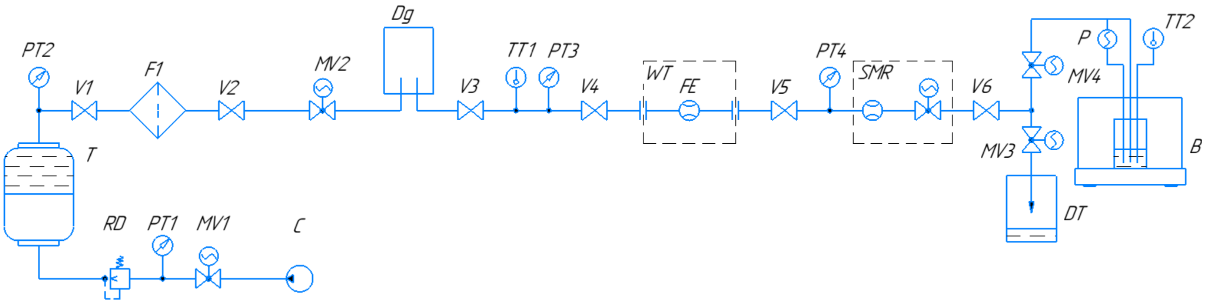

Figure 1 – Simplified schematic diagram of the measuring line of the standard:
B – balance; WT – work-table; SMR – flow measurement and control system;
Dg – degasser; PT1 – PT4 – pressure transducer; TT1 – TT2 – temperature transducer; DT – drainage tank; V1 – V6 – manual valve; MV1 – MV4 – electric valve;
C – compressor unit; T – expansion tank with a membrane; RD – reducer;
F – water purification system filter.

In terms of the operating principle, the standard represents a conditionally open hydraulic circuit. Water in the expansion tank with a membrane separating it from the air is displaced by excess air pressure created by the compressor unit. Each measuring line is equipped with high-precision instruments for measuring the temperature and pressure of the measured medium, as well as devices for mounting the investigated (calibrated, verified) measuring instruments into the standard hydraulic line (Figure 2). The flow rate setpoint is reached through the operation of the flow measurement and control system, which consists of a Coriolis flow meter and an electrical valve located in a control loop with feedback. After passing through the hydraulic path, water is fed into a weighing container installed on the balance. Electric valves provide flow switching functions as well as overflow protection of the weighing container. In order to protect the equipment from clogging and breakdown, filter elements with a pore size of 2 microns or higher are installed in the hydraulic lines of the standard.

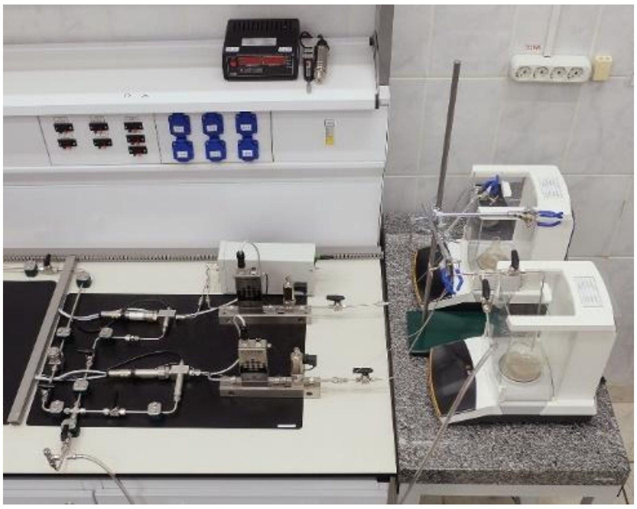

Figure 2 – Appearance of the standard

When measuring the mass of liquid, the temperature of distilled water in the weighing container is determined. These values are used to introduce a correction for air buoyancy. When measuring the volume of liquid in a stream and the volumetric flow rate in the measuring path, the pressure and temperature of distilled water passing through the measuring line are additionally measured at the time of measurements. These values are used to determine the density of water corresponding to the conditions in the measuring line.

4. Main sources of uncertainty

The main sources of uncertainty, identified for the dynamic measurement model, affecting the metrological characteristics of the standard (see Fig. 1):

– uncertainties of mass measurement: calibration uncertainty, time and temperature drift, repeatability, linearity and reproducibility of balance readings;
– uncertainties caused by measurements of the density of air, distilled water, corrections for air buoyancy;
– uncertainties caused by geometric changes in pipes and valves;
– uncertainties caused by measurements of time intervals and synchronization;
– uncertainties caused by water evaporation from the weighing tank;
– uncertainties caused by the surface tension coefficient of water in the weighing container.

In evaluating the above sources of uncertainty, particular attention should be paid to water evaporation and liquid surface tension, as these are the sources of greatest contribution to standard's uncertainty budget.

5. Assessment of the main sources of uncertainty typical for the low flow rate range

Studies have shown that water evaporation from a weighing container can contribute up to 0.6% to the uncertainty budget, which is 12 times higher than the target value of the uncertainty of reproductions and transfer of units from the standard to measuring instruments. The formation of oil film on the water surface in the weighing container excludes water evaporation, but the effect of the surface tension coefficient increases to 0.016% [16], which is approximately 30% of the target value of the standard's uncertainty.

In order to reduce the impact of the above sources of uncertainty, new design solutions in the implementation of the standard are being developed and researched. A program of research of all sources of uncertainty affecting the metrological characteristics of the standard was developed.

Studies of the metrological characteristics of the balance were carried out (the uncertainty caused by balance readings contributes from 5 to 10% of the target value of the standard's uncertainty), the requirements for the operating conditions were determined, which would allow obtaining the lowest values of measurement uncertainty. The influence of free and forced convective air streams in the standard's room on the metrological characteristics of the balance was determined. Technical solutions were developed to achieve the necessary operating conditions in the standard's room, and separately for the location of the balance. A distributed air supply system with the required values of temperature and relative humidity of air in the standard's room was designed. The design of the module for stabilizing the ambient conditions in the vicinity of the balance was developed and implemented. This module includes a laboratory cabinet with installed measuring instruments for ambient conditions measurements and equipment for maintaining relative humidity.

6. Conclision

1) A critical review of design solutions, algorithms of operation and experience of operating foreign standards in the low flow range was performed; 2) a hydraulic diagram of the standard and a program of research of metrological characteristics were developed; 3) the equipment of the main modules of the standard was installed; 4) the sources of uncertainty affecting the metrological characteristics of the standard based on a dynamic model of measuring units were determined; 5) new technical solutions to minimize the main sources of uncertainty were identified.

References:

1. Bohl, Elmendorf. Technische Strömungslehre, Verlag Vogel Fachbuch, ISBN 978-3-8343-3129-8, 2008
2. W. Press, S. Teukolsky, W. Vetterling, B. Flannery, Numerical Recipes in C. New York: Cambridge University Press, 1992, ch. 15.3, pp. 666 – 670
3. BEDIAT N. Faibles debits. ARATEM. 2005
4. Benkova M., Mikulecky I.. Primary standard and traceability chain for microflow of liquids. 16th International Flow Measurement Conference 2013, FLOMEKO 2013. 44-49
5. Thailand testing procedure for medical measuring device handbook 2016 Standard procedures for testing of infusion pumps ISBN: 978-616-11-2153-2
6. Batista E., Almeida N., Godinho I., Filipe E., Uncertainty calculation in gravimetric microflow measurements, AMCTM X, 2015
7. Website of the EMRP Project HLT07 MeDD, www.drugmetrology.com
8. Bediat N. La métrologie des debits de liquide inférieurs à 1 litre par heure. Proceedings of the 12th International metrology congress, Lyon, France. 2005
9. Clarkson D M Accuracy estimations of testing of infusion devices using weighing balances // Medical Engineering & Physics. 2002. Vol 24. Pp. 229–35
10. Chinarak T Leetang K and Wongthep P Calibration guideline for the infusion pump analyzer applied in secondary laboratories in Thailand 2016 Int. Conf. Flomeko, Australia
11. JCGM 100:2008 Evaluation of measurement data – Guide to the expression of uncertainty in measurement
12. BIPM et al, Guide to the Expression of Uncertainty in Measurement (GUM), 2nd ed., International Organization for Standardization, Genève, 1995
13. Sirenden, Bernadus. (2015). Development of Volumetric Micro-Flow Calibration System Using FPGA for Medical Application
14. Melvad, Claus. 2013. The progress of gravimetric primary standards for liquid flow calibration at the danish technological institute from 500 m^3/h to 1e^{-9} m^3/h. 218-221
15. James W. Schmidt, John D. Wright. Micro-Flow Calibration Facility at NIST. 9th ISFFM
16. Platenkamp, Tom & Sparreboom, Wouter & Ratering, Gijs & Katerberg, Marcel & Lötters, Joost. (2015). Low Flow Liquid Calibration Setup. Micromachines. 6. 473-486
17. Christopher David, Pierre Claudel. Novel water flow facility in France. Range extension to low flow rates. 15th Flow Meas. Conference. Flomeko. 2010 Taipei, Taiwan

AN AUTOMATION APPROACH TO PERFORM ROCKWELL HARDNESS MEASUREMENTS

M. Zackaria, F. Menelao, A. Felgner
Physikalisch-Technische Bundesanstalt (PTB),
Braunschweig and Berlin, Germany
Tel. +49 531 592-5168,
Email: mutaib.zackaria@ptb.de

Abstract

It is challenging to calibrate hardness reference blocks in compliance with the prevailing standards without performing time-consuming pre-measurements. A new method developed at the PTB uses data obtained during the preload phase of a Rockwell hardness measurement to automate the test cycle and thereby eliminates the need for pre-measurements. The new approach accelerates the overall calibration process and increases the user-friendliness of the Rockwell hardness testing equipment. This report gives an overview of the developed method.

1. Introduction

The Rockwell hardness test is one of the most popular methods to characterize the hardness of metals. Despite being an empirical indentation test, it has established itself in the field of material testing due to its simplistic testing principle. Furthermore, the test is attractive because of the speed of operation, low-cost and non-destructive nature of testing. However, a strict compliance with the regulations of the standard is necessary to obtain meaningful measurement results with low measurement uncertainty [1]. The procedure for performing a Rockwell hardness test is described in the ISO standard 6508 [2]. Amongst other parameters, the norm defines the loading rate, hold time and indenter geometry.

Certified reference blocks play a key role in ensuring the traceability of the measurement and are widely used by end-users to test their instruments. Hence, its calibration has been standardized in a separate part of the same standard with considerably stricter requirements. The ISO 6508-3 sets the loading time of the additional test force and the indentation speed during the final stage of the indentation process (between 80 % and 99 % of the total test force). However, it does not define the indentation speed during the initial stages, i.e. between 0 % and 80 % of the total test force, making the compliance with the standard extremely difficult. Thus, up until the automation, multiple pre-measurements were required to ensure a compliance with the standard.

2. Basic Principle

The initial indentation speed needs to be set depending on the hardness of the tested material. Fig. 1 shows the section of the depth vs. time curve during the additional load application and its holding time for two materials with different hardness values. It is clear that the initial indentation speed varies with the hardness of the material because the final indentation speed and the total loading time have been fixed by ISO 6508. The missing information about the initial indentation speed can be determined with the help of test indents or pre-measurements. This, however, is very time-consuming and requires an expert user. Instead, a new and innovative method developed at the PTB extracts the needed information from the pre-load phase and allows to determine the initial indentation speed without the need of pre-measurements [3]. To achieve this, a database with functional relationships between the maximum indentation depth (h_{max}) and hardness as well as the indentation depth at pre-load (h_0) and hardness are created. A typical characteristic curve for steel applicable for the Rockwell scale C is shown in Fig. 2 [4]. The initial indentation speed is then calculated with the help of the following equation 1:

$$v_1 = \frac{(1 - \frac{0.2F}{F - F_0}) * h_{max}}{T_{aa} - \frac{(\frac{0.2F}{F - F_0}) * h_{max}}{v_2}} \qquad (1)$$

where,

ν_1 is the initial indentation speed for the loading phase (0 % to 80 %)

ν_2 is the final indentation speed (80 % to 99 %)

T_{aa} is the total loading time

F is the total test force and

F_0 is the pre-load.

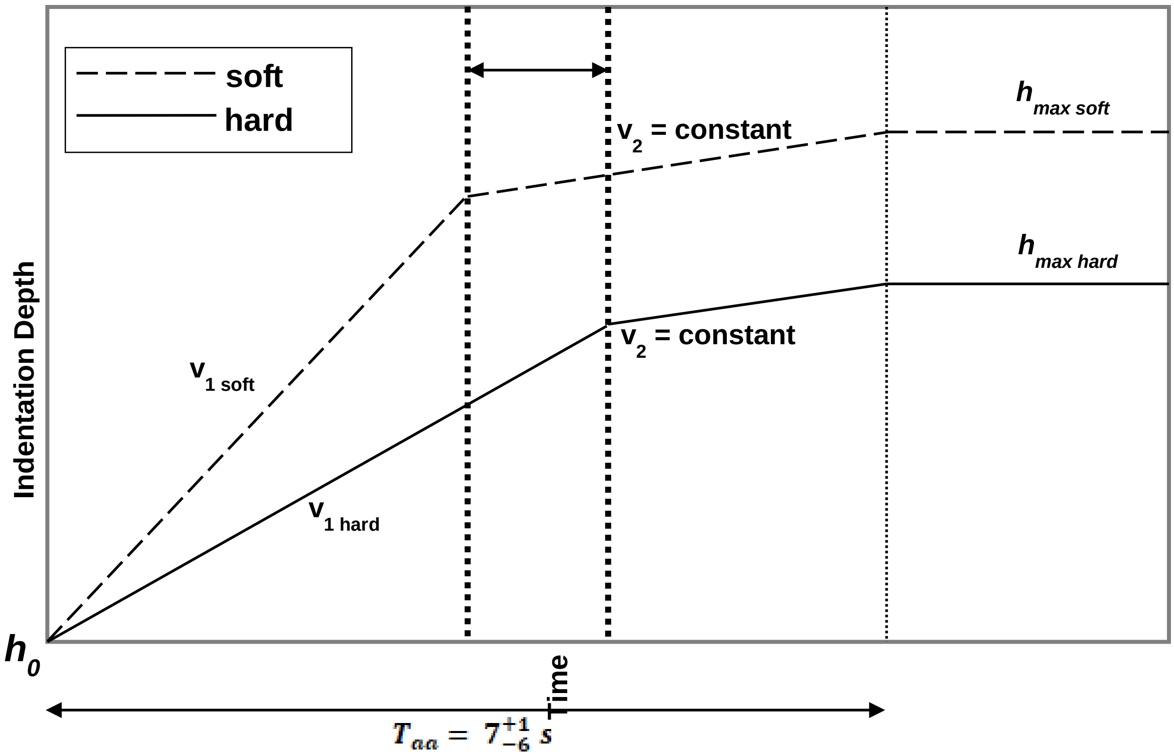

Figure 1: Depth vs. time plot for an arbitrary soft and hard material

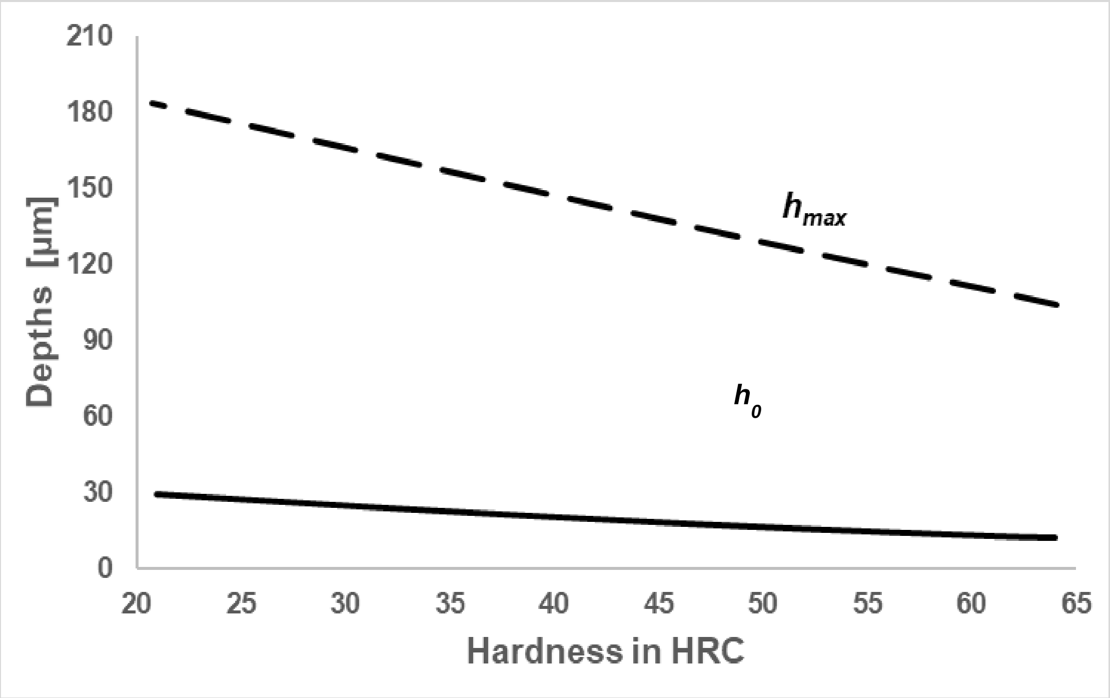

Figure 2: Characteristic curves for Rockwell scale C for steel with maximum indentation depth h_{max} and indentation depth at pre-load h_0

3. Machine Stiffness

In the framework of the automation, the machine stiffness plays a crucial role. Primarily, the determined characteristic curves need to be universally applicable for every hardness testing equipment. Secondly, the indentation depths at preload and maximum load are affected differently by the machine stiffness. In a normal Rockwell hardness test, the depth readings are measured at the minor load (during loading and unloading) making the determination of the precise machine stiffness redundant. On the contrary, absolute values of indentation depth at minor and major loads are required for a machine independent automation. These absolute values can only be determined if the machine stiffness is known. The extent of elastic deformation during a hardness test depends substantially on the machine design or type.

There are different ways in which machine stiffness can be measured. The method stated in ISO 6508 ensures that the machine hysteresis is minimized but is insufficient to calculate the absolute value. It also does not include the deformation of the indenter, the indenter holder and most importantly the elasticity of the material placed under the indenter. One possible solution is to use a length measuring system such as an interferometer. Owing to the difficulties in alignment, logistics and availability, this isn't preferred.

At PTB, an approach similar to the measurement of machine compliance in instrumented indentation testing is followed. A hardness reference block is indented at the same position multiple times until the Rockwell hardness value reaches its maximum and stays constant even upon further indentation (approx. 10 indents). The force and displacement values of the final indentation are used to determine the stiffness. Repetitive indentations ensure that surface effects such as roughness, unevenness etc. and material plasticity are compromised. Furthermore, a large spherical indenter and high loads are preferred to reduce errors due to non-ideal indenter geometry and to capture maximum hysteresis effects respectively [5]. Assuming the deformation in the machine parts are purely elastic, these can be quantified using Hooke's law. The measured depth is a combination of the machine deformation and the material-indenter interaction. This can be modelled as two springs in series [6]. The material-indenter interaction follows the Hertzian theory of contact:

$$\delta = \left[\frac{3}{4E^*}\right]^{2/3} F^{2/3} R^{1/3} + F * S \qquad (2)$$

where,

δ is the measured depth [μm]

E* is the reduced indentation modulus [GPa]

F is the force [N]

R is the radius [μm] and

S is the machine stiffness [N/μm]

Considering two pairs of force and measured depth data enables the calculation of the machine stiffness without the knowledge of the indenter radius and the material properties. Care must be taken while interpreting the results as many assumptions such as purely elastic deformation in the entire system, a constant indenter radius and constant reduced indentation modulus at varying depths, etc. might not be correct.

4. Indenter Geometry

Another important aspect to be considered is the deviation of hardness measurement results caused by a deviation of the form of the indenter from the ideal geometry. However, due to manufacturing difficulties, deviations from the desired ideal geometry are unavoidable. Moreover, the indenter wears with progressing usage and changes its form gradually. Therefore, a precise measurement of the indenter geometry and appropriate correction factors are required to ensure worldwide comparability of hardness results. Fig. 3 shows the plot of the effective radius vs. depth for three used Rockwell hardness testing indenters EDK1, EDK2 and EDK3 obtained using a confocal laser scanning microscope. An ideal indenter of this kind is a sphero-conical diamond indenter with an opening angle of 120° and a radius of 200 μm at the tip. In the literature we find various approaches to correct the hardness deviations [7,8]. The finite element method supersedes most of them due to its ability to import the entire indenter topography into the simulation.

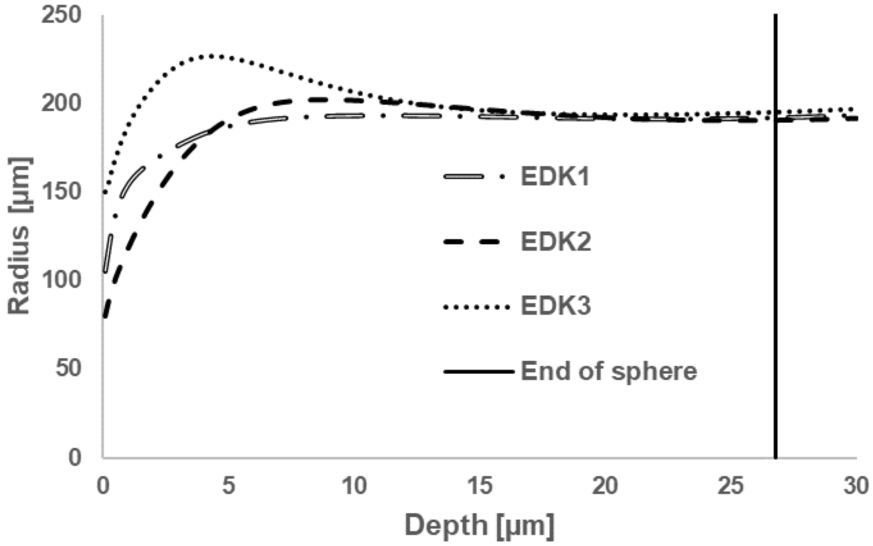

Figure 3: Measured tip radius vs. depth for three used indenters

5. Conclusion

This report provides a basic insight into the automation of Rockwell hardness testing machines. The developed method helps to perform measurements much more efficiently, simplifies the compliance with the necessary standards and eliminates the need for an expert user. The basic principle has been tested and implemented for a single Rockwell hardness scale. The report also highlights the need for the determination of machine stiffness and the importance of indenter geometry correction factors. Nonetheless, the impact of further factors such as surface roughness, type of material and surface detection still needs to be investigated.

References:

[1] Rockwell Hardness Measurement of Metallic Materials, Samuel R. Low, NIST Recommended Practice Guide, Special Publication 960-5, January 2001

[2] DIN EN ISO 6508-1:2014 (E) Metallic materials - Rockwell hardness test - Part 1: Test method

[3] D. Grziwotz, et al., Automation of the Rockwell standard measuring machine of the PTB, IMEKO international conference, 2017

[4] D. Grziwotz, Automation of a standard measuring device for Rockwell hardness tests, TU Braunschweig, Master thesis, 2016

[5] Anthony C. Fischer-Cripps, Nanoindentation, Springer-Verlag New York, 2004

[6] W.C. Oliver and G.M. Pharr, An improved technique for determining hardness and elastic modulus using load and displacement sensing indentation experiments, J. Mater. Res., Vol. 7, No. 6, June 1992

[7] D. Schwenk and D. Dengel, Zum Einfluß der Eindringkörperform auf die Rockwell Härte, Härtereitechnische Mitteilungen, Ausgabe 54, Heft-Nr. 6, S-385-391, 1999

[8] G. Dai et al., Progress in the Characterization of the geometry of Rockwell diamond indenters, XIX IMEKO World Congress, 2009

Dimensional Characterization and Effective Area Estimation of the 35 mm Piston/Cylinder Assembly - PG0806

Yulieth Fernanda Gutiérrez León - David Alonso
Plazas Fernández - Mayckol Jesid Morales Castro
Instituto Nacional de Metrología - INM,
Bogotá D.C., Colombia
Phone: 57 315 543 99 60 Fax: 571 254 22 22
Email: fernanda.ferguti@gmail.com

Abstract

Piston/cylinder assemblies are widely used in the calibration of pressure measuring equipment whose principle of operation is to generate pressure by positioning non-standard weights, which generate radial forces when compressing the fluid. The pressure can be determined by knowing the combined mass of the weights, the local acceleration of free fall and the effective area of the piston/cylinder assembly. Often the effective areas are determined through a calibration to another piston gauge or from dimensional measurements; we are going to develop the second method. The dimensional characterization of the piston/cylinder assemblies is fundamental to the realizations the pressure measurement made with piston/cylinder assemblies. There diameter, straightness and roundness measurements were made for the PG 0806 of the pressure laboratory of the INM - Colombia, both for the cylinder and the piston itself. To do this measurement the Brown & Sharpe coordinate measuring machine (CMM) of the dimensional laboratory of the INM was used. With the measuring method described, we were capable to measure the effective area with a relative uncertainty about 9.7x10^{-5}.

1. *Relevance in terms of* its scientific and practical meaning

The present investigation is relevant for the realization of the pressure scale, because with the geometric method the value of the effective area of the PG0806 piston/cylinder system is obtained thanks to the roundness and diameter measurements. Moreover, together with the determination of the coefficient of deformation, the area of the piston/cylinder system is then obtained and, knowing the mass of the set of weights, the pressure value is obtained. Here is the importance, that it would no longer be required to send the pressure standards to be calibrated by the Physikalisch Technische Bundesanstalt (PTB) as it has the primary standard. Now the PG0806 piston/cylinder assembly will be the primary standard of the pressure laboratory of the Nacional Institute of Metrology (INM) - Colombia, which reduces time and costs in guaranteeing metrological traceability.

2. Purpose of the paper

The procedure to determine the effective area of piston-cylinder assemblies from the dimensional properties of the pistons and cylinders is very well documented [1], for the straightness, roundness, and diameters, and the contributions to the uncertainty of them should be determined [1]. Therefore, the purpose of this paper is to determine the effective area with the geometric method. The measurement of the dimensional properties of diameter and roundness of the PG 0806 were made with the coordinate measuring machine (CMM) Global Performance size 07.10.07 [3]. The selected stylus tip was a ceramic hemispherical 18 mm diameter [4].

3. Scientific novelty or practical (applied) significance

By developing the method to realize the dimensional characterization to calculate the effective area of the PG 0806 of the INM Pressure Laboratory a new branch of dimensional metrology has been developed.

A method to measure the effective area for the PG 0806 was successfully developed, unfortunately the uncertainty of the measure is too high to allow a geometric realization of the Pascal. Nevertheless, with data from higher precision machine it would be possible to reach the desired uncertainty, because with the coordinate measurement machine the accuracy is 2 x 10^{-3} mm.

4. Tasks

In order to measure the diameter and roundness both for piston and cylinder the CMM Brown & Sharpe model 07.10.07 Performance was chosen. The diameter of the cylinder was measured from top to button at the heights: [1, 4.25, 11.25, 14.75, y 18.25] mm. Each circumference was measured three times with: 36, 72, 84, 96, 108 and 120 contacts each. The diameter of the cylinder was measured from top to bottom at this heights: [3, 6, 9, 12, 15, 18, 21, 24, 27, 30, 33, 36, 39, 42, 45, 48, 51, 54, 57] mm [1], as can be seen on Figure 1. With this data the roundness can be determined. Each circumference was measured three times with 120 points. The environmental conditions of the measurements were: ambient temperature between 19 °C - 21 °C and relative air humidity between 40% to 60 %.

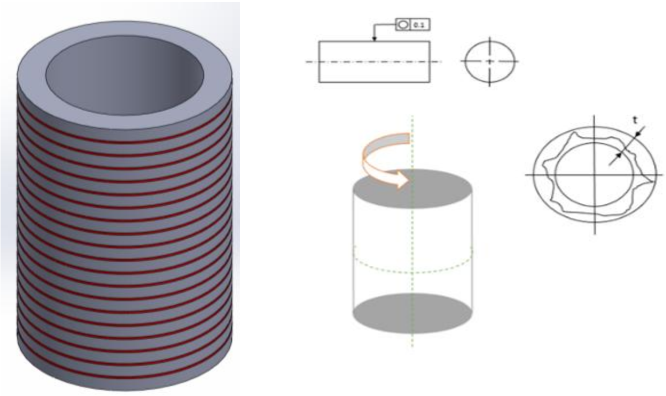

Figure 1. Heights for the roundness measure.

5. Description of the paper

5.1. Effective area by geometric measurement.

The effective area of the piston cylinder assembly is assumed to be the average between piston and cylinder:

$$A_0 = \frac{(A_{0c} + A_{0p})}{2} \quad (1)$$

Where A_{0p} is the mean piston cross sectional area and A_{0c} is the mean cylinder cross sectional area. Both are calculated by using the equation:

$$A_{0c,p} = \pi \frac{d^2{}_{c,p}}{4} \quad (2)$$

Where $d_{c,p}$ is the inner diameter of the cylinder or the external diameter of the piston. For the uncertainty budget we use the equation 3 [5]:

$$\frac{u(A_0)}{A_0} = \left[\left(\frac{u_d(A_0)}{A_0}\right)^2 + \left(\frac{u_{nr}(A_0)}{A_0}\right)^2\right]^{\frac{1}{2}} \quad (3)$$

Where $u_d(A_0)$ is calculated by using the equation 4:

$$\frac{u_d(A_0)}{A_0} = \frac{\sqrt{u_p^2 + u_c^2}}{2R_0} \quad (4)$$

Where u_p and u_c are the uncertainties of the piston and cylinder measurement, respectively. Finally, $u_{nr}(A_0)$ is the uncertainty due to the lack of roundness and is obtained from equation 5:

$$\frac{u_{nr}(A_0)}{A_0} = \frac{\sqrt{u_{nr\,p}^2 + u_{nr\,c}^2}}{2R_0} \quad (5)$$

5.2 Measurements

5.2.1. Cylinder Measurements.

The mean values of the cylinder diameter at different heights. Whereas contacts number has an impact about the spend time to get a measure, the uncertainty does not change significantly when the contacts number are 36 or 120. The average diameter of the cylinder with 36 contact is 35.334 4 ± 0.003 4 mm. Twelve sources of uncertainty were considered for that measurement.

5.2.2. Piston Measurements.

The mean values of the piston diameter at different heights with 120 contacts. The mean diameter is 35.332 8 mm.

6. Results

6.1 Effective Area

The effective area of the piston cylinder assembly is calculated using Equation 2 with the mean values of the diameters of the cylinder and the piston taken from the Table 1 and Table 2 with 84 and 120 number of contacts each, the area values are in the Table 1:

Table 1. Mean diameter and area for Piston and cylinder

Piston		Cylinder	
d (mm)	Sd (mm)	d (mm)	Sd (mm)
35.332 8	0.000 2	35.334 4	0.000 4
Area (mm^2)	Sd (mm)	Area (mm^2)	Sd (mm)
980.496 4	0.011 7	980.585 2	0.000 4

Starting from the Equation 1 and using the values of the area of the piston and cylinder, the effective area was calculated by 980.540 7 mm^2. The known cross-floating effective area (PTB 2007) is 980.533 mm^2, then there is a difference of 0.008 mm^2.

6.2 Effective Area Uncertainty.
From equation 3 the uncertainty of the effective area was calculated, see Table 2.

Table 2. Variables for the determining the uncertainty of the effective area.

Quantity	Symbol	Value
Coverage factor	k	2
Piston Diameter Combined Uncertainty	u_p	1.7×10^{-3} mm
Cylinder Inner Diameter Combined Uncertainty	u_c	1.7×10^{-3} mm
Cylinder Roundness Combined Uncertainty	u_{pr}	1.65×10^{-3} mm
Piston Roundness Combined Uncertainty	u_{cr}	1.7×10^{-3} mm
Diameter Uncertainty	u_d	6.87E-05 $\times 10^{-3}$ mm
No Roundness Uncertainty	u_{nr}	6.77E-05 $\times 10^{-3}$ mm

Then the effective area relative uncertainty is 9.64 x 10^{-05}.

References:

[1] S. R. Gonzales, Desarrollo de un Nuevo patrón nacional de presión. Desde la columna de mercurio a patrones primarios de vacío., Valladolid: Universidad de Valladolid: Escuela de Ingenierías Industriales, 2011.

[2] V. Ramnath, "Experimental measurement of pressure balance distortion coefficient characterization. Application of an electrical capacitance technique.," [Online]. Available: https://vramnath.files.wordpress.com/2012/10/nmisa-11-0184.pdf.. [Accessed 29 September 2011].

[3] C. M. - M. Inc., "CMMXYZ Canadian Measurement-Metrology Inc.," [Online]. Available: https://www.cmmxyz.com/cmm-scanning-probes.html?ditto_paginate=0&ditto_display=all. . [Accessed Marzo 2018].

[4] R. a. i. TM, Palpadores de presición, Barcelona, 2009.

[5] F. Sharipov, Y. Yang, J. E. Ricker and J. H. Hendricks, "Primary pressure standart based on piston-cylinder assemblies. Calculation of effective cross sectional area based on rarefied gas dynamics.," *Metrologia,* pp. 1177-1184, 2016.

[6] D. Flack, "National Physical Laboratory," May 2014. [Online]. Available: https://www.npl.co.uk/special-pages/guides/gpg41_cmm. [Accessed 22 August 2019].

Methods for researching the absolute value of the spectral irradiance of standard lamps

Kateryna Hovorova, Mykola Huriev,
National Scientific Centre "Institute of Metrology",
61002, Ukraine, Kharkiv, Myronosytska Str., 42, +38 057 700 34 47,
E-mail: nickgurev@gmail.com,
english.beatles2015@gmail.com

Abstract
This paper describes the method for studying the absolute value of the spectral irradiance of OSRAM FEL standard lamps based on the use of the filter radiometer developed at NSC "Institute of Metrology". The method reduces the measurement uncertainty.

1. INTRODUCTION

Measurements of the absolute value of the spectral irradiance are necessary for the calibration of spectrometers and other measuring instruments, which are widespread in such areas as medicine, industry, and others. Therefore, reducing the measurement uncertainty is an actual task.

A widespread method for measuring the absolute value of spectral irradiance is the method using a spectrometer, which has a significant measurement uncertainty and low stability due to the design features of spectrometers. Therefore, for accurate measurements of the absolute value of spectral irradiance from OSRAM FEL reference lamps (widely used for storing and transferring spectral irradiance units), it is necessary to simultaneously calibrate the spectrometer using an absolute black body. For this, it is necessary to install a diffuser on the entrance slit of the spectrometer monochromator, which significantly reduces the signal level, for increasing of which it is necessary to expand the entrance slit of the monochromator, and this leads to an increase in the measurement uncertainty.

To reduce the measurement uncertainty of the absolute value of spectral irradiance, the measurement method with a filter radiometer can be used [1], this method is not as popular as the first one and has own drawbacks, the elimination of which is the focus of this work.

2. DESCRIPTION OF THE METHOD AND EQUIPMENT FOR MEASURING THE SPECTRAL IRRADIANCE

2.1 Measurements of the relative irradiance of OSRAM FEL lamps

To study the relative value of the spectral irradiance of FEL lamps at the NSC "Institute of Metrology", we used the spectrometer based on MSA-130 dual monochromator and detectors based on Hamamatsu 1337-1010 BQ photodiodes (250 nm – 1100 nm) and Hamamatsu G12183-010K (1100 nm – 2500 nm), the scheme is shown in Figure 1.

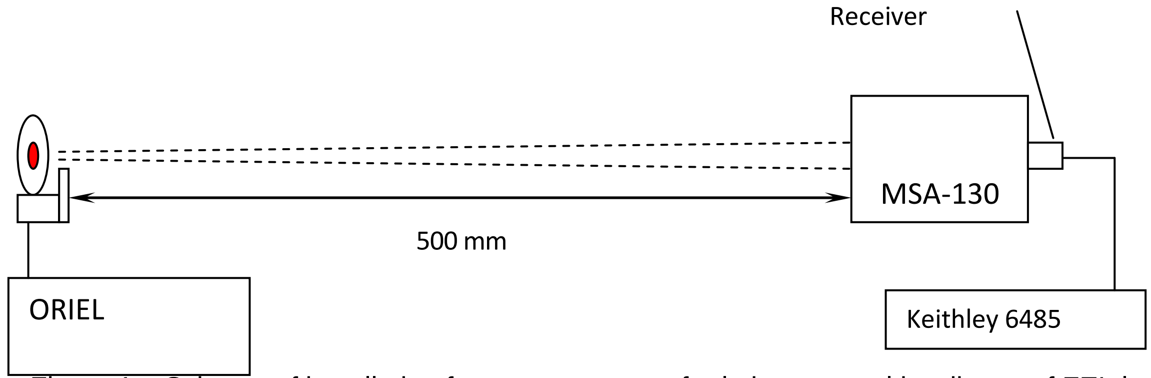

Figure 1 – Scheme of installation for measurement of relative spectral irradiance of FEL lamps

The results of the study of the relative value of the spectral irradiance of FEL lamps are shown in Figure 2

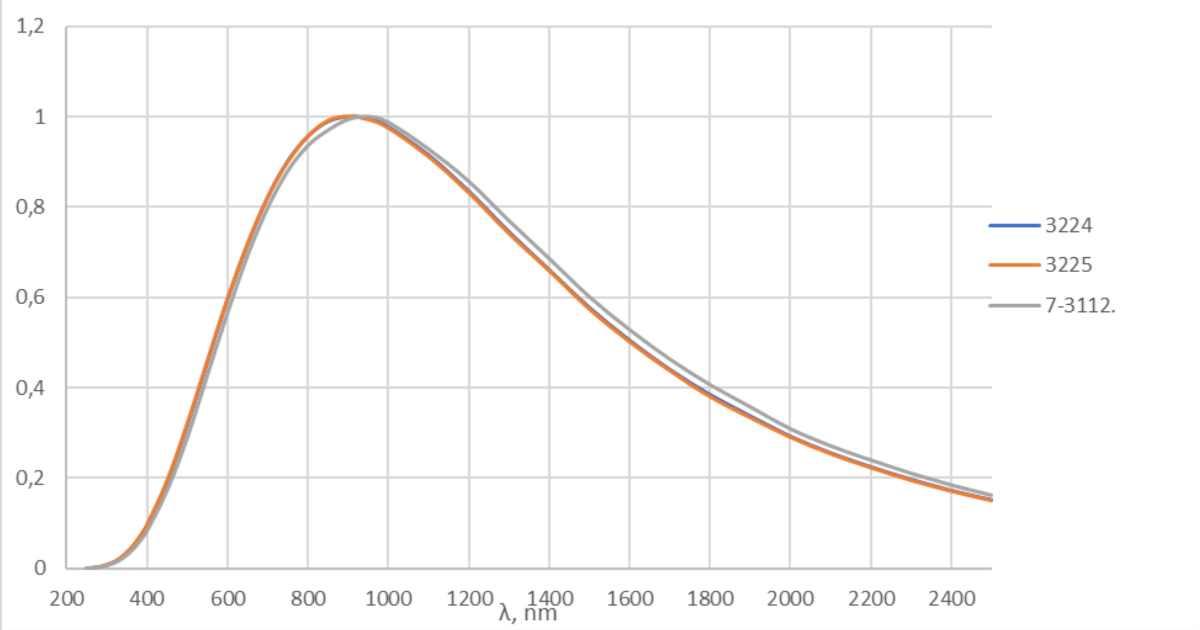

Figure 2 – Graph of relative spectral irradiance of FEL lamps

As can be seen from the above results, the relative spectral characteristic has a flat area in the range from 840 nm to 940 nm. Measurements with a filter radiometer in this area makes it possible to significantly reduce the measurement uncertainty of the absolute value of spectral irradiance caused by the measurement uncertainty of the spectral characteristics of the filter radiometer associated with the accuracy of setting the wavelengths of the monochromator and its slit width at the input and output.

2.2 Design and research of the filter radiometer

To study the absolute value of the spectral irradiance of FEL lamps, the filter radiometer was developed at the NSC "IM" which based on the trap-detector with Hamamatsu 1337-1010 BR photodiodes, filter turret from Newport with a bandpass filter with nominal value of 900 nm and a 4.3 mm aperture. The external view of the filter radiometer is shown in Figure 3.

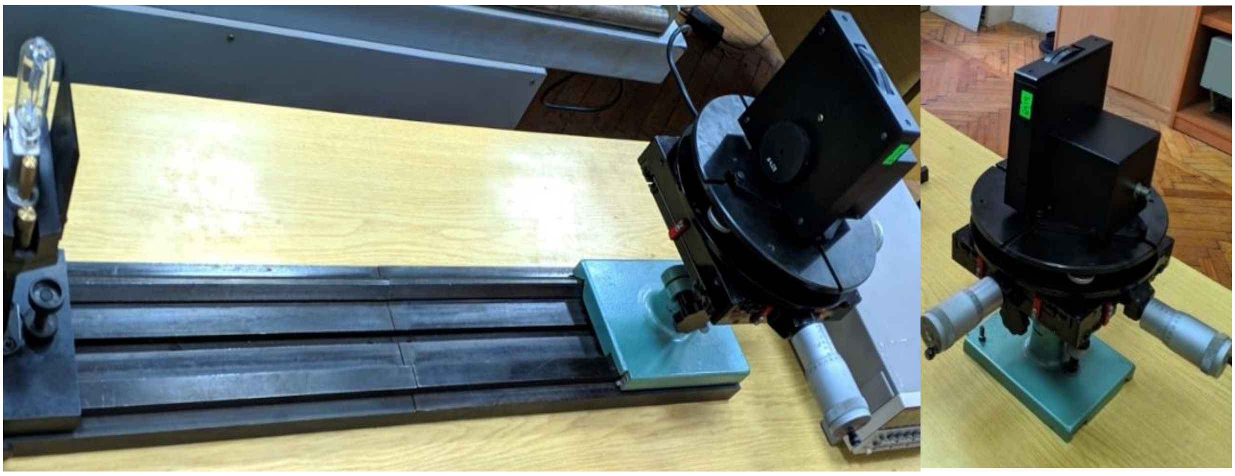

Figure 3 – Filter radiometer with spectral sensitivity in the spectral area of 900 nm

A filter radiometer in this design eliminates the component of the uncertainty of measurement, which is associated with the re-reflection of radiation between the filter and the receiver. The study of the bandpass filter was carried out using the National primary standard of the units of spectral coefficients of regular transmission, regular and diffuse reflection in the wavelength range from 0.2 μm to 25.0 μm DETU 11-09-08. The study of spectral sensitivity of the trap-detector was carried out using the National primary standard of the units of spectral density of the radiance, spectral density of radiant intensity and spectral density of irradiance, of the radiant power and irradiance DETU 11-06-06. The results of the spectral sensitivity study are shown in Figure 4.

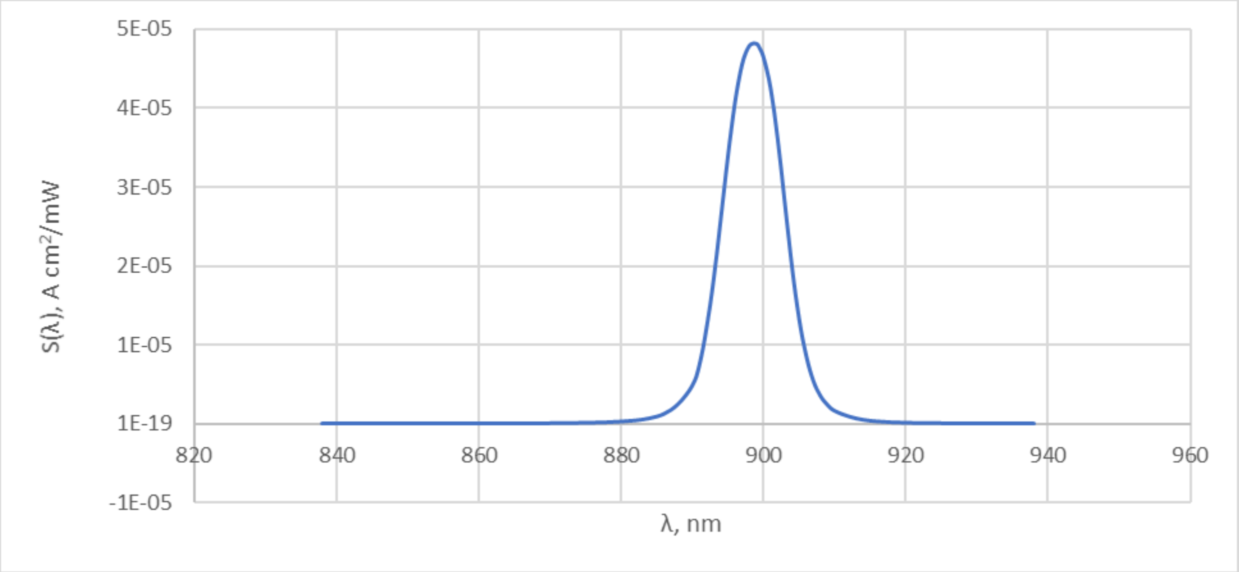

Figure 4 – Graph of the study of spectral sensitivity (A·cm^2/mW) of the filter radiometer with the bandpass filter with a nominal value of 900 nm

2.3 Installation and method of research of the absolute value of spectral irradiance of FEL lamps

The scheme of the Installation for measuring the signal with the filter radiometer at the wavelength of 900 nm from the FEL lamp is shown in Figure 5.

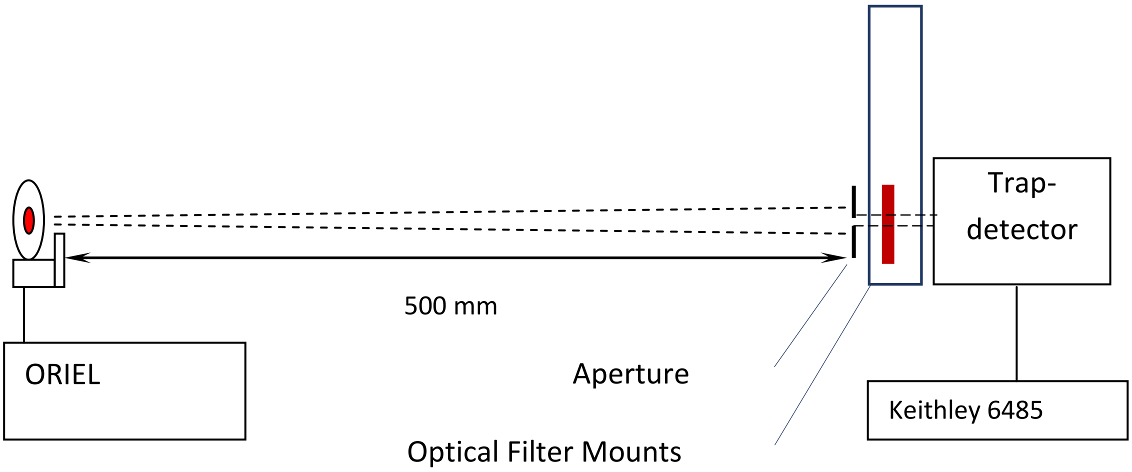

Figure 5. Scheme of the installation of measuring the signal of the filter radiometer (with bandpass filter with the nominal value of 900 nm) from a FEL lamp

On the basis of the signal from the FEL lamp measured by the filter radiometer, the absolute values of the spectral irradiance are calculated for the entire range according to formulas 1-3:

$$I = \int_0^{\infty} E_{max} \cdot E(\lambda)_{rel} \cdot S(\lambda) d\lambda \tag{1}$$

$$E_{max} = \frac{I}{\int_0^{\infty} E(\lambda)_{rel} \cdot S(\lambda) d\lambda} \tag{2}$$

where I is the signal (current, A) of the filter radiometer, E_{max} is the maximum value of the spectral irradiance from FEL lamps, $E(\lambda)_{rel}$ is the relative value of the spectral irradiance from FEL lamps, $S(\lambda)$ is the spectral sensitivity of the filter radiometer.

The spectral irradiance of FEL lamps is calculated from the formula:

$$E(\lambda) = E_{max} \cdot E(\lambda)_{rel} \tag{3}$$

The combined standard uncertainty of measuring the spectral irradiance of the filter radiometer consists of sources, the names and values are given in Table.

Table – Budget of uncertainty of determination the maximum value of the spectral irradiance from FEL lamps E_{max}

Source of uncertainty	Value, %
Uncertainty of spectral transmittance measurements of the bandpass filter in the range from 838 nm to 938 nm	0.05
Uncertainty of trap-detector calibration measurements in the range from 838 nm to 938 nm	0.10
Uncertainty of measuring the aperture area of the filter radiometer	0.14
Combined standard uncertainty	0.18

The small value of the uncertainty E_{max} for OSRAM FEL lamps is due to a flat area of the relative spectral characteristics of the spectral irradiance lamps in the bandpass of the filter.

3 CONCLUSIONS

1. The method for measuring the absolute values of the spectral irradiance of illuminance using a filter radiometer was improved.
2. The use of a trap-detector in a filter radiometer as a receiver makes it possible to eliminate the uncertainty component associated with the re-reflection of radiation between the filter and the receiver.
3. Since the spectral sensitivity of a filter radiometer with a bandpass filter with the nominal value of 900 nm is in the flat area of the FEL lamps, this significantly reduces the components of measurement uncertainty associated with the setting of radiation wavelengths and the width of the monochromator slit.

REFERENCES:

1. CCPR K1-a Key Comparison of Spectral Irradiance (250 to 2500 nm). Final Report: p. 25, p. 82, p. 160, p. 198.

STANDARD REFERENCE MATERIALS OF FLUORESCENCE AND RAMAN SCATTERING BASED ON INORGANIC GLASSES AND THEIR APPLICATION FOR QUANTITATIVE ANALYSIS

T.A. Goidina, A.A. Yushina
All-Russian Research Institute of Optical and Physical Measurements, 119361, Russia, Moscow, Ozernaya str., 46
e-mail: **leighstranger@yandex.ru**, **t.goidina@yandex.ru**

Abstract

Standard reference materials of fluorescence and Raman scattering based on phosphate glasses, one of which was activated by terbium and europium ions, and the other by thulium ions, have been developed. Their fluorescence spectra measured on a spectrofluorometer and a Raman spectrometer are presented. The possibility of using the developed standard reference materials for correction of emission spectra measured on different spectrofluorometers, systematic monitoring and correction of the sensitivity fluctuations of instruments, as well as control the error of instruments on a wavelength scale during their testing and verification is shown. It has been proven that the standard reference materials have photostability and intense fluorescence in the range from 200 to 4000 cm^{-1} and can be used as a means of metrological support in Raman spectroscopy, namely for calibrating Raman spectrometers on the wavenumber scale and on the relative intensities of Raman peaks. The possibility of using the developed standard reference materials for quantitative analysis without building a calibration graph by establishing a correspondence between the intensities of the peaks on the spectra of fluorescence or Raman scattering of standard reference materials and the intensities of the peaks on the spectra of analytes with further calibration of the selected peaks in units of the concentration of the measured substances is considered.

Relevance Fluorescence spectroscopy is used increasingly for the control of medicines and food products, in medical diagnostics and environmental monitoring. The advantages of these methods are the non-destructive nature of the control, the minimum requirements for sample preparation, the possibility of rapid analysis and the relative availability of equipment. However, the use of these methods for quantitative and, in many cases, qualitative analysis is hindered by the hardware dependence of the spectra measured by Raman and fluorescent spectrometers. The shape of the spectrum and the intensity of the lines depend on the device which they were measured. Standard reference materials are required to ensure the hardware independence of the fluorescence and Raman spectra. Until recently, there were used liquid solutions, that have a limited service life, require special storage conditions and are prone to photodegradation. The use solid samples for this purpose has so far been very limited. The development of new approaches to the creation of such standard reference materials and the expansion of their application is an actual problem.

The purpose of this work was to develop standard reference materials based on inorganic glasses suitable for calibration on the spectral and photometric scales of both fluorescent and Raman spectrometers. This is one of the elements of the novelty of the approach implemented in the work. Other elements of novelty were the presence of several narrow spectral lines in the developed standard reference materials in a fairly wide range (less then 10 nm), as well as the possibility of using the standard reference materials for calibration on the concentration scale in quantitative analysis. To solve these problems, together with ITMO University (St. Petersburg), two special fluorescent glasses based on a phosphate matrix were developed. One of the glasses was activated by europium and terbium ions, and the other by thulium ions.

The optical properties of the standard reference materials, including their fluorescence spectra, were studied on an SFF-2 Fluoran spectrophotometer/fluorimeter (developed in the All-Russian Research Institute of Optical and Physical Measurements). To refine the calibration procedure for Raman spectrometers, an InSpektr R 532 Raman luminescence spectrometer (developed by InSpektr,Ltd, Russia) was used. The results are described in [1].

Ensuring the uniformity of measurements of the fluorescence spectra

The fluorescence spectrum of the standard reference materials based on terbium and europium at an excitation wavelength of 365 nm, which is optimal for it, contains nine rather narrow (about 10 nm) and clear spectral lines in the range of 400–730 nm (Figure 1). In turn, the fluorescence spectrum of the standard reference materials based on thulium at an excitation wavelength of 358 nm, which is optimal for it, contains four lines in the range of 500–850 nm (Figure 2).

The standard reference materials can be used to correct the fluorescence spectra measured on various spectrofluorometers, as well as to systematically monitor and correct the sensitivity fluctuations of the instruments. This makes it possible to bring the spectra to a instrument-independent form, thus ensuring the unity of measurements in fluorometry. Another application of the standard reference materials is the control of the error of spectrofluorometers on the wavelength scale during their testing and verification. The most intense peaks of standard reference materials based on terbium and europium ions were calibrated in relative fluorescence units (RFU) corresponding to the set values of the concentration of sodium fluorescein, a known fluorescent dye. Similarly, a correspondence can be established between the peak intensities on the fluorescence spectra and the concentrations of other substances of interest to a particular laboratory. It will allow using measures to conduct a quantitative analysis without building a calibration graph for comparison solutions.

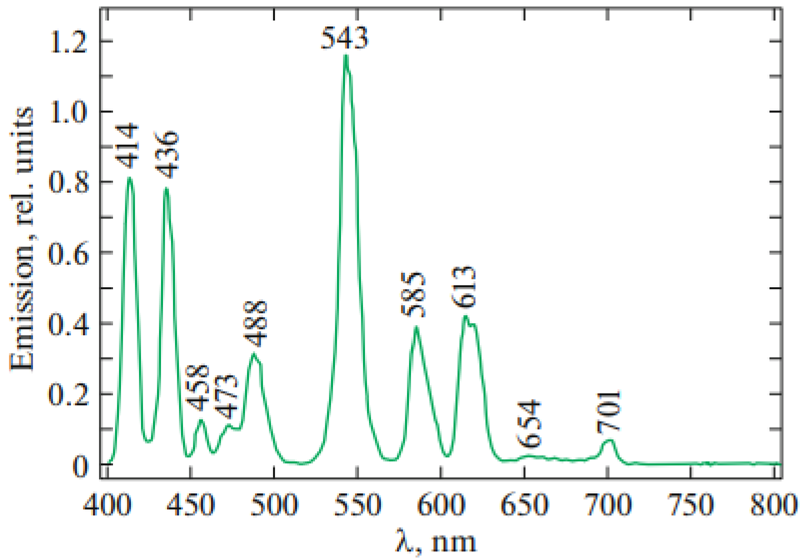

Figure 2 - Emission spectrum of the fluorescence standard reference materials based on phosphate glass activated with europium and terbium ions

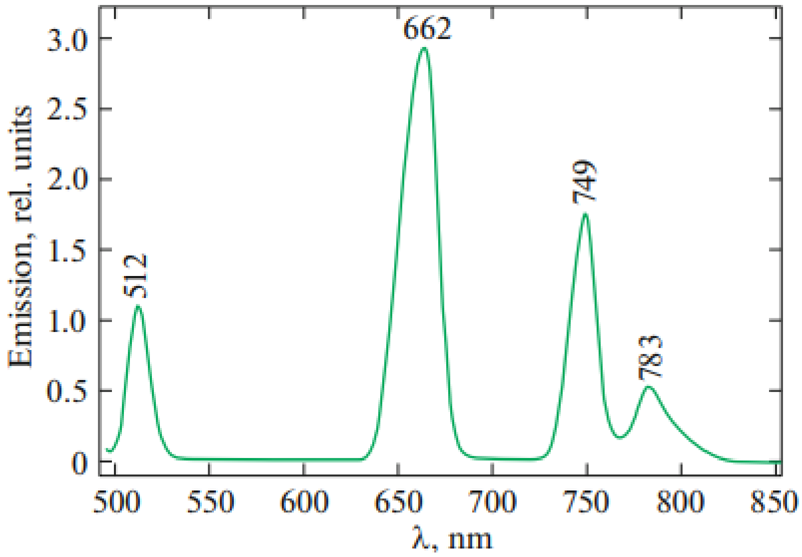

Figure 3 - Emission spectrum of the fluorescence standard reference materials based on phosphate glass activated with thulium ions

Ensuring the uniformity of measurements of Raman spectra

The increasing use of Raman spectroscopy for the qualitative and quantitative analysis of substances and materials requires the measurement of accurate and instrument-independent spectra. This is particularly useful for the detection of substances by comparing the experimental Raman spectra with the library. In this case, it is necessary to compare the spectra measured on different instruments.

The possibility of using the developed fluorescence standard reference materials as a means of metrological support in Raman spectroscopy was investigated. For this purpose, the fluorescence spectra of both standard reference materials discussed above were measured by the "Inspector R 532" spectrometer, in which the Raman spectra are excited by a laser at a wavelength of 532 nm. The results are shown in the wave number scale (Figure 3, Figure 4).

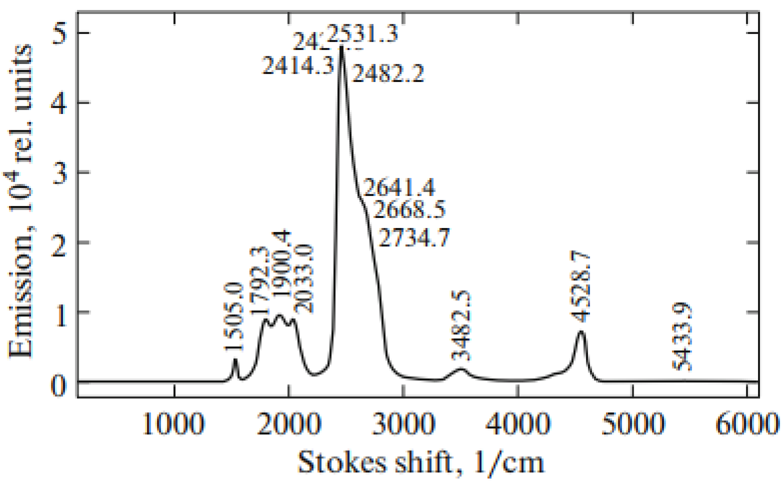

Figure 4 - Fluorescence spectra in the scale of Stokes shifts for a standard reference materials based on phosphate glass activated with terbium ions

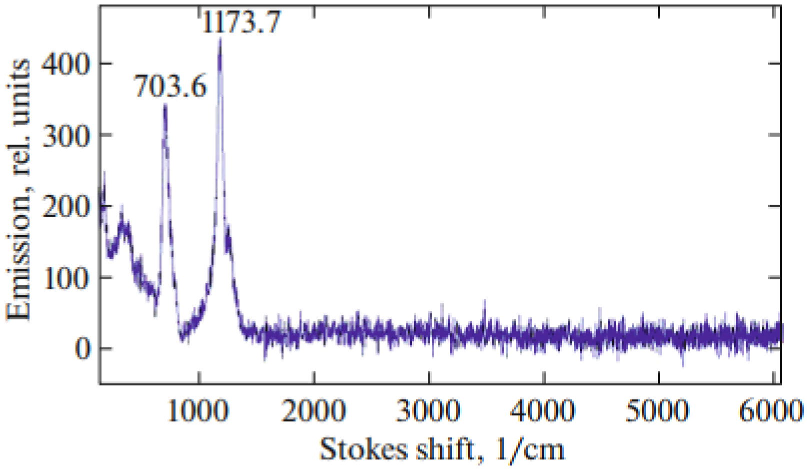

Figure 5 - Fluorescence spectra in the Stokes shift scale for a standard reference materials based on phosphate glass activated with thulium ions

The provided spectra show that the standard reference materials together reproduce peaks in the range from 200 to 4700 cm^{-1}, in the region where Raman shifts of the majority of interesting substances are observed. Multiple measurements carried out with standard reference materials of both types have shown that the intensity of all recorded peaks remains unchanged. This indicates the photostability of the investigated standard reference materials when exposed to laser radiation that is used for excitation of Raman spectra. These results indicate the possibility of using the developed standard reference materials also for calibrating Raman spectrometers with respect to both the wavenumber scale and the shape of the spectra, i.e., on the basis of relative spectral sensitivity.

In addition, a relationship can be established between the intensities of the peaks on the spectra of the standard reference material and the peaks on the spectra of specific substances measured on the same Raman spectrometer or microscope. Thus, the selected peaks can be calibrated in units of the concentration of these substances. It will allow for quantitative analysis using Raman spectra, similar what was described above for fluorescence spectra.

Currently, this approach is used in the development of a nanosensor system based on SERS (surface enhanced Raman scattering) using silver nanoparticles, for the detection and quantitative determination of reduced glutathione in biological fluids. It is a low-molecular compound that plays an important role in the vital activity of the body and can act as a marker of ischemic stroke and a number of other diseases. The operation concept of this system consists in the interaction of reduced glutathione molecules with the surface of silver nanoparticles, which leads to the charge transfer between the metal surface and the analyte molecules adsorbed on it and the appearance of intense spectral scattering lines of reduced glutathione.

Figure 5 shows the SERS spectrum of reduced glutathione in aqueous solutions in the concentration range from 0 to 100 μM, measured on a Confotec NR500 scanning laser Raman microscope (manufactured by SOL Instruments, Belarus).

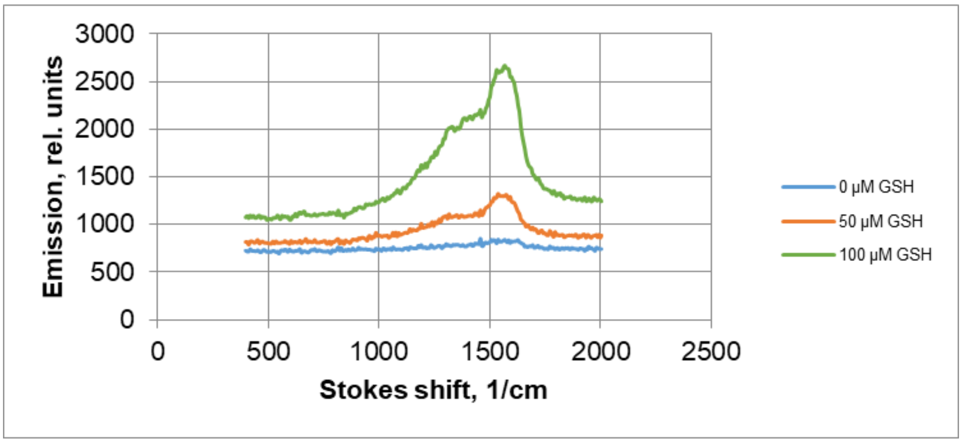

Figure 6 - SERS-spectrum of reduced glutathione aqueous solutions, measured on a Confotec NR500 Raman microscope

Figure 6 shows the spectrum of the standard reference material described above based on phosphate glass activated with europium and terbium ions, measured on the same microscope under the same conditions.

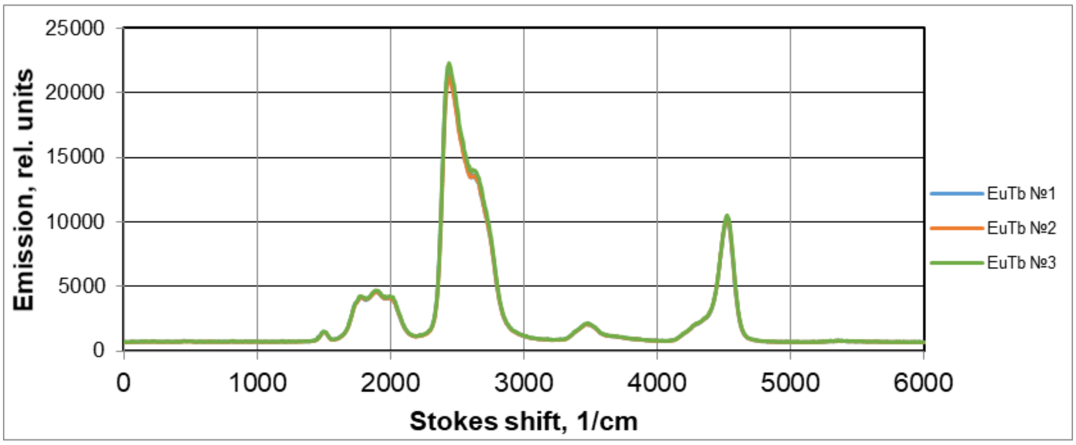

Figure 7 - The spectrum of the standard reference material based on phosphate glass activated by europium and terbium ions, measured on a Confotec NR500 Raman microscope

Comparison of these spectra will allow approximate calibration of the selected peaks on the spectra of the standard reference material in units of reduced glutathione concentration. The results of this calibration can be used to estimate the concentrations of this analyte from the Raman spectra of new samples without using of calibration splutions.

Conclusions

Two types of fluorescence standard reference materials based on phosphate glass activated by metal ions have been developed. The standard reference materials can be used to calibrate spectrofluorimeters and Raman spectrometers on the spectral and photometric scales, as well as to facilitate quantitative analysis of the fluorescence and Raman scattering spectra.

References:

1. Sadagov, A.Y., Goidina, T.A., et al. Spectral Standards Based on Glasses Activated with Rare-Earth Element Ions for the Calibration of Fluorescence and Raman Spectrometers. Opt. Spectrosc. 128, 1658–1666 (2020).

Investigation of methods for measuring the displaced volumes of gas-air environment

Shevel K. P., Bardonov A.I.
RUE "Belarusian State Institute of Metrology"
220053, Belarus, Minsk, Starovilensky tr., 93
tel. (375-017) 221-03-92
e-mail: bardonov@belgim.by

Abstract

The results of work on the implementation of the gravimetric method for measuring displaced volumes of gas-air environ are presented. This method is intended for measuring the volumetric flow rate during verification and calibration of measuring instruments, in particular, to reduce the uncertainty in measurements and increase the accuracy characteristics of the working standard. The previous and new (gravimetric) methods of measuring the displaced volumes of gas-air environ were investigated, and their comparative analysis was carried out, during which clear advantages of using the second method were observed. The gravimetric method made it possible to more accurately determine the displaced air volumes, which, in turn, made it possible to more accurately determine the volumetric flow rate. This made it possible to calibrate critical outflow Venturi nozzles, which expanded the range of calibrated measuring instruments, as well as auxiliary means at BelGIM. This was reflected in the metrological activities within the institution, in the economy of the country and society in general, and in ensuring traceability. Labor costs for carrying out work within the organization have decreased due to the departure from a large number of measuring procedures and calculations, which, as already mentioned, affects the accuracy of measurements.

To date, to ensure the procedure of verification or calibration of household gas meters, installations are used, which include measuring nozzles – the most important element of metrological control systems for household gas meters.

The relevance of this work is to obtain the possibility of calibration of critical flow Venturi nozzles (hereinafter referred to as nozzles), and, as a result, to expand the range of calibrated measuring instruments based on BelGIM.

Calibration of critical flow Venturi nozzles was previously only possible in Russia or Ukraine.

The purpose of this work is to study methods for measuring the displaced volumes of gas-air media to further improve the metrological characteristics of the installations used, and, thus, to expand the range of calibrated measuring instruments.

The objective of the work is a comparative analysis of studies of geometric and gravimetric methods by studying the metrological characteristics of the REOVG-004 installation using these two methods.

The practical significance of the gravimetric method lies in the fact that this method allows you to:

- move away from the geometric method, thereby repeatedly reducing the number of measuring instruments and labor resources used;
- more accurately determine the displaced volumes of air, thereby reducing the error in determining the volume flow itself.
- get the necessary margin of accuracy to calibrate the nozzles.

For metrological control of gas volume and flow measuring instruments, as well as auxiliary elements during measurements, a bell-type gas volume and flow unit REOVG-004 is used.

The principle of operation of the installation is based on the displacement of the volume of air due to the pressure created by the bell gauge, immersed in the liquid and moving under the influence of the measured pressure difference (the difference between the pressure under the bell and outside).

Metrological characteristics of the installation before using the new volume measurement method:

- Range of reproducible flow rates, m^3/h: from 0.016 to 2.5;
- Reproducible control volumes, m^3: 0.010; 0.020; 0.040;
- Confidence limits of the relative error of the volume flow measurement (P = 95), %: ±0,25;
- Confidence limits of the relative error of volume measurement (P = 95), %:

1. For a volume of 40.5169 dm^3 - ± 0.13;
2. For a volume of 20.1632 dm^3 - ± 0.13;
3. For a volume of 10.1045 dm^3 - ± 0.25.

It should be noted that on a small control volume, the measurement error is much higher than the values related to large volumes, which means that for calibration, for example, measuring nozzles with an error of 0.5%, there is no necessary margin of accuracy, and, accordingly, the ability to perform calibration. Thus, the main contribution to the uncertainty is made by measurements on a small control volume.

In the measuring unit REOVG-004, the volume flow values are expressed in terms of the values of the air volumes displaced from under the bell. When studying the metrological characteristics of this installation, it was revealed that the main contribution to the error in determining the volume flow rate is made by the geometric method of measuring the displaced air volumes. The disadvantage of this method is a large variety of measurement operations (Figure 1), which affects both the labor costs when performing these operations, and the measurement error of the displaced volumes. Due to the large measurement error, it was not possible to calibrate the nozzles, since a threefold margin of accuracy was required.

The values of measurement uncertainty volume in the installation of gas volume and flow rate bell type REAUG, in addition to addressing the components of the temperature, pressure, humidity, was determined by taking into account a set of measuring instruments for measuring geometric parameters of the installation, namely the geometric volume.

The geometric volume of the installation was determined by the calculation method based on the results of measurements of the dimensions of the bell, the installation body and the ruler. These measurements were carried out according to the following scheme:

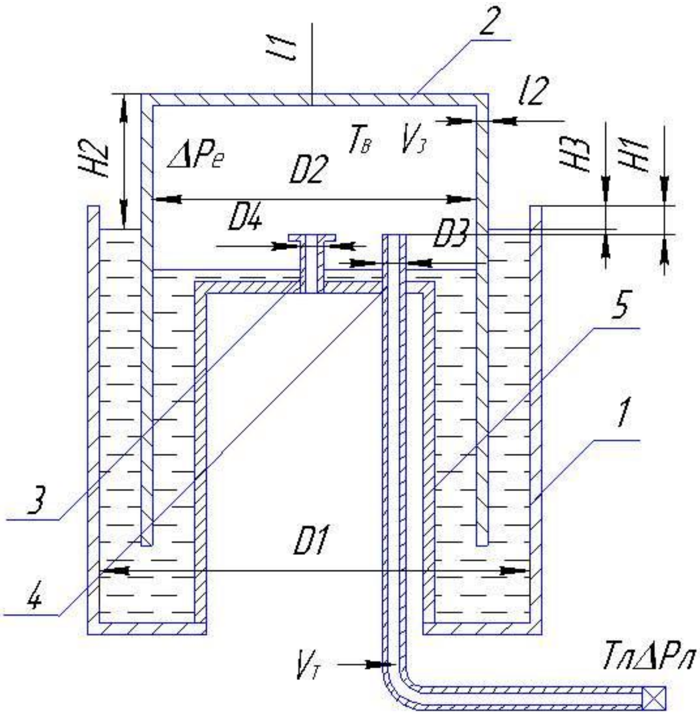

Figure 1 - Diagram of measuring the size of the bell in the “Stop " position”
Symbols: 1-installation body; 2-bell (measuring gauge);
3, 4 - outlet pipes of the displacer; 5 – the displacer

Studies were also conducted on the channels for measuring pressure, temperature, time, and liquid density in the installation.

Based on the results of all the above studies, the measured volume of air coming from under the bell to the counter input was calculated using the formula:

$$V_C = \frac{P_{Э} T_C}{P_C T_{Э}}\left(\frac{V_K \tau_C}{2\tau_K}\left(1+\frac{P_{1H}T_{1K}}{P_{1K}T_{1H}}\right)+\left(P_{И1H}-P_{И1K}\right)\left(2-\frac{P_{1H}T_{1K}}{P_{1K}T_{1H}}\right)A+\left(\frac{P_{1H}T_{1K}}{P_{1K}T_{1H}}-1\right)V_{ОСТ}\right),$$

$P_{Э}$ – the average value of the absolute pressure under the bell during the meter verification, Pa;

P_C – the average value of the absolute pressure in front of the meter during the meter verification, Pa;

$T_{Э}$ – the average value of the absolute temperature of the air coming out from under the bell during the meter verification, K;

T_C – the average value of the absolute air temperature in front of the meter during its verification, K;

P_{1H}, P_{1K} – initial and final absolute air pressure under the bell when checking the meter, Pa;

$P_{И1H}$, $P_{И1K}$ – the initial and final overpressure of the air under the bell when checking the meter, Pa;

T_{1H}, T_{1K} – the initial and final absolute temperature of the air at the top of the bell when checking the meter, K;

V_K – geometric volume of the bell, m^3;

A – correction factor for the change in the volume of air displaced from under the bell from the change in the overpressure under the bell, m^3/Pa;

V_{OCT} – the volume of air under the bell when it is at the "Stop " position, m^3;

τ_C – the time corresponding to the volume of air measured by the meter, s;

τ_K – the time corresponding to the movement of the bell between the slots on the the line, s.

Using the REOVG unit, the volumetric flow rate was determined through the volume of air displaced from under the bell.

Together with the speaker, a device was designed that allows measuring the displaced volume of air not by geometric, but by gravimetric method. The operating principle of the devices is as follows: gas pressure bell displaces the liquid density in a special container, which is weighed in the balance of high precision, which is why we're getting rid of a large number of measuring instruments and come only to the scales and density, which reduces the number of factors influencing the accuracy and uncertainty.

The gravimetric method was used to determine the values of the displaced volume of air, reduced to the required parameters, for a single observation, according to the formula:

$$V_i = \left(\frac{k_V \cdot m_И}{\rho}\right) \cdot \frac{t_i}{293.15} + \delta\overline{V_i}$$

where $\delta\overline{V_i}$ is the correction due to the spread of the measured volume values, m^3;

$m_и$ – the measured value of the mass of the liquid according to the indications of the balance, kg;

k_V – the coefficient of correction of the water mass, due to the difference in the value of the ejection force when calibrating the weighing mechanism with weights and when weighing the equivalent mass of water, is calculated in accordance with Annex D of OIML 111;

ρ – measured value of the density of the liquid displaced from the measuring gauge, kg/m^3;

ti - the measured value of the temperature on the calibrated SI during the i – th observation, K.

The uncertainty of the volume measurement is taken into account when calculating the uncertainty of the flow measurement.

The error of reproduction by setting the unit volume of air is determined for each measured volume in%, according to the formula:

$$\delta_{V_C} = K \cdot \frac{\sqrt{S^2_{V_C} + \frac{1}{3}\theta^2_{V_C}}}{V_C} \cdot 100,$$

where S_{V_C} is the estimate of the COE of reproduction of the unit volume of air by the installation, m3;

θ_{V_C} – NSP - units of air volume.;

V_C – the volume of air transferred from the installation to the input of the meter to be checked, m^3;

K is a coefficient that depends on the ratio of random and non-excluded systematic errors.

Metrological characteristics of the installation during the use of the gravimetric volume measurement method:

- Range of reproducible flow rates, m^3/h: from 0.016 to 2.5;
- Reproducible control volumes, m^3: 0.010; 0.020; 0.040;
- Confidence limits of the relative error of the volume flow measurement (P = 95), %: ±0,16.

Conclusion

Studies of methods for measuring the displaced volumes of gas-air media are carried out.

A device has been developed to replace the geometric method with a gravimetric one.

Experimental studies of the influence of the gravimetric method on the metrological characteristics of measuring devices were carried out.

Using the gravimetric volume measurement method, the following results were achieved:

1. More accurate volume measurement;
2. Improvement of metrological characteristics, namely the relative error and uncertainty of measurements;
3. Expanding the range of calibrated SI and auxiliary devices based on BelGIM;
4. Reduction of labor costs for volume measurement.

References:

1) СТБ ISO 9300-2018. Измерение расхода газа с помощью сопел Вентури критического истечения. – 36 с.

2) ГОСТ 8.324. Счётчики газа. Методика поверки. – 7 с.

3) Жагора Н.А. Сборник трудов. Выпуск 5/Т.И. Дикун, Г.А. Вечер//Исследование метрологических характеристик установок объёма и расхода газа колокольного типа РЕОВГ: Сборник трудов БелГИМ. – Минск, 2007. – С. 25-34.

ANALYSIS OF MEASURING THE OIL DENSITY IN A PIPELINE

Kamalov Yessimzhan Ishanbekovich
KazTransOil JSC
Engineer of the Automated Control Systems for Technological Processes and Metrological Support Department.
e-mail: kamalov.e@kaztrancoil.kz

Abstract
The article analyzes the process of measuring the oil density in a pipeline using an automated density transducer, by collating it with a high-precision standard pycnometric installation. The purpose of this analysis is to evaluate in detail the given measurement and to expose the values that affect measurement accuracy adversely.

Introduction

When organizing a system for quantitative accounting of oil, the method that is widely spread is the direct method of dynamic measurements of the oil mass, on the basis of direct measurements of the oil mass using measuring instruments for the mass flow rate in pipelines. To control the metrological characteristics of a mass flow meter, calibration facilities (compact provers) are used, which, in its turn, work in conjunction with a density transducer to transfer the dimensions of the units of physical quantities. As a result, we encounter a situation in which the density converter, not having direct participation in the accounting process, nevertheless, is a key measurement tool for ensuring the accuracy of accounting the amount of oil.

In the proposed experiment, our goal is to determine the external factors affecting the measurement of oil density by an automatic density meter in transportation conditions, as well as to assess their value and contribution to the final result.

To measure the density of commercial oil, a modern density transducer with the double parallel tubes technology that vibrate at a frequency of its own fluctuations is equipped. Fluctuations may vary depending on the density of the liquid filling the tube (*Figure 1*).

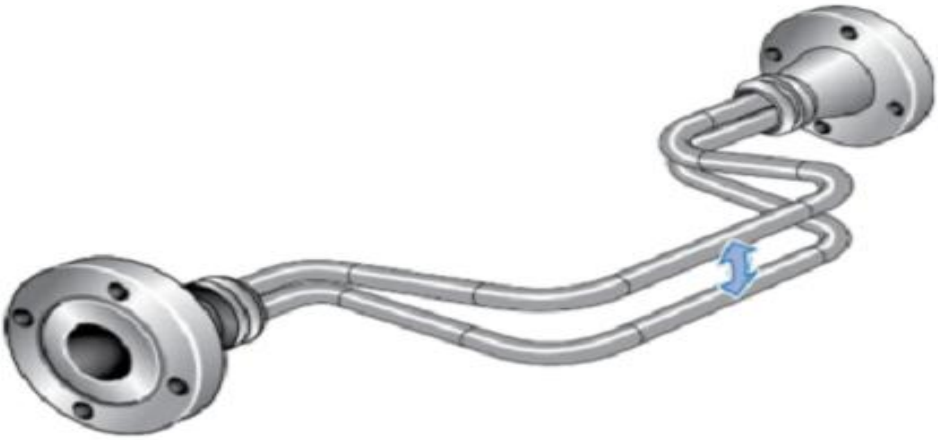

Figure 1. Parallel Tubes of a Density Meter.

The density transducer automatically measures the period between oscillations of parallel tubes and converts it to a density unit (kg/m^2) according to the calibration coefficients. The absolute permissible error of this density meter is $\pm 0.3\ kg/m^2$.

The work is carried out in the oil quality measurement block, through which the transported commercial oil is circulated from the main oil pipeline. The measurement conditions are shown in the table below:

Ambient Temperature	Temperature of the working environment (of oil)	Pressure in the pipeline
21 °C	29 °C	2,8 MPa

The density meter is installed on the technological pipeline inside the quality measurement block.

For the reading credibility of the densometer itself, it is opposed with the pycnometric installation in parallel, with an admissible absolute error of $\pm 0.1\ kg/m^2$. The given setup is connected to the conduit in series with the density meter through the outlets via flexible hoses, providing the circulation of oil through pycnometers without any excessive vibration. Additionally, a thermometer and a manometer are used to measure the conditions of the working environment simultaneously.

Measurements begin after oil parameters in the density transducer and pycnometers are stabilized, at the time when the change in oil temperature over time does not exceed $0.1\ °C/min$, the pressure change does not go over $0.05\ MPa/min$, and change in period is not beyond $0.02\ \mu s/min$.

Measuring and processing the results of pycnometers provided the following results:

Liquid Temperature		Liquid Pressure		Pycnometer's liquid density measurement	Average oscillation period	Densometer's liquid density measurement	Absolute error
in densometer t_d	in pycnometer t_p	in densometer P_d	in pycnometer P_p	ρ_p	T	ρ_d	$\Delta\rho$
$°C$	$°C$	bar	bar	kg/m^3	µs	kg/m^3	kg/m^3
32,0	**32,3**	**8,10**	**8,20**	**852,554**	**3673,281**	**852,652**	**0,098**

To determine the contribution of the selected factors to the initial result, the standard uncertainty of each variable was calculated:

Stages	**Varialbe**	**Calculations**		
Measurement process model		$Y = X_P + X_{DD} + X_M + X_t + X_{C20} + X_{C21}$		
Standard uncertainty in estimating input values	Density measured by pycnometer, X_P	$U_A(X_P) = \sqrt{\frac{\sum_{i=1}^{N}(X_{Pi} - X_{PC})^2}{(N-1)*N}} =$	0,000678215	kg/m^2
	Density Measurement with Temperature Corrected Flow Density Meter, X_{DD}	$U_A(X_{DD}) = \sqrt{\frac{\sum_{i=1}^{N}(X_{DDi} - X_{DDC})^2}{(N-1)*N}} =$	0,001380078	kg/m^2
	Absolute error of Manometer, X_M	$U_B(X_M) = \frac{X_M}{\sqrt{3}} =$	0,288675135	bar

	Absolute error of Thermometer, X_t	$U_B(X_t) = \frac{X_t}{\sqrt{3}} =$	0,115470054	°C
	Pressure Coefficient, X_{C20}	$U_B(X_{C20}) = \frac{X_{C20}}{2\sqrt{3}} =$	2,88675E-10	bar^{-1}
	Pressure Coefficient, X_{C21}	$U_B(X_{C21}) = \frac{X_{C21}}{2\sqrt{3}} =$	2,88675E-08	bar^{-1}

Budgeting uncertainty:

Value of X_i	Evaluation of X_i	Unit	Standard uncertainty $U(X_i)$	Unit	Type of uncertainty
1	2	3	4	5	6
Density measured by pycnometer, X_p	852,554	kg/m^3	-0,001	kg/m^3	A
Density Measurement with Temperature Corrected Flow Density Meter, X_{DD}	852,652	kg/m^3	0,03	kg/m^3	A
Absolute error of Manometer, X_M	0,5	bar	0,028	bar	B
Absolute error of Thermometer, X_t	0,2	°C	-0,090	°C	B
Pressure Coefficient, X_{C20}	0		0,008	bar^{-1}	B
Pressure Coefficient, X_{C21}	0,09710754		0,002	bar^{-1}	B
Probabilities Distribution	**Sensitivity Coefficients**	**Unit**	**Interest contribution,%**		
7	**8**	**9**	**12**		
Rectangular	-1	kg/m^3	0,01		
Rectangular	1	kg/m^3	9,13		
Rectangular	0,09710754	$kg/m^3/bar$	7,96		
Rectangular	-1,195882759	$kg/m^3/°C$	82,21		
Rectangular	6900,109369	$kg/m^3 * bar$	0,65		
Rectangular	8,10	bar	0,04		

Total uncertainty	Uc	0,099262279	kg/m^3
Expanded uncertainty	Up	0,198524558	kg/m^3

For visualization, a diagram featuring the contribution of sources (components) of uncertainty into total uncertainty was composed.

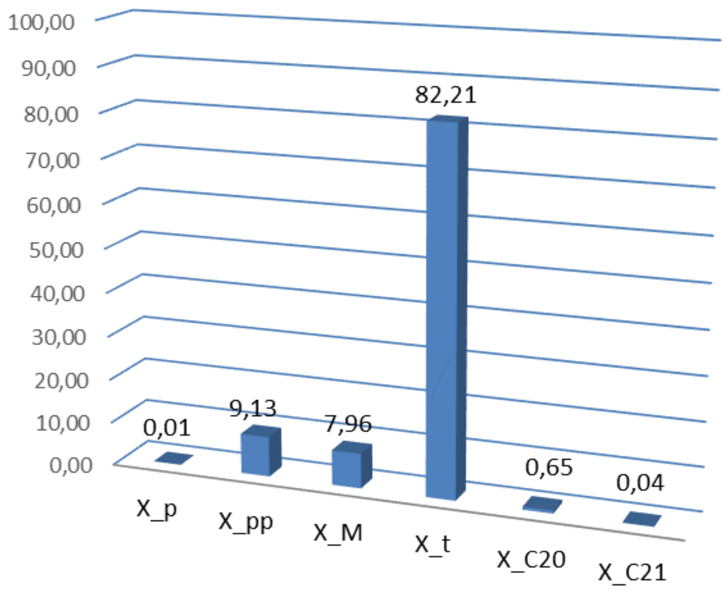

The density transducer, considering the corrections for the temperature change, showed an outstanding result - $0.03\ kg/m^2$, which fully meets the established metrological characteristics. Density meters of this design and construction minimize the impact of the work and ambient environments and deserve a high level of trust

Among the sources of uncertainty, the greatest impact (82.1%) was displayed by the accuracy of thermometer readings. This is a natural phenomenon since the slightest change in temperature and pressure is known to directly affect the density of the environment. This once again underlines the importance of using high-precision temperature instruments in the oil industry.

Reference:

[1] Standards of Republic of Kazakhstan 2.147-2008 «On-site verification methodology using a pycnometric setup. »

[2] RMG 43-2001 «State system for ensuring the uniformity of measurements. Application of the “Guide to the Expression of Measurement Uncertainty” ».

Development of a method and means of transferring a unit of absorbed dose of neutron radiation in a tissue-equivalent substance for devices used in radiation therapy

Sergey G. Fedorov
The Federal State Unitary Enterprise «Russian metrological institute of technical physics and radio engineering» − FSUE «VNIIFTRI», Mendeleevo, Moscow Region, Russia, 141570,
Mobile phone: +7 (903) 594-81-81
E-mail: fedorov911@gmail.com

Abstract

In this work, the authors provide a justification for the need to develop a method and means of transferring a unit of absorbed dose rate of neutron radiation to nuclear facilities used in neutron radiation therapy. A team of authors has studied and analyzed the main methods of neutron radiation registration in mixed gamma-neutron fields. Metrological and technical features that impose restrictions on the existing methods of reproduction and transmission of a unit of absorbed dose rate of neutron radiation are described. Work has been carried out on the design, development and manufacture of a meter of the absorbed neutron radiation dose rate for transferring a unit to nuclear installations. That was based on a registration unit, the operating principle of which is based on the scintillation method. The paper describes the design of the absorbed neutron radiation dose rate meter. Experimental studies of the components of the uncertainty budget of the transmission means during the transfer of a unit to nuclear facilities were carried out.

Introduction

For the purposes of radiation therapy, various types of ionizing radiation are used: photon (gamma and X-ray), proton, electron, neutron. The choice of a specific type of ionizing radiation is conditioned by the need to solve certain therapeutic problems. The type of radiation is chosen depending on the depth and the type of tissue where the damaged cells are located. In the case when damaged cells exhibit radioresistance to traditional types of radiation therapy (photon, proton) or remission occurs, neutron radiation therapy, namely fast neutron therapy, is used.

The success of radiation therapy depends on the accuracy with which the irradiated organ receives the specified absorbed dose of neutron radiation; it should not differ from the specified one by more than 5% [1-4]. If the absorbed dose received by the patient is less than necessary, then some of the malignant cells will not be destroyed. If the absorbed dose received by the patient exceeds the specified value, the ionizing radiation will harm healthy tissues, thereby aggravating the patient's condition [5]. This leads to very high requirements for the accuracy of measurements of radiation doses in medical practice and for the system of metrological support of these measurements. The dependences of the probabilities of healthy cells survival and malignant cells destruction during radiation therapy on the radiation dose are shown in Figure 1.

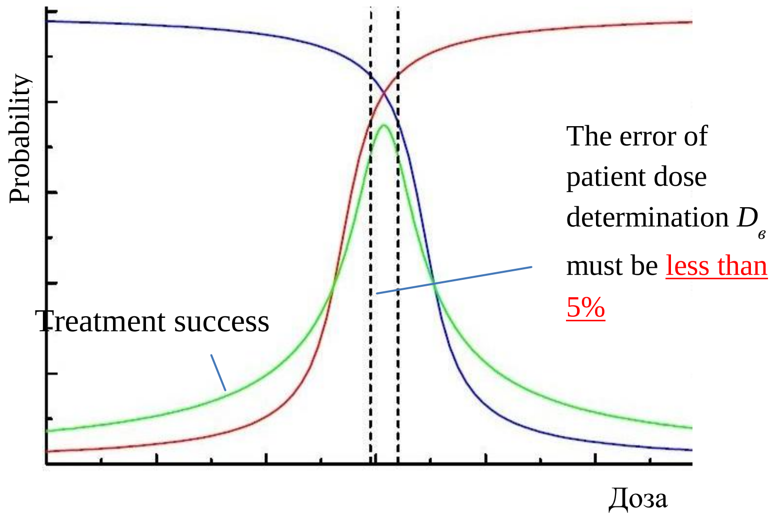

Figure 1 Dependences of the probabilities of survival of healthy cells and destruction of malignant cells on the radiation dose

Analysis of medical statistics [6] shows that the number of people registered in oncological institutions was about 4 million in 2018. The prevalence of malignant neoplasms is 2561 per 100,000 of the population. In 2018, 624,709 new cases of malignant diseases were detected in Russia. Among them, women accounted for 54% and men for 46%. The number of cases over the past ten years has increased by more than 27%. Analysis of the morbidity statistics shows that in 17.3% of cases the patient needs neutron radiation therapy, of which two-thirds are associated with relapses after primary treatment with photon radiation therapy. In the mortality rate, oncological diseases rank second (15.6%) after diseases of the cardiovascular system (46.3%).

Nowadays the unit of the absorbed dose rate of neutron radiation is reproduced and transmitted by the ionization method. The standard includes two independent methods for reproducing the unit of absorbed neutron radiation dose, which are used for direct transfer of the unit to standard installations such as UKPN-1M, UKPN-2M-D, KIS-NRD-MB, etc.:

– meter of absorbed dose of neutrons with a set of abdominal ionization chambers;
– meter of absorbed dose rate of neutrons with a cylindrical counter.

These installations are equipped with sealed radionuclide sources of neutron radiation based on radionuclides ^{238}Pu, ^{239}Pu, ^{252}Cf, that create reference fields of neutron radiation with a small admixture of gamma radiation.

The meter of the absorbed dose of neutrons with a set of abdominal ionization chambers can be used to reproduce and transfer a unit to neutron generators in open geometry, where the neutron energy equals 14 MeV. The main approaches, design principles and composition of a meter of neutron absorbed dose rate with a set of abdominal ionization chambers are described in [7-10].

Nowadays in medical institutions various types of nuclear physics facilities (NPF) are used. They implement neutron fluxes by accelerating particles and then bombarding these particles onto a target to knock out neutrons. Depending on the type of reaction of neutron production, their energy distribution can be very complex. The selection of nuclear-physics installations used in practice is presented in Table 1

Table 1 Nuclear Installations Used in Neutron Radiation Therapy

Name	Tomsk	Snezhinsk	Obninsk
Installation type	Cyclotron У-120	NG-12I (14 MeV) Up to year 2003 (reconstruction)	PNG type NG-24

Neutron production reaction	${}^{2}_{1}d(13{,}5\ \mathrm{MeV}) + {}^{9}_{4}Be \rightarrow$ $\rightarrow {}^{10}_{5}Be + {}^{1}_{0}n$	${}^{3}_{1}H + {}^{2}_{1}d \rightarrow {}^{4}_{2}He + {}^{1}_{0}n$	${}^{3}_{1}H + {}^{2}_{1}d \rightarrow {}^{4}_{2}He + {}^{1}_{0}n$
Average spectrum energy	6,3 MeV	10,5 MeV	About 14 MeV
Absorbed dose rate	0,15 Gy/min	11,5 sGy/min	
Collimator size	6x6 и 15x15 sm		$\varnothing\, 30\ mm$
Distance to the patient	110 sm	105 sm	Up to 100 sm
Background gamma radiation	About 10 %	4-8 %	5-10 %

The analysis of the technical and metrological parameters of the NPF [11-14] used in neutron radiation therapy and the medical rules and recommendations for irradiation of patients [15] imposes a number of restrictions:

- neutron field intensity by flux density is from 10^{7} up to $10^{10}\ \frac{1}{sm^{2}\cdot s}$;
- average energy of neutrons emitted by NPF is in the range from 2.5 to 14 MeV;
- the size of the exit window of the collimator should not exceed the size of the tumor and should be in the range from 3 to 15 cm;
- distance from the radiation source to the patient is from 0.5 to 1 m;
- the proportion of the gamma radiation component in the beam is from 4 to 15%.

These restrictions impose significant requirements on the methods and means of transferring the unit of absorbed dose rate of neutron radiation in mixed gamma-neutron fields and make the methods and means of measuring the absorbed dose of neutron radiation that were implemented in the standard not applicable.

Objective

Development of a method and means of transferring a unit of absorbed dose rate of neutron radiation, which provides the transfer of a unit to nuclear physics facilities used in radiation therapy for the cancer treatment.

Research object

Dosimetry of neutron radiation in the energy range from $2.5 \cdot 10^{-8}$ to 20 MeV.

Scientific novelty

A method and means of measuring of the absorbed neutron radiation dose have been developed, which allows the transfer of a unit to nuclear physics installations used in neutron radiation therapy for the radiation of oncological diseases.

Practical significance:

A method and a measuring instrument that allow the transfer of units of the absorbed dose of neutron radiation with the required accuracy for the purposes of radiation therapy have been implemented.

Main part

The presence of a collimator, in addition to focusing the neutron flux, also serves as a shadow shield for healthy tissues of the patient. Tungsten or iron is used as the collimator material; these materials have the ability to be activated by neutron radiation, which in turn leads to an increase of the proportion of gamma radiation. Neutrons, passing through the collimator, slow down, losing part of their energy when interacting with matter, which is converted into secondary charged particles and gamma quanta. Scattered neutrons make an additional negative contribution to the value of the absorbed dose of neutron radiation from 14 MeV neutrons that are required for neutron radiation therapy. Thus, the average energy of the neutron spectrum in the collimated beam becomes less than 14 MeV, which is critical, since the stopping power and relative biological efficiency for particles of different types and energies are strongly dependent on the particle energy. Therefore, neutrons with energy of less than 14

MeV will be absorbed on the way to the tumor and thereby cause significant harm to the patient's healthy tissues.

The absorbed dose in the beam from nuclear physics installations used in the treatment of oncological diseases can be represented as:

$$D= D_б+ D_{n,n'} + D_{n,n'\gamma} + D_\gamma+ D_{noise} + D_{вy} + D_{th} \quad (1)$$

where $D_б$ – target neutron contribution, $D_{n,n'}$ $(E_{n'})$ – scattered neutron contribution, $D_{n,n'\gamma}$ (E_γ) – contribution of instantaneous gamma quanta from the target and environment, $D_{n,n'\gamma} \sim D_{n,n'}$, D_γ – contribution of activation gamma quanta, $D_a = f\ (D_{n,n'}, t_{exp}, t_{exc})$, where t_{exp} – object exposure time, t_{exc} – time elapsed after object irradiation, D_{noise} – contribution of cosmic radiation and intrinsic noise of the recording system, D_{br} – contribution of bremsstrahlung gamma quanta from the accelerating system of the generator, D_{th} – thermal neutron contribution.

The components D_{th} (less than 0,1%) and D_{noise} (0,001%) can be neglected. The proportion of activation gamma quanta contributing during irradiation is rather small (less than 1%) and is taken into account when measuring the dose from gamma radiation, and the contribution of activation of long-lived components when calculating the absorbed dose during irradiation can be neglected. Taking into account the contribution from bremsstrahlung gamma quanta is very difficult, since the functional relationship between their yield and the neutron yield is complex; therefore, it is recommended to install a lead filter with a thickness of 2-2.5 mm in all measurements and irradiation options. With an average energy of ≈ 100 keV, to attenuate their flux of 10,000, a filter thickness of ≈ 1.5 mm is required, and taking into account experimental data, the recommended thickness of the lead layer is 2-2.5 mm. In this case, the neutron flux from the target is attenuated by 2%, however, this attenuation is automatically taken into account when calibrating nuclear physics facilities, when using a lead plate of the same thickness in this case. Considering the above, you can write equation 1 in the form:

$$D = D_f + D_{th} + D_\gamma \quad (2)$$

where $D_{th} = D_{n,n'} + D_{n,n'\gamma}$.

In order to experimentally separate the components of the mixed gamma-neutron field, at least three measuring channels are required. To minimize the error of reproduction and transmission of the unit of absorbed dose rate of neutron radiation, it is advisable to carry out measurements simultaneously at one point. This is due to the technical features of nuclear physics facilities, since the number of particles in the beam exhibits small but very noticeable fluctuations, especially for pulsed radiation.

Analysis of published data [16-21] methods and means of joint measurement of the absorbed dose rate of neutron radiation in mixed fields of gamma-neutron radiation with the possibility of separating gamma-neutron components showed that the most suitable transmission method is the scintillation method.

The main requirements for the development of a transmission medium are:

– the geometric dimensions of the detecting unit, since the minimum collimated beam size is 40 mm in diameter;

– the presence of several scintillation detectors working together, but at the same time independently of each other, since it is necessary to know the absorbed dose not only from neutrons with an energy of 14 MeV, but also the contribution of gamma radiation and the scattered neutron radiation;

– the use of materials that are little or not at all activated by high-energy neutron radiation, but at the same time provide a reliable design of the registration unit, light and moisture protection;

– the design of the registration unit provides the combined use of three different types of cylindrical scintillation detectors with dimensions: 1x1, 2x2, 3x3, 4x4, 8x8, 11x11 mm. Such a nomenclature of standard sizes is necessary for the selection of the optimal ratio of the dead time depending on the intensity of the fields and operating modes of nuclear physics installations, to which the unit of the absorbed dose of neutron radiation is transferred;

– it is necessary to provide three channels of independent power supply and amplification for the possibility of adjusting the measuring signal from each scintillation detector;

– it is necessary to provide three independent channels for collecting and digitizing the signal coming from the registration unit for subsequent mathematical processing of the instrumental spectra by means of a personal computer (PC).

The measuring system of the means of transmitting the unit of absorbed neutron radiation dose rate is designed to make it possible to measure the dosimetric values of neutron radiation directly at the locations of nuclear physics facilities. The general view of the measuring system is shown in Figure 3. The measuring system includes a registration unit (an assembly drawing is shown in Figure 2), a signal processing unit, including: a power supply unit with three independent channels, an amplification unit that provides the adjustment of the measured signal, an analog-to-digital converter that's designed to collect, process and accumulate information necessary to collect the instrumental spectrum; personal computer for control, storage and further processing of the measured results.

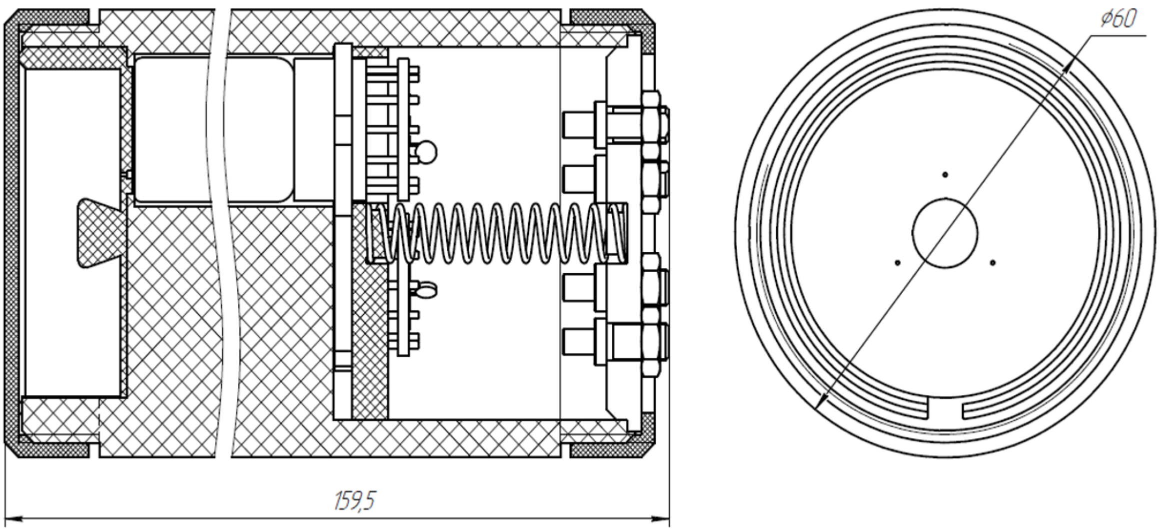

Figure 2 Block of registration

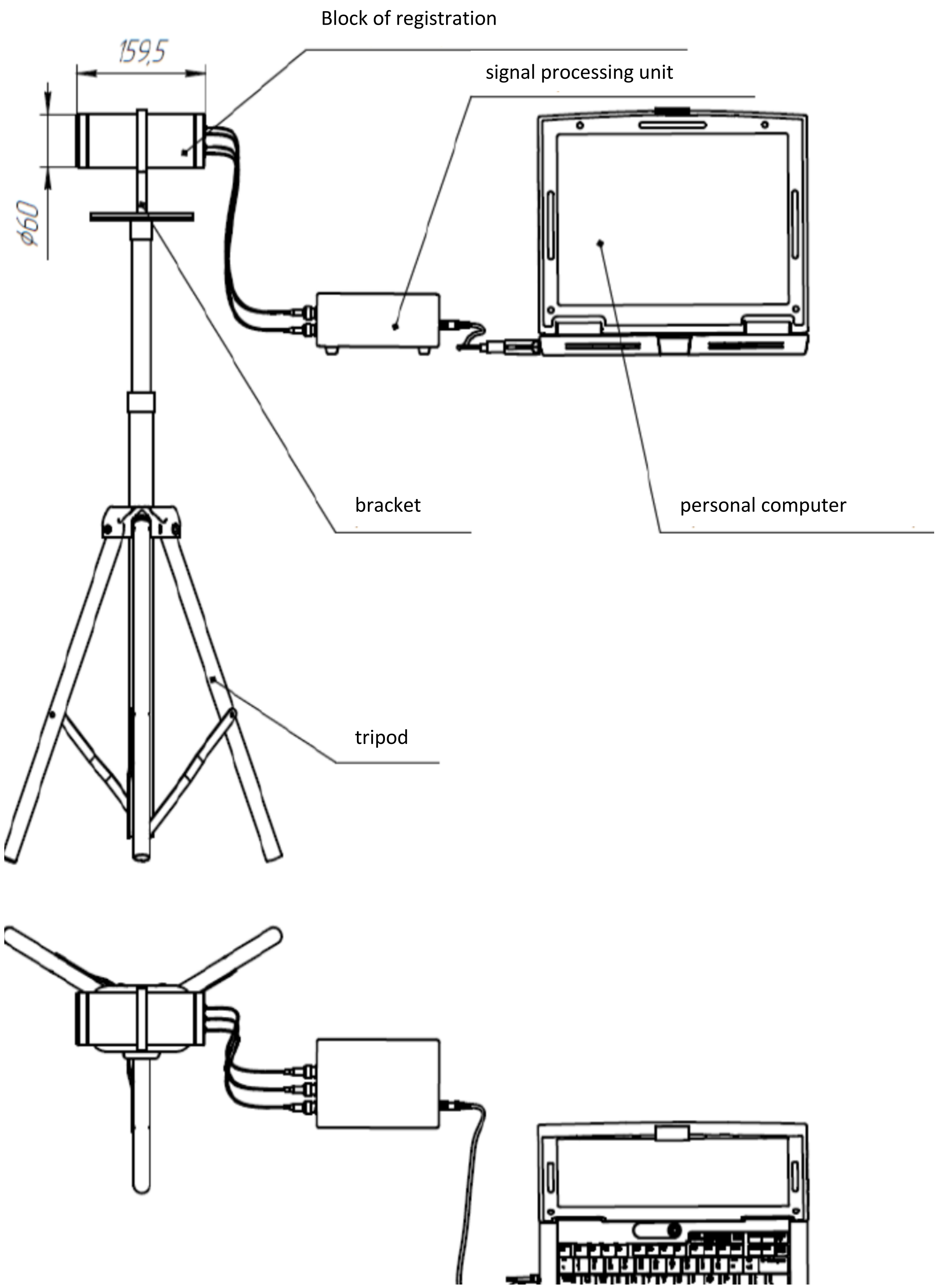

Figure 3 General view of the measuring system

The developed means of transmitting a unit of absorbed dose rate of neutron radiation allows to measure three components simultaneously: the absorbed dose of high-energy neutrons, the absorbed dose of gamma radiation and the absorbed dose of thermal neutrons.

The unit of measurement for each scintillation detector from the composition of the developed transmission device is transmitted by means of calibration at the reference point. For a fast neutron scintillator, this is a neutron field generated by a neutron generator with the average spectrum energy of 14 MeV. For a gamma-ray scintillator, it is a gamma-ray field generated by a sealed radionuclide source based on the Co-60 or Cs-137 radionuclide. For a thermal neutron scintillation detector, these are the neutron radiation fields generated by a sealed radionuclide source based on the PuBe or Cf-252 radionuclide and the gamma radiation field created by a sealed radionuclide source based on the Co-60 or Cs-137 radionuclide, where the value of the absorbed thermal neutron dose is determined by the difference between the readings of a scintillation detector sensitive to gamma-neutron radiation and a scintillation detector sensitive only to thermal neutrons.

The main metrological characteristic of the transmission device (comparator) is stability. To identify the stable mode of operation of the PMT, studies of the dependence of the PMT gain factor on the supply voltage in the range from 850 to 1150 V were carried out. The research results are shown in Figure 4.

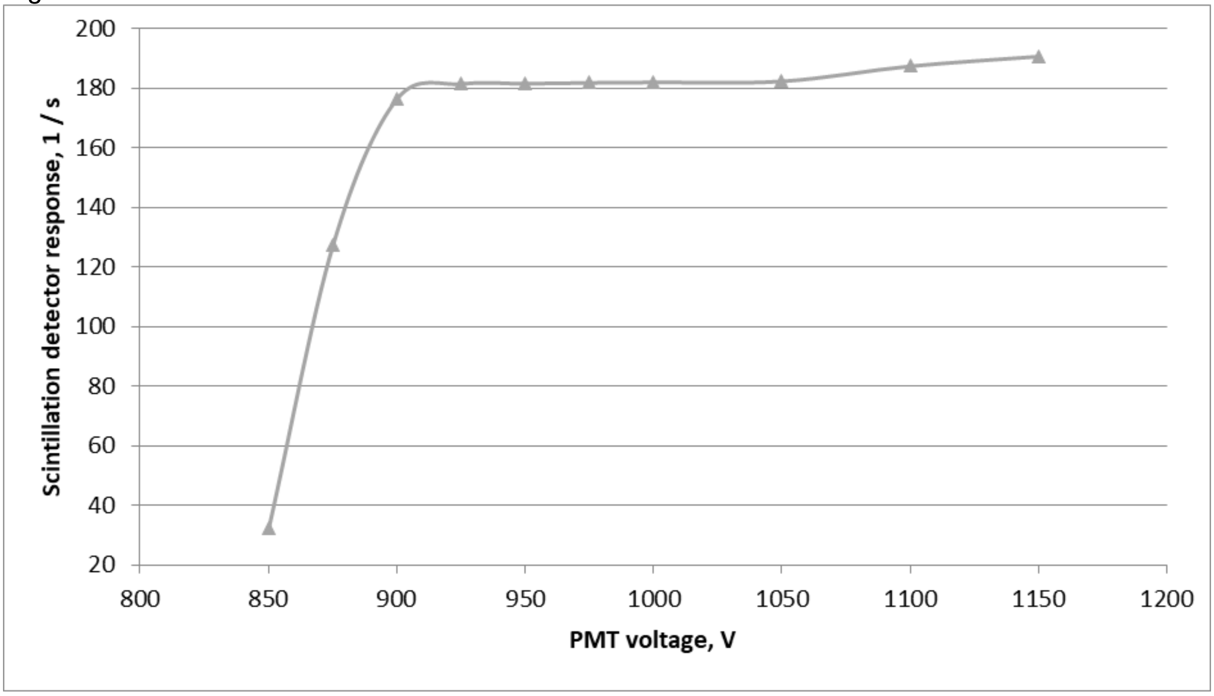

Figure 4 Results of measurements of the dependence of the amplification factor on the supply voltage of the PMT

In the voltage range from 930 to 1050 V, a stable mode of PMT amplification is observed; the standard deviation of the PMT gain factor does not exceed 0.3%.

To determine the operation stability of the means of transmitting the units of absorbed dose (absorbed dose rate) of neutron radiation, studies were carried out for a time interval of 1, 2, 12 and 24 hours. The research results are presented in Figure 5.

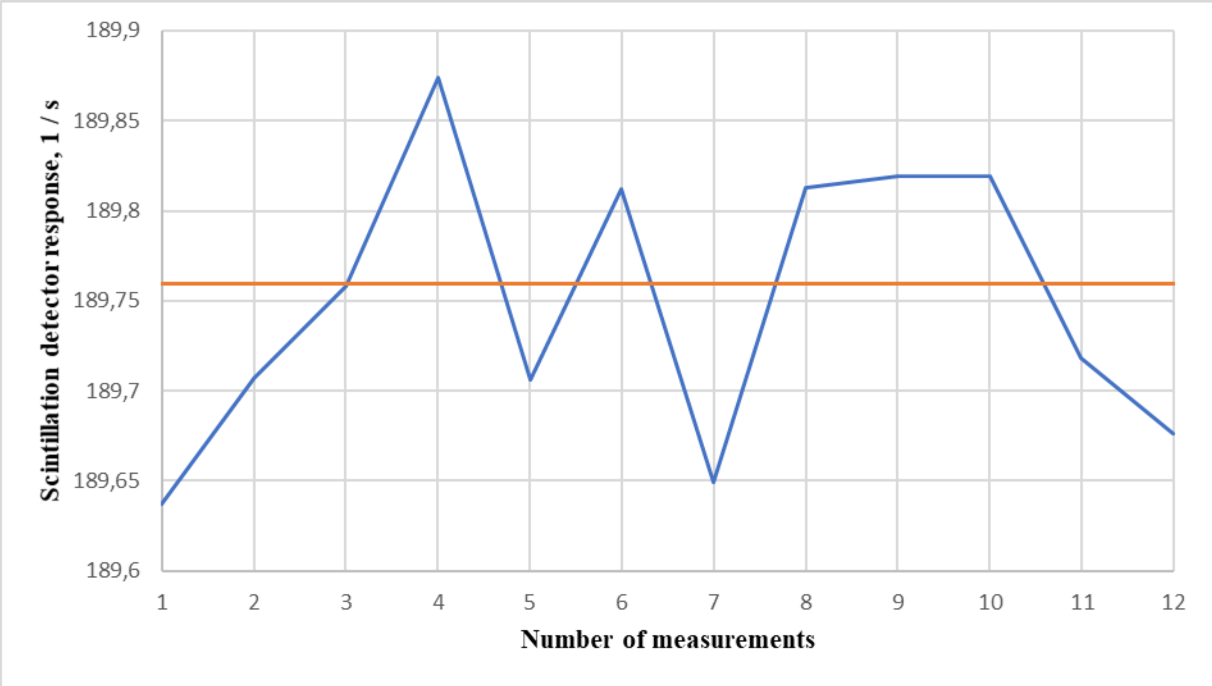

Figure 5 Results of measuring the stability of the transmission means

The results of the standard deviation of the transmission device stability do not exceed 0.1%. In Figure 5, the values 5 and 9 of the measurement correspond to the daily operation stability of the means of transmission of the units of the absorbed dose of neutron radiation.

Conclusion

The developed method and means of transmission provide the transfer of a unit of absorbed dose rate of neutron radiation in mixed gamma-neutron fields in the energy range from 0.05 to 14 MeV in the range of absorbed dose rate from $2 \cdot 10^{-10}$ to $1 \cdot 10^{-3}$ Gy·s^{-1} to nuclear physics installations used in practice in neutron radiation therapy for the treatment of oncological diseases.

References:

1. Ставицкий Р.В., Аспекты клинической дозиметрии / Р.В. Ставицкий – Москва: МНПИ, 2000 г.
2. Booth J.T., Modeling the impact of treatment uncertainties in radiotherapy: thesis – Adelaide, 2002
3. Brahme A. Dosimetric precision requirement in radiation therapy – Acta Radiological Oncology, №24, 1984
4. Custin-Savard A., Dose delivery uncertainty in photon beam radiotherapy: thesis, Montreal, 1995
5. Struelens L. Characterization of the scattered radiation field around an x-ray tube, Phys. Med. Biol., №56, 2011 г.
6. Здравоохранение в России 2018: статистический сборник – Москва, Росстат 2018 г.
7. Ю.И. Брегадзе, П.Ф. Масляев, О погрешности раздельного определения поглощенной дозы нейтронов и гамма-излучения ионизационными камерами, Измерительная техника, - № 8, - с. 70, - 1973;
8. В.П. Антипенко, Б.В. Артемов, Ю.И. Брегадзе, Б.И. Ермилов, П.Ф. Масляев, Автоматическое определение поглощенной дозы из дифференциального спектра импульсов, Измерительная техника, - № 4, - с. 90-91, - 1973;

9. Ю.И. Брегадзе, А.В. Марченко, П.Ф. Масляев, Л.М. Сидоренко, Государственный первичный эталон единиц мощности поглощенной и эквивалентной доз нейтронного излучения, Измерительная техника, - №10, - с. 3-6, 1979;
10. Ю.И. Брегадзе, П.Ф. Масляев, Комплекс средств высшей точности для определения поглощенной дозы быстрых нейтронов, Измерительная техника, - № 7, - с. 14-17, - 1974;
11. В.В. Великая, Л.И. Мусабаева, Ж.А. Старцева, В.А. Лисин, Быстрые нейтроны 6,3 МэВ в комплексном лечении больных местными рецидивами рака молочной железы, Вопросы онкологии, - Том 61, - с. 583-585, - 2015;
12. Е.М. Слонимская, Л.И. Мусабаева, В.А. Лисин, Р.А. Шагиахметова, Ж.А. Жогина, Комплексная терапия местнораспространенного рака молочной железы с применением нейтронно-фотонной терапии, Сибирский онкологический журнал, - с. 30-36, - 2002;
13. В.А. Новиков, Л.И. Мусабаева, В.А. Лисин, Результаты комбинированного лечения опухолей полости носа и околоносовых пазух с применением нейтронной терапии, Сибирский онкологический журнал, - с. 21-26, - 2002;
14. В.А. Лисин, Способы определения относительной биологической эффективности нейтронов в дистанционной нейтронной терапии, Сибирский онкологический журнал, - Том №5, - с. 36-41, - 2017;
15. IAEA TRS-398 Absorbed dose determination in external beam radiotherapy: 5an international code of practice for dosimetry based on standards of absorbed dose to water: Technical report. – Vienna: International Atomic Energy Agency, 2000;
16. C.P.J. Raaijmakers, P.R.D. Watkins and etc., The neutron sensitivity of dosimeters applied to boron neutron capture therapy, The International Journal Medical Physics Research and Practice, - T. 23, - p. 1581-1589, - 1996;
17. A. Buffler, A.C. Comrie, F.D. Smit, H.J. Wortche, Neutron spectrometry with EJ299-33 plastic scintillator for En = 10-100 MeV, Transactions on Nuclear Science, - Vol. 62, - p. 1422-1428, - 2015;
18. J. Paepen, F. Schulte, P. Mastinu and etc., Characterisation of plastic scintillators used as an active background shield for neutron detection, JRCTechnical report, - Belgium, European Atomic Energy Community, - 2016;
19. H. Klein, Neutron spectrometry in mixed fields: NE213/BC501A liquid scintillation spectrometer, Nuclear Technology Publishing, - Vol. 107, - p. 95-109, - 2003;
20. V.V. Verbinski, W.R. Burrus, T.A. Love, W. Zobel, N.W. Hill, Calibration of an organic scintillator for neutron spectrometry, Nuclear Instruments and Methods, - Vol. 65, - p. 8-25, - 1968;
21. Ю.А. Кащук, Сцинтилляционные спектрометры нейтронного и гамма-излучения для диагностики термоядерной плазмы, диссертационная работа, - с. 198, - 2007.

Secondary standard for the units of alpha, beta emitting radionuclides activity, flux of alpha, beta particles

N.K. Mamyrbek,
JSC «NCEC»,
Secondary standard dosimetry laboratory
Kazakhstan, Kapshagay, Koichumanov str. 10A,
tel. (7-727)3916333
e-mail: ssdlkz@gmail.com

Abstract

Metrology of ionizing radiation provides reliable measurements in such critical areas of human activity as scientific research, nuclear medicine, nuclear industry, environmental protection and radioecology. It so happened that at the head of the system for ensuring the uniformity of measurements used in the radiometry of alpha and beta radiation of the Republic until now were reference radionuclide sources of alpha and beta emitting. In this regard, there was a need for periodic removal of radionuclide sources outside the borders of the country to ensure metrological traceability. Difficulties in organizing international transportation and physical protection of nuclear and other radioactive materials, the high cost of transportation of radioactive sources led to the need to develop a radiometric installation used as a secondary standard for units of radionuclide activity and particle flux, which would meet the requirements for such standards. The author presents an approach designed to eliminate the risks of removal and transportation of radioactive sources. The results of work on the creation of a secondary standard of units of activity of alpha-, beta-emitting radionuclides and the flux of alpha, beta particles are presented. The paper describes the metrological characteristics of the radiometric installation and the results of comparison with the UEAP-1 and UEAPP-2 installations from the state primary standard of the Russian Federation GET 6-2016.

The article presents the results of work on the creation of secondary standard for the units of alpha, beta emitting radionuclides activity, flux of alpha, beta particles. Its metrological characteristics and the results of comparison with the UEAP-1 and UEAPP-2 installations of the structure of the state primary standard of the Russian Federation GET 6-2016 are describe.

The problem of measuring radioactivity arises in many areas where sources of ionizing radiation are used. Methods for measuring radioactivity found applications in the search and extraction of minerals, technological processes using irradiating devices, in the operation of nuclear power plants, in the production of radioactive raw materials, in medicine. One of the main issues of environmental protection is the control of the content of radioactive substances and their migration in the atmosphere, soil, vegetation.

The variety of directions where it is necessary to deal with the measurement of radioactivity is very wide [1].

At the head of the system for ensuring the unity of measurements used in alpha, beta radiometry of our country until now there were reference radionuclide sources of alpha, beta emitting. Reference radionuclide sources have traceability to the state primary standard of units of activity of radionuclides of the Russian Federation, stored at VNIIM D.I. Mendeleev All-Russian Institute for Metrology.

The tightening of the requirement for the organization of international transportation and physical protection of nuclear and other radioactive materials, the high cost of transportation of radioactive sources led to the need to develop a radiometric installation used as a secondary standard for the units of alpha, beta emitting radionuclides activity, flux of alpha, beta particles. Which would meet the requirements of the interstate standard [2]. In this case, the radiometric installation had to meet the criteria of small size, have a relatively small mass with the ability to measure alpha and beta emitting sources with an active part area from 1 cm^2 to 160 cm^2. Based on the above criteria, we have created a radiometric installation based on the 2πα/β counting method.

The 2πα/β counting method is design to measure the flux of alpha and beta particles and is implement in our case, based on a proportional 2π counter. In international practice, gas flow proportional counters used as a national primary standard for calibrating reference radiation sources [3-4].

Structurally, the radiometric installation consists of a windowless gas flow proportional counter, a high-voltage power supply, an amplifier, and a pulse counter. The gas flow proportional counter consists of a multi-wire grid that covers a large sensitive area. The source to be calibrate is introduce directly into the sensitive volume of the counter. The particle flux emitted by the source is measure through the ionization of the gas. Ar+CH4 (CH4 - 10%) mixture is used as a filling gas in the counter.

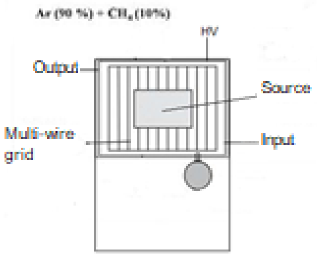

Figure 1. Illustrative diagram of a windowless gas flow proportional counter

To confirm the compliance of the metrological characteristics of the radiometric installation with the requirements of secondary standards, the operating parameters and the main metrological characteristics of the installation were determined, such as operating voltage, dead time, instability and unevenness of the counter efficiency, measurement uncertainty.

Comparisons with the UEAP-1 and UEAPP-2 units from GET 6-2016 carried out.

To determine the positions of the operating voltages within the plateau of the counting characteristic, alpha and beta sources put in series in the gas flow proportional counter. The supply voltage of the counter gradually increased up to the voltage of the beginning of counting, at which the counting circuit began to register pulses from charged particles.

The results of measuring the count rate used to construct the counting characteristic of the proportional counter.

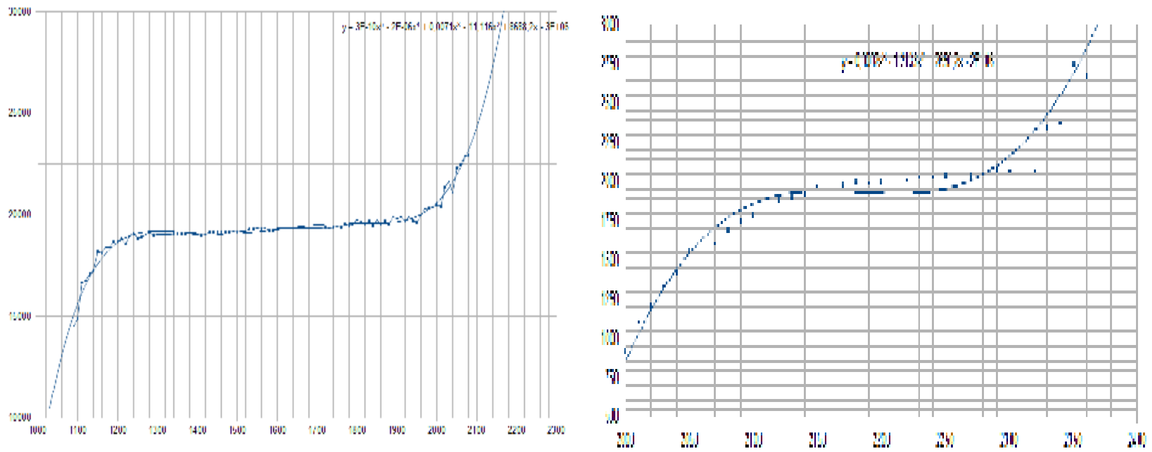

Figure 2. Counting characteristics of the proportional counter for alpha and beta sources

Based on the results of the counting characteristics, the operating voltages of the gas flow proportional counter are determined: 1650 V (for alpha emitting radionuclides), 2300 V (for beta emitting radionuclides).

To determine the value of the dead time, two radionuclide sources of RES selected, each of which creates a count rate n, s^{-1}, equal:

$$n_1 \approx n_2 \approx \frac{0{,}04}{\tau_m} \tag{1}$$

Where τ_m - is the expected dead time, s;

n_1, n_2 is the count rate of pulses from radionuclide sources, s^{-1};

The background count rate of pulses of a gas flow proportional counter $n_ф$ (s^{-1}) previously measure, followed by the put and accordingly measurement of the count rate from the first radionuclide source n_1. Without changing the position of the first radionuclide source, a second radionuclide source put with the measurement of the count rate from two n_{12} radionuclide sources. The last step of was the measurement of the count rate from the second radionuclide source n_2 with the removal of the first radionuclide source.

Dead time calculated using the formula:

$$\tau_м = \frac{n_1 \cdot n_2 - n_{12} \cdot n_ф - \sqrt{(n_1 - n_ф)(n_{12} - n_1)(n_2 - n_ф)(n_{12} - n_2)}}{n_1 \cdot n_2 \cdot (n_{12} + n_ф) - (n_1 + n_2) \cdot n_{12} \cdot n_ф} \tag{2}$$

Based on the results of multiple measurements, at least five values of the dead time calculated with the determination of the average value.

$$\overline{\tau_м} = \frac{1}{z} \sum_{i=1}^{z} \tau_{м\,i} \tag{3}$$

The standard uncertainty of the dead time measurement calculated using the formula:

$$u(\tau_м) = \frac{\tau_{м\max} - \tau_{м\min}}{\overline{\tau_м} \cdot 2\sqrt{3}} \tag{4}$$

According to the measurement results, the average value of the dead time of the flowing proportional counter is 2.3 μs. The standard uncertainty in determining the dead time is 0.004 μs.

To determine the instability of a gas flow proportional counter, a radionuclide source with external radiation of at least 5000 s^{-1} used, with at least 20 measurements of the count rate n, s^{-1} and the measurement time t, 100 seconds.

The relative standard deviation of the arithmetic mean value of the pulse-counting rate is calculated:

$$S_n = \frac{1}{n_t} \sqrt{\frac{\sum_{i=1}^{20} (n_i - \bar{n})^2}{20 \cdot (20 - 1)}} \tag{5}$$

The standard deviation of the arithmetic mean value of the count rate is - 0.025%.

The relative standard deviation is calculate under the assumption that the scattering of the measurement results has a Poisson distribution:

$$S_n^{ПУАСС} = \frac{1}{\sqrt{\sum_{i=1}^{20} n_i \cdot t}} \tag{6}$$

The relative standard deviation of the scattering of the measurement results according to the Poisson distribution is - 0.022%.

Standard uncertainty due to counter instability is calculate using the formula:

$$\nu = \sqrt{(S_n)^2 - (S_n^{ПУАСС})^2} \quad (7)$$

The standard uncertainty of the counter is 0.01%.

To determine the unevenness of the gas flow proportional counter, an empty substrate with a working area of 160 cm2 was used, which, in turn, put in the working volume of the counter, followed by placing a radionuclide source of the RES type in it at positions evenly distributed on the aforementioned substrate.

Uneven efficiency of the investigated gas flow proportional counter over the area: no more than 0.1%. The standard uncertainty due to uneven efficiency over the counter area is 0.1%.

Comparisons with the UEAP-1 and UEAPP-2 installations carried out using radionuclide sources of the P9 and C0 (Pu-239, Sr(Y)-90) types. At the UEAP-1 and UEAPP-2 installations and a gas flow proportional counter, the flux of alpha and beta particles from radionuclide sources measured. The number of measurements from each radionuclide source was at least 10 the time of one measurement was at least 100 s.

Installation	Alpha particle flux in solid angle 2π sr., s^{-1}	Expanded uncertainty (k=2),%	Difference of results, %	Convergence of results of comparisons
UEAPP-2	861,1	0,6	0,07	0,08
Proportional counter	861,7	0,6		

Installation	Beta particle flux in solid angle 2π sr., s^{-1}	Expanded uncertainty (k=2),%	Difference of results, %	Convergence of results of comparisons
UEAP-1	2018	0,6	0,39	0,52
Proportional counter	2010	0,5		

Figure 3. Results of comparison of a gas flow proportional counter with UEAP-1 and UEAPP-2 units from GET 6-2016

The expanded measurement uncertainty estimated by the formula: $Up = k \cdot u_c$ (8)

Where, u_c is the total standard uncertainty equal to

$$u_c = \sqrt{\left(\frac{\bar{n}}{\bar{n}-\bar{n}_ф} \cdot u(n)\right)^2 + \left(\frac{\bar{n}_ф}{\bar{n}-\bar{n}_ф} \cdot u(n_ф)\right)^2 + (\bar{n} \cdot \tau_М \cdot u(\tau_М))^2 + u(\nu)^2 + u(\vartheta)^2 + u(\varphi_{ГЭТ})^2} \quad (9)$$

Where, $u(n)$ is the relative standard uncertainty of measuring the count rate from the source, equal to the maximum value of $u_{ср.арифм}(n)$ и $u_{Пуассон}(n)$.

$u_{ср.арифм}(n)$ - is the relative standard uncertainty of measuring the count rate according to the formula of the arithmetic mean

$$u_{ср.арифм}(n) = \frac{1}{\bar{n}} \sqrt{\frac{\sum_{i=1}^{z}(n_i - \bar{n})^2}{z \cdot (z-1)}} \quad (10)$$

$u_{Пуассон}(n)$ - is the relative standard uncertainty of measuring the count rate according to the standard deviation formula according to Poisson's law

$$u_{Пуассон}(n) = \frac{1}{\sqrt{\sum_{i=1}^{z} \cdot N_i}} \quad (11)$$

$u(n_{\text{ф}})$ - is the relative standard uncertainty of the background count rate, equal to the maximum value $u_{\text{ср.арифм}}(n_{\text{ф}})$ и $u_{\text{Пуассон}}(n_{\text{ф}})$.

$u(\varphi_{\text{ГЭТ}})$ - is the relative standard uncertainty of measuring the flux of alpha and beta particles at installations from the GET 6-2016.

According to the assessment results, the expanded uncertainty of measurements of the flux of alpha and beta particles was equal to - 0.6%, with k=2, P=0.95.

The radionuclide activity in the source calculated by the formula: $A_i = K \cdot \varphi_i$ (12)

Where K is the coefficient of transition from flux of particles in the source to activity.

According to the test results, it found that the installation has high metrological characteristics. The work performed allows improving the measuring capabilities of the laboratory. The installation is also mobile and solves the problem of transporting radionuclide sources to ensure metrological traceability of measurements.

References:

1. Ю.И. Брегадзе, Э.К. Степанов, В.П. Ярына. Прикладная метрология ионизирующих излучений. Энергоатомиздат, 1990
2. ГОСТ 8.033-96 Межгосударственный стандарт «Государственная поверочная схема для средств измерений активности радионуклидов, потока и плотности потока альфа-, бета-частиц и фотонов радионуклидных источников».
3. King, L.E. & Hutchinson, J.M.R. & Unterweger, M.P. (2008). A new large-area 2π proportional counting system at NIST. Applied Radiation and Isotopes, Volume 66, Issues 6–7, June–July 2008, Pages 877-880
4. Zhang, Junwei & Zhang, Ming & Duan, Limin & Tu, Zheng & Yang, Zhijie & Li, Yuqi & Liang, Juncheng & Liu, Haoran. The large-area multi-wire proportional counting system for 2π alpha and beta emission measurement at the NIM China. Applied Radiation and Isotopes, Volume 134, April 2018, Pages 366-369
5. Караваев Ф.М. Измерения активности нуклидов. Издательство стандартов, 1972

CERTIFICATION OF A STANDARD SAMPLE WITH ESTIMATION OF MEASUREMENT UNCERTAINTY BY MEANS OF ANALYSIS OF VARIANCE

Zhumagali Assylbek
Kazstandart, Kazakhstan
e-mail: a.zhumagali@ksm.kz
Тел.: 87172282963

Abstract

Standard samples (RM) are designed to reproduce, store and transfer the characteristics of the composition or properties of substances (materials), expressed in unit values. Standard samples must be certified with uncertainty, which ensures metrological traceability. There are two ways to determine bottom-up and top-down uncertainty. Bottom-up uncertainty definitions are the traditional method that is used to this day, determining the contribution of sources of uncertainty and using formulas to find the standard uncertainties, calculates the extended uncertainty with a set probability and coverage factor. Top-down uncertainty definitions (top-down) are definitions of measurement uncertainty using an analysis of variance involving several accredited laboratories that have proven their competence. This method in mathematical statistics, aimed at finding dependencies in the experimental data by examining the significance of differences in mean values. Dispersion analysis The definition of top-down uncertainty is easy to implement and it is easier to cover all the effects.

The relevance of the article. Currently, in the Republic of Kazakhstan, the estimation of measurement uncertainty using the analysis of variance for a standard sample is not used.

The purpose of the work. Development of methodological bases for improving the determination of the value of the component in the RM using the analysis of variance.

Scientific novelty or practical (applied) significance. This methodological framework will be useful for the field of metrology in the development of metrological traceability.

Tasks of the work. Study of the methodology of certification of RM and assessment of uncertainty.

The essence of the work. The determination of the characteristics of the RM can be performed in various ways. There are two main ways:

a) determination of characteristics by one method,

b) determination of characteristics by several methods and / or by several laboratories.

In all cases, the measurement methods used to determine the characteristics should ensure traceability to approved standards, preferably SI units..

It is required that all measurements are performed on appropriately calibrated / verified equipment, and the results of these calibrations/verifications can be compared. In particular, when several laboratories are involved in the measurement, a substance, mixture or solution may be used to verify the consistency between calibrations/verifications, which makes it possible to demonstrate the validity and comparability of the results obtained during the various stages of the program.

When choosing the certification method, it is necessary to determine the components of uncertainty that contribute to the uncertainty associated with the value of the certified parameter. Moreover, it is necessary that the certified value and its uncertainty can be demonstrated. The choice of the best method for determining the characteristics of RM depends on both the available methods and the RM matrix [2].

There are two ways to determine uncertainty bottom-up (снизу-вверх) and top-down (сверху-вниз).

The method of determining the uncertainty from the bottom-up (снизу-вверх) can be represented as follows:

a) express the ratio between the value of the certified parameter (y) and all the input values on which the parameter value depends mathematically. This relationship includes all the quantities that can make a significant contribution to the uncertainty of the parameter value, and is called the measurement model.

b) determine the values of all input values.

c) evaluate the standard uncertainty of type A and type B, the estimate of the covariance between any of the input values.

d) calculate the value of the parameter (y), i.e. the value of the certified characteristic.

e) determine the total standard uncertainty, the coverage factor k, and obtain the extended uncertainty U [3].

Example: estimation of uncertainty in the measurement of chloride ion content in RM.

The standard uncertainty of measuring the content of chloride ions in RM in accordance with the mathematical model is due to the following values: from the concentration of the standard sample, the volume of the flasks, the volume of the pipettes.

We estimate the uncertainty of the content of chloride ions in RM and fill in the uncertainty budget table (Table 1.1).

Table 1.1 Uncertainty budget

Input value, x_i	The value of the input value, x_i	Type uncer.	Law of distribution.	Standard uncer., u(x_i)	Contribution of uncer., u_i(y)	Extended uncer., k=2
Cco	1001 mg/l	A	норм.	0	0	0,94 mg/l
Δc	±2 mg/l	B	прямоуг.	1,15 mg/l	1,15 mg/l	
Vп	1 ml	A	норм.	0	0	
$Δп_1$	±0,02	B	треуг.	0,0082 ml	0,0082 ml	
$Δп_2$	±0,02	B	треуг.	0,0082 ml	0,0082 ml	
Vк	100 ml	A	норм.	0	0	
$Δк_1$	±0,2	B	треуг.	0,082 ml	0,082 ml	
$Δк_2$	±0,2	B	треуг.	0,162 ml	0,162 ml	

The content of chloride ions in RM was c=(40,04±0,94) mg/l, p=95%, k=2.

The following method of determining the uncertainty is top-down (top-down), which is determined using the analysis of variance (ANOVA).

Variance analysis is a method in mathematical statistics aimed at finding dependencies in experimental data by examining the significance of differences in mean values. Developed by Fischer to analyze the results of experimental studies. In the literature, the designation ANOVA is also found (eng. *Analysis Of VAriance*).

The essence of the analysis of variance is to study the influence of one or more independent variables, usually referred to as factors, on the dependent variable.

The variance analysis procedure consists in determining the ratio of systematic (inter-group) variance to random (intra-group) variance in the measured data. As an indicator of variability, the sum of the squares of the deviation of the parameter values from the average is used: SS (from the English Sum of Squares). The total sum of squares, SS_{Total} is decomposed into between-group sum of squares SS_{BG} and intra-group sum of squares SS_{WG}:

$$SS_{Total} = SS_{BG} + SS_{WG} \qquad (1.1)$$

Here, the intergroup sum of squares SS_{BG} and the intragroup sum of squares SS_{WG} are found using the following formulas:

$$SS_{BG}=\sum(x_{in}-x_{cpn})^2 \qquad (1.2)$$

$$SS_{WG}=n\sum(x_{cpn}-x_{cp})^2 \qquad (1.3)$$

where, x_{in} is the value of observations, x_{cpn} is the average value of observations of the n group, x_{cp} is the average value of all observations.

If the variances are equal, then the Fisher F-test is used to estimate the ratio of inter-group and intra-group variability:

$$F=\frac{MS_{BG}}{MS_{WG}}, \text{ where} \qquad (1.4)$$

$$MS_{BG}=\frac{SS_{BG}}{v_{BG}} \text{ and } MS_{WG}=\frac{SS_{WG}}{v_{WG}} \qquad (1.5)$$

Based on this, the value of F should be close to 1 if there are still no statistically significant differences. The critical value of F is determined by the significance level (usually 0.05 or 0.01) and the intra-group and inter-group number of degrees of freedom (v). It is quite difficult to calculate, so it is more common to use table values with the indication α, v_{BG}, v_{WG}.

Intergroup number of degrees of freedom:

$$v_{BG} = m - 1 \qquad (1.6)$$

m – number of observations per group.

Intragroup number of degrees of freedom:

$$v_{WG} = n - m \qquad (1.7)$$

n – total number of observations [4].

Example: Certification of a standard sample with measurement uncertainty estimation using analysis of variance.

Three laboratories for 4 days measured the content of chloride ions in RM (in mg / l) are shown in Table 1.2 below:

Table 1.2 – Measurement data of the content of chloride ions in RM

	Laboratory 1	Laboratory 2	Laboratory 3
Day 1	39,6	39,5	40,6
Day 2	40,1	39,5	40,5
Day 3	39,7	40	40,4
Day 4	39,8	41	40,5
Arithmetic mean	39,8	40	40,5

We consider the value of (1.4) of the Fisher criterion, based on the mean squares of deviations within and between the groups and the corresponding (1.6) and (1.7) degrees of freedom. Using these formulas, fill in Table 1.3:

Table 1.3 – ANOVA data estimation of RM chloride ion content

Variance	**SS**	**d_f**	**MS**	**F**
Between groups	1,04	3	0,35	3,89
Within groups	0,7	8	0,09	

The critical value of the F-distribution for probability 0.05 and degrees of freedom 3 and 8 is F_{cr}=4.07. F<F_{cr} indicates that the estimated value is correct and the uncertainty can be determined. To do this, you need to find the variance within the group and between the groups:

$$S_{WG}=\sqrt{MS_{WG}} \tag{1.8}$$

$$S_{BG}=\sqrt{\frac{MS_{BG}-MS_{WG}}{d}} \tag{1.9}$$

where, d – number of groups.

Using these formulas (1.6) and (1.7), we find the variances.

Variance within the group: $S_{WG} = \sqrt{0,35}$= 0,58 mg/l.

Variance between groups: $S_{BG} = \sqrt{(0,35-0,09)/3}$= 0,29 mg/l.

After finding the variance, you can find the uncertainties using this formula:

$$U= k\sqrt{\frac{S_{WG}}{m}+\frac{S_{BG}}{n}} \tag{1.10}$$

The uncertainty in this case is equal to if k=2:

$$U = 2\sqrt{\frac{0,58^2}{3}+\frac{0,29^2}{12}} = 0,7 \text{ мг/л.}$$

Thus, the certified RM value can be written as C = 40,09±0,7мг/л.

The results obtained:

Thus, the traditional way of determining uncertainty from top to bottom requires extensive research to find all the factors and a large risk of not determining the important factors and lead to a complex equation if many factors are affected.

Variance analysis determining uncertainty from top to bottom is easy to implement and easier to cover all effects.

References:

[1] ГОСТ 8.315-97 Государственная система обеспечения единства измерений (ГСИ). Стандартные образцы состава и свойств веществ и материалов. Основные положения (с Изменением N 1).
[2] ГОСТ ISO Guide 34-2014 Общие требования к компетентности изготовителей стандартных образцов.
[3] ГОСТ 8.532-2002 Государственная система обеспечения единства измерений (ГСИ). Стандартные образцы состава веществ и материалов. Межлабораторная метрологическая аттестация. Содержание и порядок проведения работ.
[4] Материалы курса «Use of Reference Materials and the Estimation of Measurement» Belgium-2011, 5-12 стр.

Difference between ITS-90 scale and thermodynamic temperature measured by acoustic gas thermometry at FSUE VNIIFTRI

Ghavalyan M.Yu. *, Kytin V.G. , Potapov B.G.
National Research Institute for Physical-Technical and RadioTechnical Measurements − FGUP VNIIFTRI,
Mendeleevo, Moscow Region, Russia, 141570,
http://www.vniiftri.ru
*e-mail: ghavalyan@vniiftri.ru,
phone.:+7 909 958 48 98

Abstract

A difference between temperature determined by International Temperature Scale (ITS-90) and thermodynamic measured by relative acoustic gas thermometry has been determined at 79 K and at the temperature of the triple point of Ar. Measurements were carried out using quasi-spherical acoustic resonator filled with helium at different pressures. There isotherms were fitted for four different acoustic modes simultaneously assuming the same thermal accommodation coefficient for all modes. To take into account the change in the radius and shape of the resonator with a change in temperature, we measured the frequency dependence of the complex transmittance for the TM11 mode in a resonator evacuated to a pressure of less than 1 Pa. Temperature measurements according to the current international temperature scale ITS-90 were carried out using platinum resistance thermometers calibrated at the fixed points, which are part of the State Primary Temperature Standard of the Russian Federation. Obtained values of the difference between temperature determined by ITS-90 and thermodynamic temperatures agrees with previously published data within estimated uncertainty

***Keywords**: Thermodynamic temperature, acoustic gas thermometry, International temperature scale*

a. Relevance in terms of its scientific and practical meaning

According to the new definition of temperature unit kelvin [1] the unit of temperature is not related to the temperature of the triple point of water. It is determined by a fixed value of the Boltzmann constant. In fact, this means determining the unit of temperature through the laws of thermodynamics and statistical physics. Therefore, primary temperature measurement methods based on these laws should play a key role in precision temperature measurements. At the same time, the current international temperature scale ITS-90 is easy to implement and remains extremely important for practical use. Therefore, measurements of the temperature deviation of the ITS-90 scale T90 from the thermodynamic temperature T are important, relevant and are carried out in the leading metrological institutes of the world.

b. Purpose of the paper

The purpose of this work was to present the results of T-T90 measurements at T_{90}=79 K and T_{90}=83.8058 K by relative acoustic gas thermometry.

c. Scientific novelty or practical (applied) significance

The measurements were carried out on the apparatus of relative acoustic gas thermometry, developed at VNIIFTRI. In particular, the method of simultaneous approximation of isotherms for several modes of acoustic resonance was used to determine the thermodynamic temperature, which made it possible to reduce the uncertainty in measuring the thermodynamic temperature. To implement this method, both algorithms for calculating the thermodynamic temperature and algorithms for calculating the uncertainty of its measurement were developed and implemented. The measurement of the temperature deviation of the ITS-90 scale from the thermodynamic temperature was the first carried out in the COOMET countries after the collapse of the USSR.

d. Tasks

To determine the deviation of the temperature on the ITS-90 scale from the thermodynamic temperature, the following tasks were solved:
1) Stabilization and measurement of temperature of the ITS-90 scale
2) Determination of thermodynamic temperature by the method of relative acoustic gas thermometry.

e. Description of the paper

The measurement technique is detailed in the article [2]. Below is a brief description of the technique and equipment.

1. Apparatus.

The fundamentals of the method of acoustic gas thermometry are fully described in [3]. To implement the method, a resonator of oxygen-free copper was manufactured at FSUE VNIIFTRI. The shape of resonator is shown in figure 1, By design it has spherical shape of internal cavity with 100 mm diameter. The resonator consists of two hemispheres. Internal

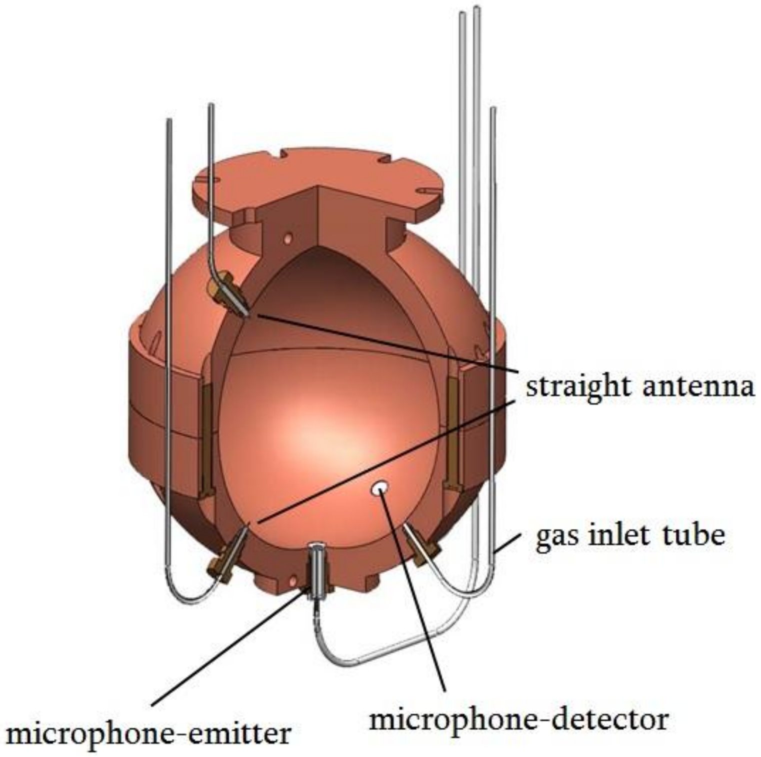

Fig. 1 Shape of resonator

surface of resonator was hand polished using special optical pastes. Two microphones were used to excite and detect acoustic signal. Microphone-emitter was mounted in the “south pole” of the resonator. Microphone-detector was mounted at 39.20 with respect to microphone-emitter to avoid detection of (3,1) acoustic mode which can overlap with (0,2) mode used to determine thermodynamic temperature. The openings for microphones were tightly fitted to the diameter of sensitive part of microphones. The surface of microphones’ membranes was fitted to the surface of resonator cavity using magnifying loop with the accuracy better than 0,1 mm. Two straight antenna were mounted in the resonator walls at 450 with respect to vertical axis in upper and lower hemispheres. Gas inlet tube with internal diameter 1,4 mm was mounted in the lower hemisphere at 450 with respect to the vertical axis of the resonator. Outlet opening with 2 mm diameter was made in the upper hemisphere at 450 with respect to the vertical axis. Two Pt resistance thermometers were mounted in the wall of upper and lower hemisphere at the opposite sides of resonator center.

2. Measurement of T90.

Pt resistance thermometers utilized for the measurement of T90 were calibrated by comparison with the group of Pt thermometers of National temperature standard of Russian Federation in the fixed points of ITS-90. This group of thermometers was calibrated in the fixed points of ITS-90 and took a part in the CCT key comparison.

The values of resistance were extrapolated to the zero current by measurements at 0.4 mA and 0.7 mA.

3. Measurement of T.

Thermodynamic temperature was determined for acoustic modes (0,2), (0,3), (0,4) and (0,6) (in following numbered as 1,2,3,4 using following expression:

$$T_l = T_W \frac{f_{a0l}^2(T)}{f_{a0l}^2(T_W)} \frac{f_{m0}^2(T_W)}{f_{m0}^2(T)} \quad (1)$$

where l is the mode number, $T_W = 273.16$ K is the temperature of the triple point of water, $f_{a0l}(T)$, $f_{a0l}(T_W)$ are the frequencies of acoustic resonance corresponding to ideal gas in the cavity with rigid walls with zero heat conductivity at T and TW, $f_{m0}(T)$, $f_{m0}(T_W)$ are the frequencies of electromagnetic resonance in empty cavity with ideally conducting walls. The determination of frequencies in expression (1) is described below.

3.1 Microwave measurements.

Microwave measurements were employed to determine variation resonator radii and shape with temperature. Frequency dependence for mode TM11 was measured in resonator pumped down to the pressure below 1 Pa. First measurement was performed at the reference point, i.e. triple point of water. Then frequency dependencies were measured at triple point of Ar and at T_{90}=79 K.

3.2 Acoustic measurements and analysis.

Frequency dependencies of acoustic signal were recorded at several pressures of helium p in the resonator. Before each measurement of the frequency dependence of acoustic signal pressure chamber with resonator was pumped down to 1 Pa and filled with helium through cryogenic trap (4.2 K) to target pressure.

Frequency dependencies were fitted by Lorentzian function

The isotherm approximation for different acoustic resonance modes was carried out simultaneously. For this, the resonance frequencies for different modes were normalized to the frequency corresponding to the minimum pressure.

4. Uncertainty analysis.

Following origins of type A uncertainties were considered: fluctuations of microwave signal, fluctuations of acoustic signal, fluctuation of the value of temperature measured by Pt thermometers, fluctuations of measured pressure [2, 4].

Following contributions to type B uncertainty of T90 measurements were taken into account: type B uncertainties of Pt thermometers calibration, type B uncertainty of thermometer resistance measurement, type B uncertainty originating from temperature gradient in the resonator [2, 4]. For type B uncertainty of T we considered uncertainties originating from pressure measurements, uncertainty of He molar mass, uncertainty of resonator shape variation.

f. Results

The obtained values of the temperature deviation on the ITS-90 scale from the thermodynamic temperature are listed in Table 1.

Table 1 T-T_{90} values and its uncertainties

T_{90}, K	T-T_{90}, mK	$u(T$-$T_{90})$, mK
83.8058	-4.81	0.93
79	-4.47	0.88

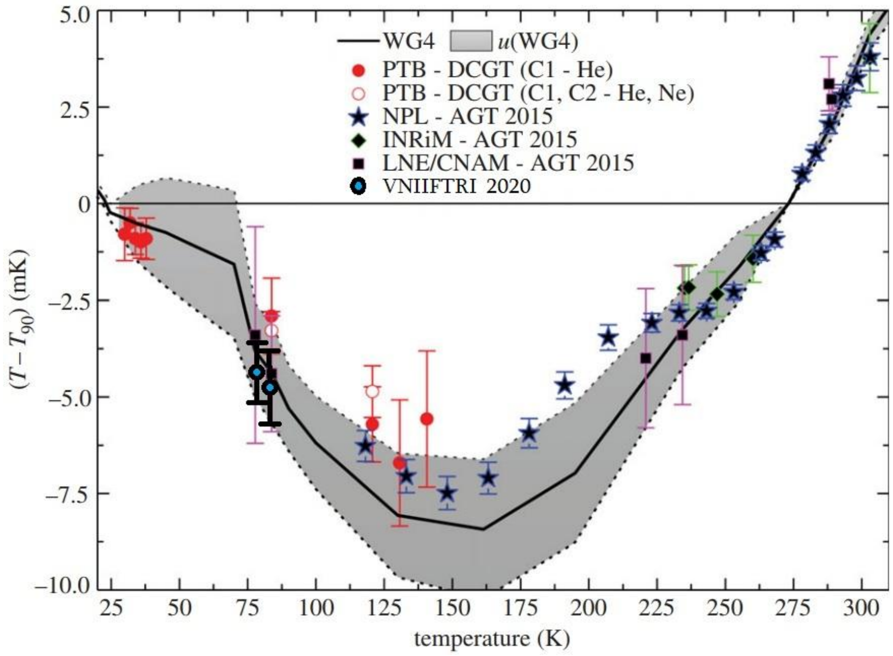

Fig. 2 T-T_{90} values obtained in the leading metrological institutes of the world

For comparison, the figure 2 shows T-T90 values obtained in the world leading metrological institutes in recent years at the leading metrological institutes of the world in a similar temperature range.

It can be seen that the obtained values agree with the previously published data within the standard uncertainty.

References:

1. Resolutions of 26th CGPM, Versailles, France (2018)
2. Kytin, V. G.; Kytin, G. A.; Ghavalyan, M. Yu.; Potapov, B. G.; Aslanyan, E. G.; Schipunov, A. N. International Journal of Thermophysics, Volume 41, Issue 6, article id.88
3. M.R. Moldover, R.M. Gavioso, J.B. Mehl, L. Pitre, M. de Podesta, J.T Zhang, Metrologia,
4. V.G. Kytin, G.A. Kytin, Measurement Techniques, 59 62 (2016)

Comparison of time scales using optical frequency references on ultracold atoms

Belotelov G.S., Gribov A.Yu.
National Research Institute for Physical-Technical and
RadioTechnical Measurements − FGUP VNIIFTRI,
Mendeleevo, Moscow Region, Russia, 141570,
http://www.vniiftri.ru
Mobile phone: +7 (909) 955-04-71
E-mail: belotelov@vniiftri.ru

Abstract

High-precision time synchronization for remote optical frequency references plays an important role in basic science and practical applications. Where possible, the solution is to use FOCL. With its help, it is possible to transmit the frequency from the optical reference in the optical range, transferring it to the radio range only if necessary at the remote end of the line. An IR laser attached to a cryogenic resonator can act as a guardian of the optical frequency range, which solves the problem of inconsistent operation of the optical reference. The ability to remotely compare the time scale in situations where the use of fiber-optic communication lines is impractical or impossible, in particular, between terrestrial and space optical frequency reference points, will provide significant progress in fundamental physics and practical applications, including testing the variability of fundamental constants, general theory of relativity , dark matter search, geodesy and global navigation satellite systems. The paper proposes an approach to the use of a laser stabilized by a cryogenic silicon resonator as a storage of the optical reference frequency in the optical range, which will improve the stability level of the local time scale. An approach to the use of mobile optical frequency references for carrying out comparisons of time scales in the absence of FOCL is also considered.

Relevance

High-precision time synchronization for remote optical frequency references plays an important role in basic science and practical applications. Where possible, the solution is to use FOCL. With its help, it is possible to transmit the frequency from the optical reference in the optical range, transferring it to the radio range only if necessary at the remote end of the line. An IR laser attached to a cryogenic resonator can act as a frequency keeper of the optical range, which solves the problem of inconsistent operation of the optical reference.

The ability to remotely compare the time scale in situations where the use of fiber-optic communication lines is impractical or impossible, in particular, between terrestrial and space optical frequency references, will provide significant progress in fundamental physics and practical applications, including testing the variability of fundamental constants, general theory of relativity , dark matter search, geodesy and global navigation satellite systems.

Purpose of work

Synchronization of local time scales of geographically separated metrological centers is not worse than 1 ns.

Applied relevance

Global trends are leading to increased requirements for the accuracy of the time scales matching, which forces researchers to look for new methods of their formation. One of the main directions for solving this problem is the creation of a scale using optical frequency references (OFR) along with cesium and rubidium reference [1]. The second approach is the use of OFR to correct the hydrogen drift [2].

We are developing an approach to the use of a cryogenic silicon resonator stabilized laser as a keeper of the optical reference frequency in the optical range, which will improve the stability level of the local time scale. We also consider an approach to the use of mobile optical frequency reference for carrying out comparisons of time scales in the absence of fiber-optic communication lines.

Work tasks

1. Development of a system for comparison the frequency of a laser stabilized by a cryogenic silicon resonator using a fiber-optic link used as a frequency keeper in the optical range with hydrogen keepers.
    - stabilization of an IR laser in a cryogenic silicon resonator;
    - development of a FOCL scheme.
2. Development of a mobile OFR:
    - development of a compact vacuum chamber of an optical spectroscope;
    - development of a laser radiation distribution system;
    - development of frequency stabilization systems and compact "watch" laser systems;
    - placing the created modules in the van.
3. Development of an algorithm for conducting comparisons using mobile OFR.

The essence of the work

Synchronizing time scales is a difficult task that can be solved using different approaches. One approach is FOCL synchronization using frequency keepers in the optical range. Another approach is the synchronization of the unit of frequency using mobile ORF [3].

OFR is a complex system in which the applied methods of controlling the states of atoms play an important role. The OFR device can be divided into several modules:

- vacuum spectroscope. It is a single vacuum system, assembled from the following separate segments: a source of hot atoms, a collimator section for narrowing the flow of atoms, a Zeeman slower section for preliminary cooling of atoms, a vacuum chamber, hetero-ion pumps, magnetic coils in the anti-Helmholtz configuration for forming a magneto-optical trap (MOT);
- laser cooling system. It consists of laser systems of first and second stage cooling for preparing atoms for loading into an optical lattice, a laser system for forming an optical lattice, a laser system for interrogating a clock transition, a laser pumping system for increasing the number of trapped atoms;
- laser stabilization system. Consists of a set of laser wavelength meters or similar equipment that allows precise control of the laser radiation frequency;
- detection system. It consists of an optomechanical scheme for interrogating a cloud of trapped atoms and a high-precision camera or PMT for photon counting.

Results

The algorithms for the operation of comparison schemes for OFR with hydrogen keepers from the composition of the primary standard GET 1 - 2018 and the system for comparison by fiber optic lines of the frequency of a laser stabilized by a cryogenic silicon resonator, used as a frequency keeper in the optical range with hydrogen keepers of the primary standard GET 1 - 2018, is discussed in detail in [4].

At FSUE “VNIIFTRI”, a variant of a system for comparing the FOCL of the frequency of a laser stabilized by a cryogenic silicon resonator is being implemented, used as a frequency keeper in the optical range with hydrogen keepers of the primary standard GET 1 - 2018.

The diagram is shown in Fig. 1. The use of the telecommunication wavelength (1.5 μm) makes it possible to transmit ultrastable signals over fiber lines over long distances.

Usually, two identical fiber lines are built to check the correct of frequency transfer, however, in our case, this possibility exists due to the simultaneous work of the circuit where the HM18 hydrogen maser, connected via an optical line to an ensemble of hydrogen masers, still acts as a frequency keeper.

Such a scheme will make it possible to implement a frequency keeper in the optical range and compare it with the ensemble of hydrogen masers from the primary standard GET 1 - 2018.

At present, a mobile OFR based on cold ytterbium atoms is being created at FSUE VNIIFTRI. At this stage:

- implemented a vacuum chamber of the optical spectroscope, including a pair of magnetic coils in anti-Helmholtz configuration;
- a laser radiation distribution system was manufactured and tuned, which includes all the necessary directions for laser cooling and trapping of atoms: first stage cooling in three mutually perpendicular directions, Zeeman slower, detection, collimating radiation. All necessary detuning frequencies achieved using acousto-optic modulators. The secondary cooling combined with the first stage one on a dichroic mirror, after which the balance of the first stage and second stage cooling capacities realized;

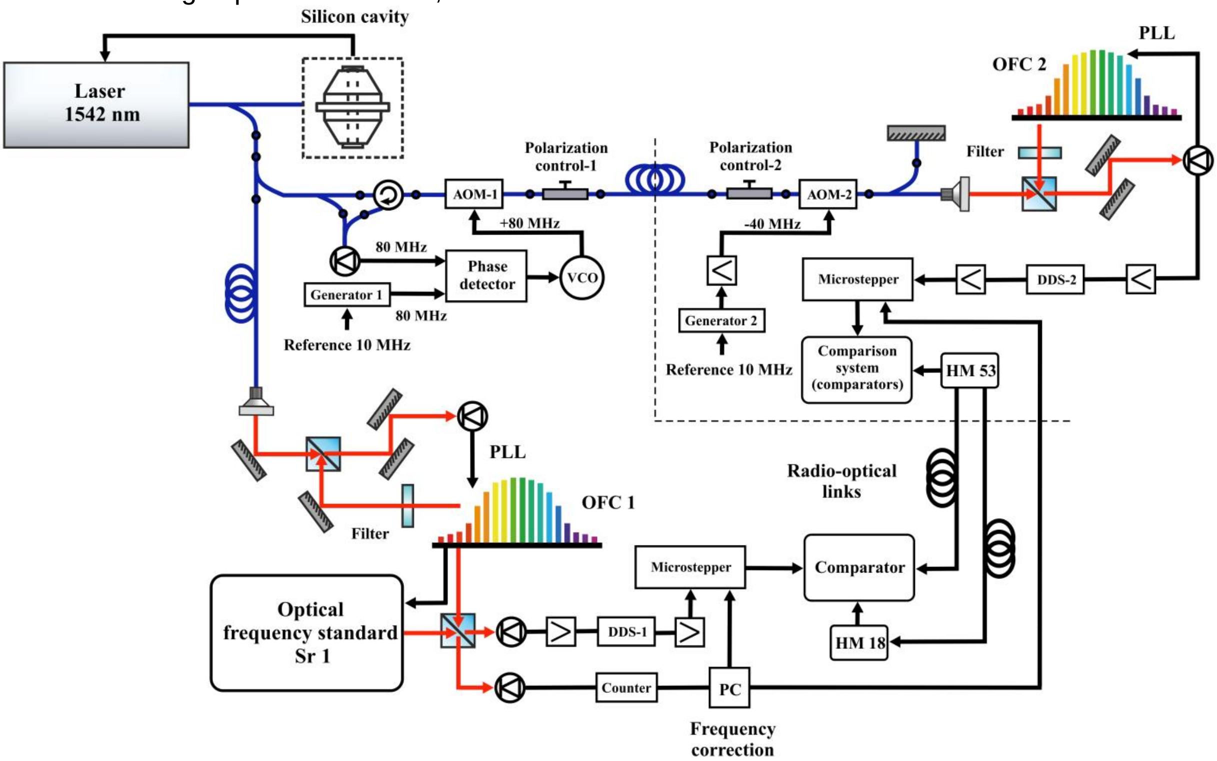

Fig. 1. Proposed frequency comparison scheme based on optical frequency keeper: Polarization control 1, Polarization control 2 – polarization controllers; VCO – voltage controlled oscillator; HM 18, 53 – main hydrogen masers for measurements; AOM-1 – acousto-optic modulator, that suppresses phase noise introduced by the line; AOM-2 – acousto-optic modulator, provides separation of reflected radiation from parasitic retroreflections along the fiber that are not shifted by frequency.

- a unique frequency stabilization unit FSU-1 [5] was created, which is an ultra-compact system used to stabilize the frequency of lasers at 798 nm (laser with a singlet transition before frequency doubling), 1112 nm (laser with a triplet transition before frequency doubling) and 759 nm (optical grating). The FSU-1 contains a 10 cm long ULE block with two embedded high-finesse optical resonators, placed in a compact vacuum chamber. The finesse at 759 nm and 798 nm equals 2 000, at 1112 nm equals 10 000.

- the first version of the compact stabilized clock laser system CLS-1 was created. It contains a vertical "vibration-insensitive" high-precision ULE resonator 10 cm long, located inside the vacuum chamber, and doubled in frequency ECDL at a wavelength of 1157 nm. The Q-factor of the CLS-1 ULE resonator is 120,000. For safe transportation, a mechanical resonator locking system is implemented.

- a system for forming an optical lattice at a wavelength of 759 nm is being prepared.

The standard method for synchronizing time scales is to carry a continuous pps signal source. The optical frequency reference is not a continuously operating device [5] and, at the same time, the formation of the pps signal with its help is not trivial [6]. An alternative could be the transportation of a continuously operating hydrogen maser, the frequency of which is adjusted according to the OFR [7], but this approach is unlikely to provide time scale synchronization at a level better than 1 ns.

A promising option is to transport a unit of frequency using an optical frequency reference. We are developing an algorithm for applying a mobile optical frequency reference in the time scale. At the first stage, a step-by-step movement of two mobile OFRs is made to the target and back, comparing the frequencies of the mobile units with each other in order to accurately establish the difference in gravitational potentials between the metrological centers.

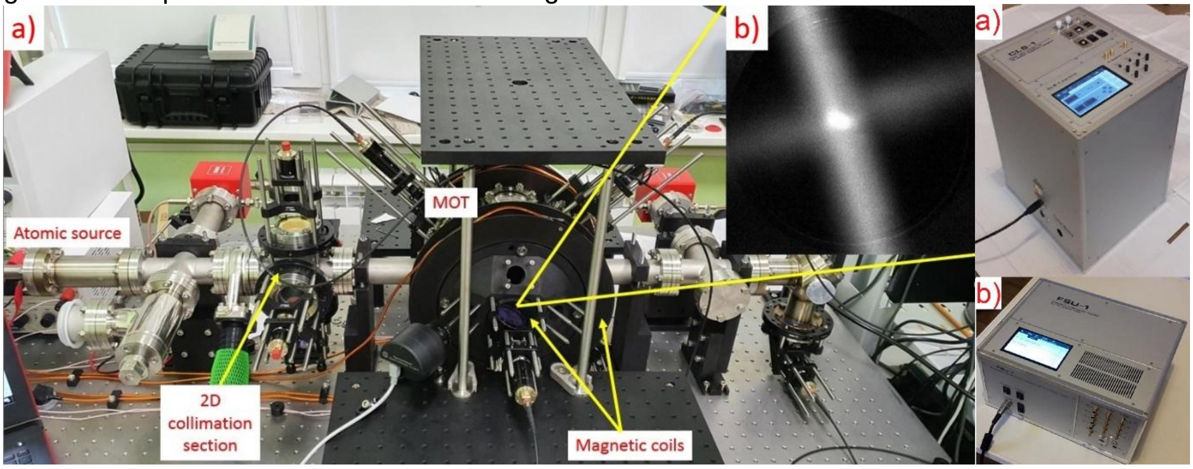

Fig. 2. Left: a) vacuum chamber of the optical spectroscope, b) cloud of trapped atoms. Right: a) compact stabilized clock laser system CLS-1, b) frequency stabilization unit FSU-1. Together they take up a volume of approx. 40 liters with an approximate power consumption of 20 W and a weight of 35 kg.

At the second stage, the mobile OFR is compared with a cesium frequency standard through measurements with a hydrogen frequency guard.

The third stage of the algorithm is the movement of the mobile OFR from the first center to the second, where the mobile OFR is compared with the local frequency standard (optical reference, hydrogen or rubidium fountain). Thus, the local time scale is synchronized according to the transported size of the unit of frequency of the cesium standard.

References:

1. Сутырин Д. В. и др. Оптический репер частоты для применения в национальной шкале времени //Квантовая электроника. – 2019. – Т. 49. – №. 2. – С. 199-204.
2. Hachisu H. et al. Months-long real-time generation of a time scale based on an optical clock //Scientific reports. – 2018. – Т. 8. – №. 1. – С. 1-12.
3. Riehle F. Optical clock networks //Nature Photonics. – 2017. – Т. 11. – №. 1. – С. 25-31.
4. *A. Gribov et al.* “Time-scale Generation Methods Based on an Optical Clock”, 2020 Joint Conference of the IEEE International Frequency Control Symposium and International Symposium on Applications of Ferroelectrics (IFCS-ISAF), Keystone, CO, USA, 2020, pp. 1-4, doi: 10.1109/IFCS-ISAF41089.2020.9234906.
5. Бердасов О. И. и др. О продолжительности непрерывной работы оптического стандарта частоты на атомах стронция //Квантовая электроника. – 2018. – Т. 48. – №. 5. – С. 431-437.
6. Herman D. et al. Femtosecond timekeeping: Slip-free clockwork for optical timescales //Physical Review Applied. – 2018. – Т. 9. – №. 4. – С. 044002.
7. КАРАУШ А. А. и др. ОЦЕНИВАНИЕ СМЕЩЕНИЯ ШКАЛЫ ВРЕМЕНИ ПЕРЕВОЗИМОГО СТАНДАРТА ЧАСТОТЫ, НАХОДЯЩЕГОСЯ В ДВИЖЕНИИ, ПО СИГНАЛАМ ГНСС //Гироскопия и навигация. – 2020. – Т. 28. – №. 3. – С. 110.